UNIVERSITY OF ALBERTA

HYDROGEOLOGY OF THE DEVONIAN RIMBEY-MEADOWBROOK REEF TREND OF CENTRAL ALBERTA, CANADA

BY
DEBASHISH PAUL

A THESIS SUBMITTED TO THE FACULTY OF GRADUATE STUDIES AND RESEARCH IN PARTIAL FULFILLMENT OF THE REQUIREMENTS FOR THE DEGREE OF MASTER OF SCIENCE

DEPARTMENT OF GEOLOGY

EDMONTON, ALBERTA
SPRING 1994

ISBN 0-612-11319-1

UNIVERSITY OF ALBERTA

RELEASE FORM

NAME OF AUTHOR: DEBASHISH PAUL

TITLE OF THESIS: HYDROGEOLOGY OF THE DEVONIAN RIMBEY-MEADOWBROOK REEF TREND OF CENTRAL ALBERTA, CANADA.

DEGREE: MASTER OF SCIENCE

YEAR THIS DEGREE GRANTED: 1994

Debashish [signature]

68/232, Gandhinagar,
Opp. Tikonia Park,
Lucknow (U.P.)
INDIA 226 019

Date: Nov. 25, 1993

UNIVERSITY OF ALBERTA

FACULTY OF GRADUATE STUDIES AND RESEARCH

The undersigned certify that they have read, and recommend to the Faculty of Graduate Studies and Research for acceptance, a thesis entitled *"Hydrogeology of the Devonian Rimbey-Meadowbrook reef trend of Central Alberta, Canada"* submitted by *Debashish Paul* in partial fulfillment of the requirements for the degree of Master of Science.

Dr. József Tóth,
Supervisor

Dr. H. G. Machel,
Co-supervisor

Dr. Carl Mendoza

Dr. Peter Steffler

Date: Nov. 23, 1993

Dedicated to my parents, sister
and
Christine

ABSTRACT

The Devonian Rimbey-Meadowbrook reef trend of Central Alberta comprises a series of isolated dolomitized Leduc Fm. reefs surrounded and capped by Ireton Fm. shales. Based on potentiometric surface, pressure-depth and water chemical analyses, the study has revealed interesting features of the present-day fluid flow pattern and distribution in the Nisku Formation and the underlying Leduc and Cooking Lake Formations. The regional fluid flow direction is north northeast and follows the slope of the land surface. Along the reef trend the potentiometric surface of the Nisku Formation is subdued compared to that of the Leduc and Cooking Lake Fms.; however, in the Bashaw reef a close correspondence is noted. Along the pre-Cretaceous unconformity energy is dissipated more rapidly within the Nisku Formation than in the Leduc and Cooking Lake Formations. Fluid flux along the Nisku Formation is 1.2mm/day as compared to 0.5mm/day along the Cooking Lake Formation.

During the Late Cretaceous to Early Eocene fluid flow within the Alberta Basin was updip and ascending. Hydraulic continuity on a geological time scale exists between the Nisku and Leduc Fms., especially where the Ireton shales thin over the Leduc reefs. The thin, relatively permeable Ireton shales capping the Bashaw reef allow ascending Leduc waters with a vertical flux of 1.3mm/day to move up into the Nisku Formation. Gravity-driven cross-formational flow of dolomitizing fluids is a possible mechanism for the post-depositional dolomitization noted in the structurally downdip portions of the Nisku Formation. Near the southern end of the Leduc-Woodbend reef, similar salinities between the Nisku and Leduc Fms. waters indicate that the reefs in the trend were filled by upward moving feedstock fluids.

In the structurally updip regions, the Nisku, Leduc and Cooking Lake Fms. waters are diluted to varying degrees by mixing with Cretaceous Fm. waters. The pre-Cretaceous unconformity controls the extent of the mixing zone within these formations. The relationship of salinity to Mg/Ca ratio in the Devonian formation waters show a scatter in the data points across the calcite and dolomite saturation fields, indicating a continuous fluid flow within these formations.

ACKNOWLEDGEMENTS

I wish to extend my sincere gratitude to my supervisor Prof. József Tóth under whose tutelage (the "hard way"-no spoonfeeding) I realized the important role groundwater plays as a subsurface transport agent. The casual discussions that we had over coffee-breaks were extremely fruitful as most of the intangible problems and queries were solved. I am thankful to my co-supervisor, Dr. H.G. Machel for his critical comments and suggestions during the course of my research work. His enthusiasm in my research problem always kept me on my toes. Thanks to Dr. Carl Mendoza for his supervision during the latter phase of the thesis.

Many thanks to Mike Ranger for providing the plotting program to generate the maps used in the study. A special token of appreciation goes to Hydro Petroleum Canada, Ltd. for supplying some of the pressure data that were used. I am indebted to my colleague, Dan Barson, for his willingness to teach and give suggestions at different stages of my research. A truck load of thanks to my other colleagues in the Petroleum Hydrogeology Group. I could always rely on Ben Rostron before embarking on any method and procedure of analysis. Liane was always there to lend her ears to the accomplishments of my daily work, but more so to my lamentations and frustrations. The amicable group of Kriengsak, John, and Kent provided the perfect working environment.

I would like to thank the Department of Geology for granting me the financial support in the form of Research and Teaching Assistantships.

This study was funded by the research grants held by Prof. J. Tóth and by a Strategic Grant of the Natural Sciences and Engineering Research Council of Canada held jointly by Dr. H.G. Machel and Dr. E.W. Mountjoy (McGill University), and a grant from the American Association of Petroleum Geologists Grant-in-Aid held by the author.

Table of Contents

List of Tables

List of Figures

Chapter 1 Introduction

1.1 Selection of Study Area and Previous Work

In the petroleum industry optimizing strategies for hydrocarbon exploration requires knowledge of the timing of hydrocarbon generation, the location of suitable traps and the pattern and distribution of fluid flow. Tóth (1978) has strongly advocated that in geologically mature sedimentary basins, topography driven flow is the principal agent in the transport (secondary migration) and accumulation of hydrocarbons.

The Western Canada Sedimentary Basin (WCSB) is a geologically mature sedimentary basin. Since the discovery of oil in the Upper Devonian Leduc reefs of Central Alberta in 1947, the WCSB has been the focus of hydrocarbon exploration activity in Canada. In the Alberta part of the WCSB, the Devonian System ranks as the major hydrocarbon producing interval, accounting for over 60% of recoverable conventional crude oil reserves and about 20% of recoverable gas reserves (Burrowes and Krause, 1987). Reefs of the Leduc Formation contain almost a quarter of the total conventional oil reserves in Alberta.

The spatial distribution of oil and gas pools and the patterns of dolomitization within the individual reefs of the Devonian Rimbey-Meadowbrook reef chain of Alberta, have led to various speculations about possible fluid flow patterns (Stoakes and Creaney, 1984; Machel and Mountjoy, 1987; Hugo, 1990). The present study, therefore, focusses on understanding the hydrogeology of this reef trend (Figure 1.1). The Rimbey-

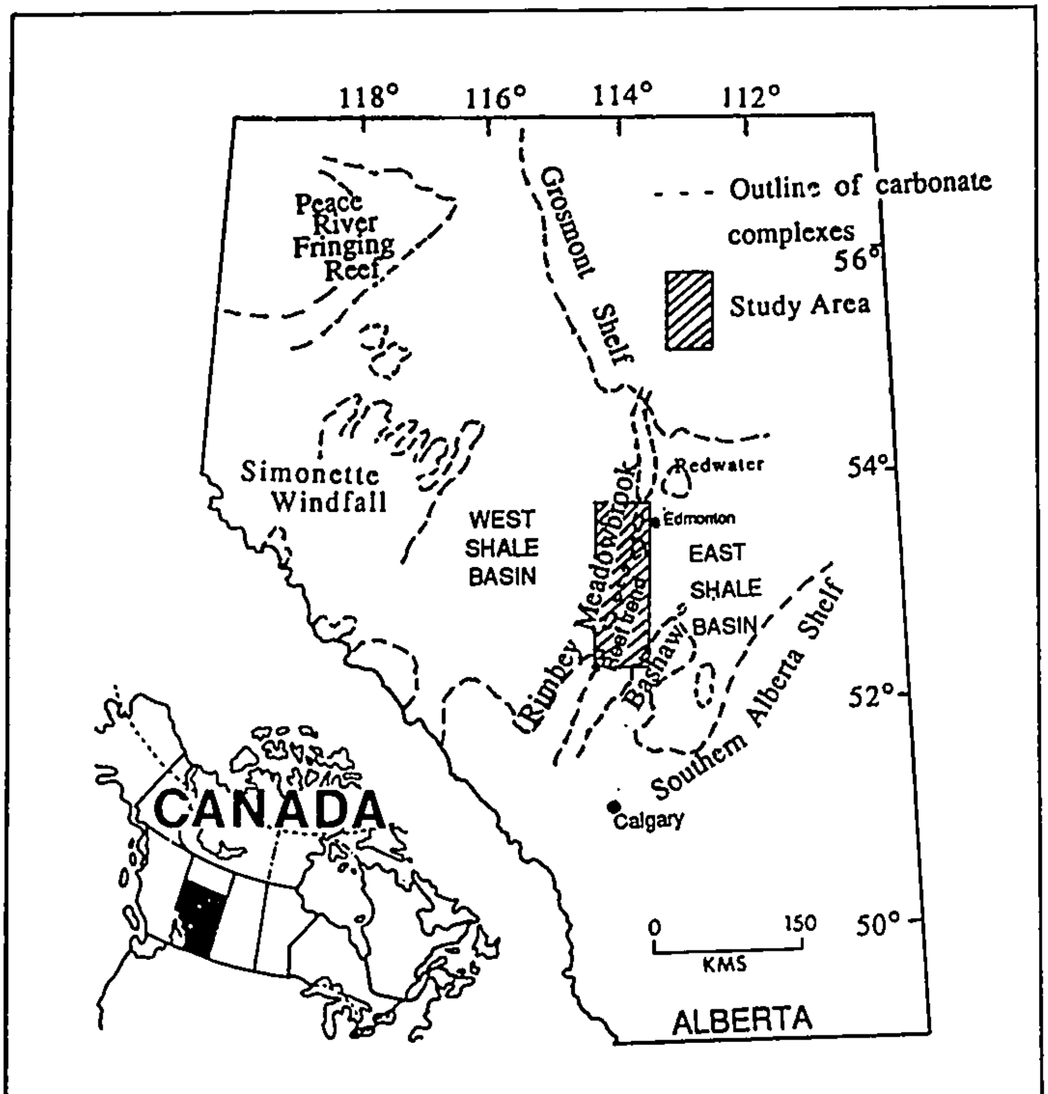

Figure 1.1 Distribution of upper Devonian carbonate complexes (Leduc Frm. and equivalent) and intervening shale basins (modified from Stoakes, 1980)

Meadowbrook reef trend which is oriented NNE-SSW, lies below the Central Alberta Plains between latitudes 52°25'N-53°45'N and roughly along longitude 114°W (Tps.40-54 Rs.23W4-2W5). It comprises a series of "isolated" Leduc reefs, ten of which are major hydrocarbon reservoirs. From the southern to the northern end of the study area they are: Rimbey, Westrose South, Westrose, Bonnie Glen, Wizard Lake, Glen Park, Leduc-Woodbend, Acheson, Big Lake and St. Albert.

The stratigraphy of this area has been extensively studied by numerous researchers (Imperial Oil Limited, 1950; Belyea, 1952, 1955; Andrichuk, 1958a, 1958b). The Rimbey-Meadowbrook reef trend served as an example of the principle of differential entrapment of hydrocarbons in contiguous structures (Gussow, 1954). Hitchon (1969) cited this region in his analysis of the effect of topography and geology on the regional fluid flow in the Western Canada Sedimentary Basin while Hugo (1990) described fluid flow within the Leduc reefs. McNamara and Wardlaw (1991) have given a detailed geological description and statistical analyses of the Leduc Formation permeabilities and porosities in the Westrose reef.

There are some intriguing peculiarities concerning these reefs. Most reefs along the Rimbey-Meadowbrook trend overlie the Cooking Lake Formation platform, and all except the Golden Spike and Redwater (outside the study area, see Fig.1.1) reefs are fully dolomitized. Machel and Mountjoy (1987) suggested that the Cooking Lake platform served as a conduit for the dolomitizing fluids and that the Golden Spike reef was not dolomitized because it lies west of the main reef trend and is hydraulically disconnected from the Cooking Lake conduit. The Redwater reef, however, is rooted on the Cooking Lake Formation so its incomplete dolomitization remains an enigma for the Machel and Mountjoy hypothesis.

Stoakes and Creaney (1984) suggested that the Cooking Lake platform served as a conduit for petroleum migration. Gussow (1954) had earlier propounded the principle of differential entrapment or, as it is more commonly known, the "spill-point theory", with the Rimbey-Meadowbrook reef trend as an example. However, the theory is not valid throughout the trend. Stoakes and Creaney (1984) believe that simple updip migration with successive traps filling to spill point, fails to account for the distribution of gas and oil in the reefs north of Glen Park, while the hydrocarbon distribution within individual reefs south of Glen Park (inclusive) can be explained by the spill-point theory. However, a close scrutiny of the known hydrocarbon distribution actually renders the spill-point theory untenable throughout the reef trend.

Hitchon (1969) and Hugo (1990) describe uninterrupted NNE directed flow in the aquifers of the Woodbend Group - the Leduc and Cooking Lake Formations. Studies of pool pressure histories for individual Leduc reefs suggested varying degrees of pressure communication between the reefs which could be explained by the existence of hydraulic barriers along the reef trend (Hnatiuk and Martinelli, 1967; Barfoot and Ko, 1987). Since their study is based on pool pressure histories over the past 45 years of hydrocarbon production in the reef trend, their conclusions should not be incorporated for assessing hydraulic communication between reefs on a geologic time scale. Hnatiuk and Martinelli (1967) also concluded that all pools in the reef trend are, to varying degrees, in pressure communication through the underlying Cooking Lake Formation.

1.2 Purpose of Study

This study was undertaken primarily to determine the present-day formation fluid flow distribution in the Leduc and Cooking Lake Formations of the Rimbey-Meadowbrook trend and in the overlying Nisku Formation. It is hoped that this study will resolve the ambiguity arising from the contrasting flow models/patterns proposed by Hitchon & Hugo on one hand and Hnatiuk & Martinelli and Barfoot & Ko on the other.

Ireton shales cap the Leduc pools (reefs) and separate them from the conformably overlying Nisku Formation. A qualitative assessment of the effectiveness of the Ireton shale seal was made in this study. Concerning the hydraulics and the distribution of hydrocarbons the result of this assessment is considered crucial. This will also indicate whether the Rimbey-Meadowbrook reef trend has influenced the hydraulics and hydrochemistry of the Nisku Formation.

In this study, fluid fluxes were estimated to evaluate the intensity of fluid flow within and among the Leduc reefs as well as in the Nisku and Cooking Lake Formations. Such estimates provide a foundation for additional research on mass balance calculations by incorporating the geometry of the individual reefs.

Establishing a possible relation between the present-day flow pattern and the hydrochemistry of formation waters was another aspect of this study. The results from the entire study may also yield insight into the relations between flow and dolomitization, through rigorous determination of present-day fluid migration paths. For the interest of the Petroleum Hydrogeologist a method has been proposed to calculate equivalent freshwater head when bottom-hole pressure measurements are made within a hydrocarbon pool.

Chapter 2 Geological Setting and Stratigraphy

2.1 Introduction

The Western Canada Sedimentary Basin is bounded to the northeast by the Precambrian Shield and to the west by the Rocky Mountain Thrust Belt, which forms the easternmost subdivision of the Canadian Cordillera. The Interior Plain comprising gently dipping sedimentary rocks forms the central part of the Western Canada Sedimentary Basin. The Interior Plain is divisible into three regions, the Alberta and Williston basins, separated by the Sweetgrass Arch.

The present study area is located in the central plains of the Alberta Basin and the focus is on the Rimbey-Meadowbrook reefs of Upper Devonian (Frasnian) age in the Woodbend Group. This group comprises, in ascending order, the Cooking Lake, Leduc and Ireton Formations in the reef region; and, Majeau Lake Member and Duvernay Formation as the basinal equivalents for the first two, in the off-reef region (Imperial Oil Limited, 1950; Stoakes, 1980). The Nisku Formation which is the lowermost unit in the overlying Winterburn Group has also been considered in this study. Figure 2.1 illustrates the stratigraphic relationship of the different geologic formations. The geological history and stratigraphy of the Woodbend Group of Central Alberta has been described by Imperial Oil Limited (1950), Belyea (1952, 1955), Andrichuk (1958a, 1958b), Stoakes (1980) and others.

The Cooking Lake carbonate platform is the foundation on which the Rimbey-Meadowbrook reef trend striking NNE-SSW is developed. The Cooking Lake Formation is deposited on an extensive

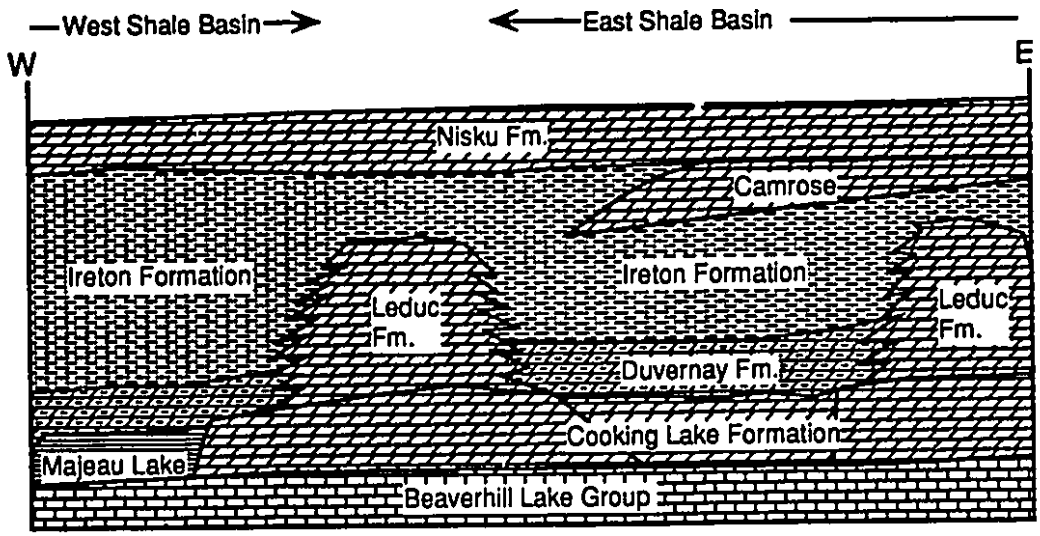

Figure 2.1 Schematic cross-section and stratigraphic terminology of the Rimbey-Meadowbrook Reef Trend (modified from Stoakes, 1980)

Late Devonian bank and has a distinct margin directly west of the reef trend (Andrichuk, 1958a). Conformably overlying the Cooking Lake platform, in the off-reef areas, are the black bituminous shales and dense argillaceous limestones of the Duvernay Formation deposited under euxinic conditions (Stoakes, 1980). The Duvernay Formation is overlain by the green shales of the Ireton Formation deposited under marine conditions. These thick, basin-filling Ireton shales surround and cover individual Leduc reefs that are along the reef trend. Therefore, the regions on either side of the Rimbey-Meadowbrook reef trend are categorized as the East and West Shale Basins. The Ireton Formation varies in thickness throughout the study area, averaging 10m over individual Leduc reefs (Stoakes, 1980). In the south east corner of the study area, over the Bashaw reef, the Ireton Formation is less than 10m thick; and it is negligible or absent in Tp.42 R23W4.

Structural cross-sections have been constructed along A-A' and B-B' on the map shown in Figure 2.2. These cross-sections were constructed with the aid of well logs and PUBCO (1990) formation picks (Figures 2.3 and 2.4). Wells used in these two cross-sections have been listed in Table 1. A typical log response for an off-reef well over the stratigraphic interval of interest is depicted in Figure 2.5.

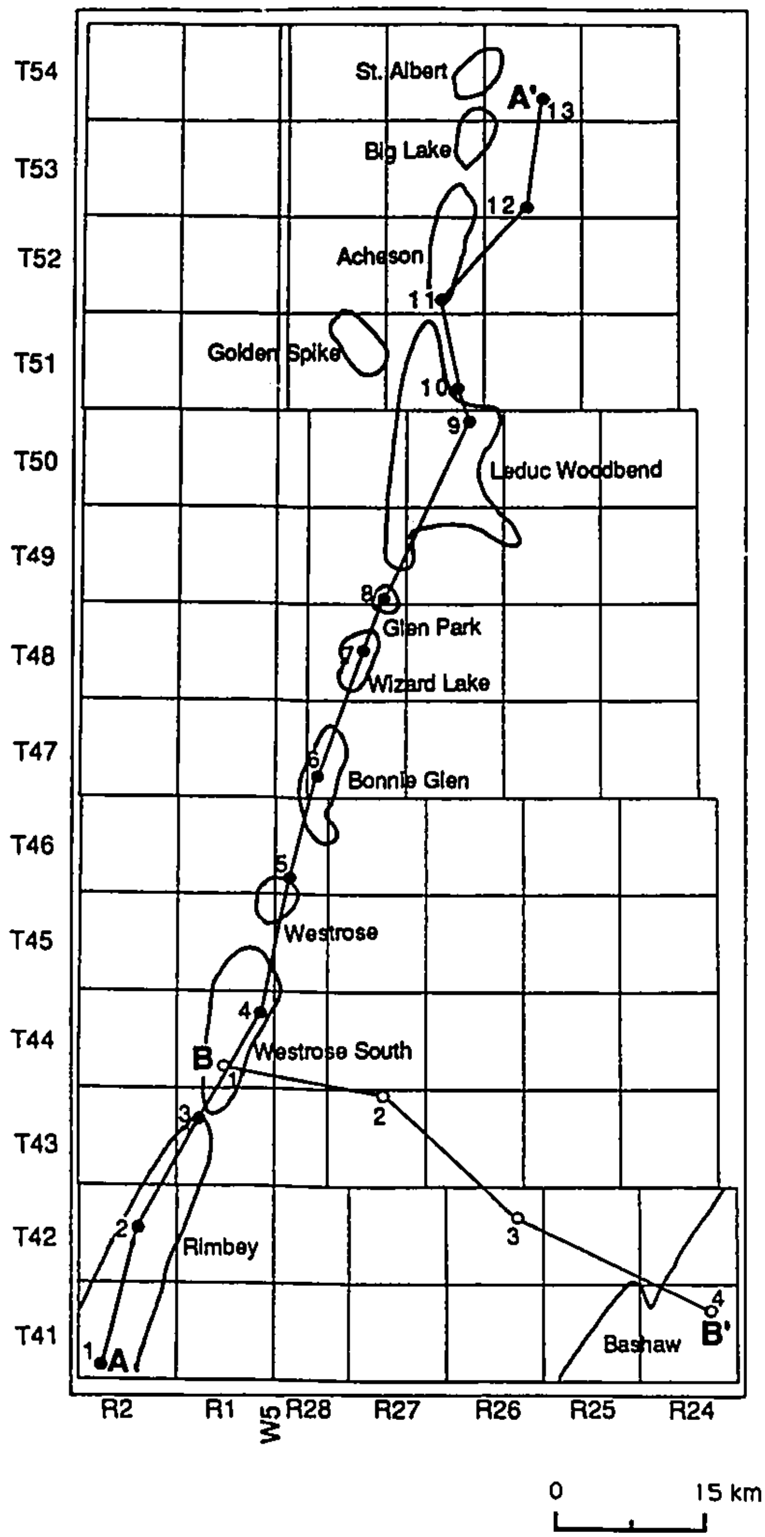

Figure 2.2 Locations of cross-sections (A-A' & B-B')
(with outiine of the Leduc reefs)

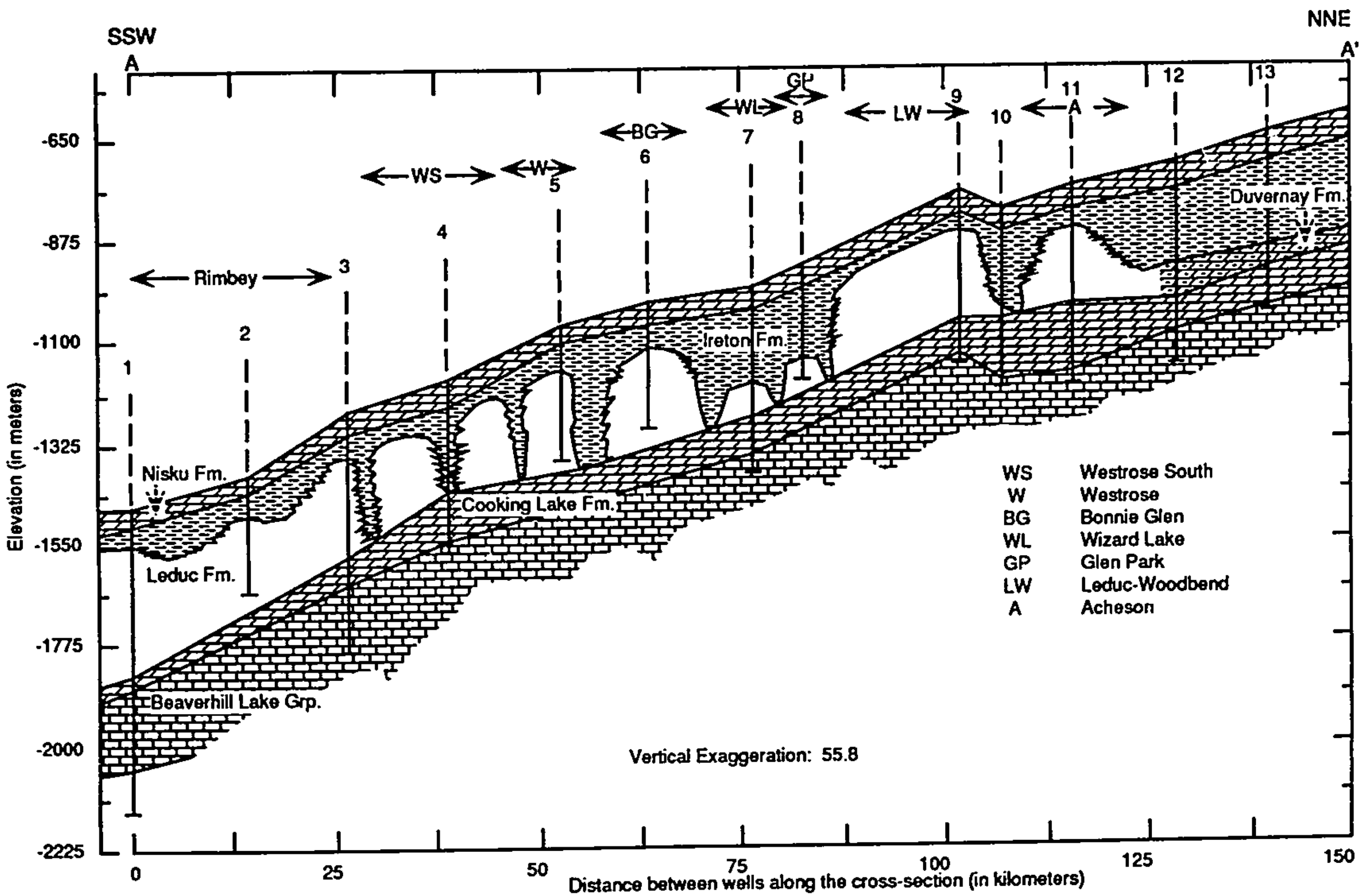

Figure 2.3 Structural cross-section (A-A') along the reef trend (strike section)

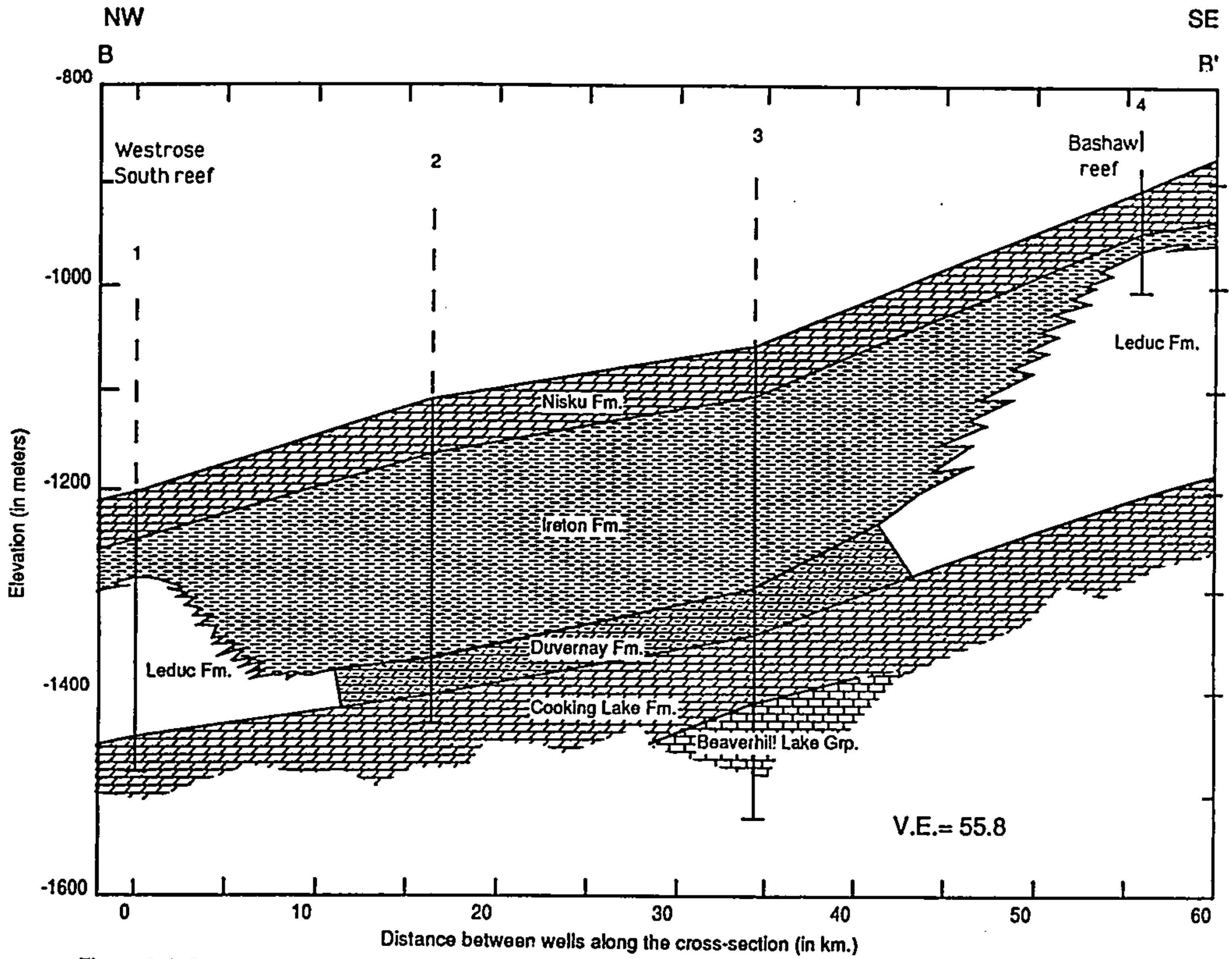

Figure 2.4 Structural cross-section (B-B') across the reef trend (dip section)

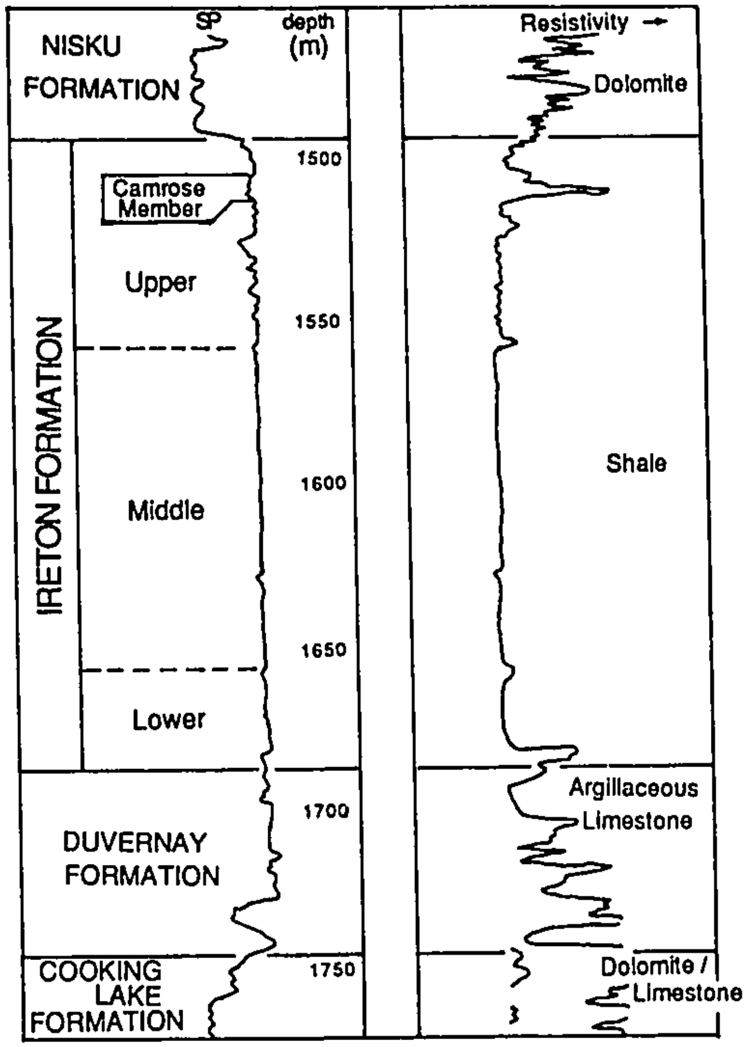

Figure 2.5 Typical off-reef showing log response and stratigraphic divisions (modified from Stoakes, 1980)

2.2 Geologic Formations

2.2.1 Cooking Lake Formation:

The Cooking Lake Formation is the basal unit of the Woodbend Group and is a result of marine transgression with concomitant deepening within the Alberta Basin. The upper contact of the Cooking Lake Formation appears transitional with the black bituminous shales of the Duvernay Formation in the off-reef region, and especially with the overlying dolomitic Leduc reefs. The type section for Cooking Lake is in Calmont Leduc's well No.3 (04-14-051-21W4).

In most of the off-reef region of east-central Alberta the Cooking Lake Formation is biostromal in character while in the reefal region it develops biohermal characteristics. Andrichuk (1958) has divided this formation into four units - upper calcarenite, middle argillaceous, lower calcarenite, and basal dolomitic unit, with the vertical variations in the limestone being attributed to the changing energy conditions that varied from quiet to highly agitated water environments. The average thickness of the Cooking Lake Formation is 70m, with the calcarenite units being the thickest.

Conformably overlying the Cooking Lake Formation is the dolomitized Leduc Formation. Along the reef trend the Cooking Lake Formation is generally fully dolomitized making lithological differentiation from the Leduc Formation problematic (Imperial Oil Limited, 1950). However, in British American's Pyrcz well No.1 (12-25-50-26W4) the Cooking Lake Formation is partially dolomitized making it easily identifiable (Andrichuk, 1958b). Andrichuk also observed that the lower boundary of the completely dolomitized lower calcarenite unit which extends from the west side of Acheson and Leduc-Woodbend reefs varies in extent up to the top of the upper calcarenite unit on the east side. Further, complete dolomitization of the limestone has taken place in the Leduc-Woodbend and Wizard Lake reefs. The Cooking Lake Formation has a hydraulic conductivity in the order of 10^{-6}m/s (Hugo,1990). The Cooking Lake Formation is hypothesized to have acted as a highly permeable conduit for secondary hydrocarbon migration (Stoakes and Creaney, 1984) and dolomitizing fluids (Machel and Mountjoy, 1987).

2.2.2 Leduc Formation (D-3):

According to Imperial Oil Limited (1950) -

"A reef is a distinct lithologic unit of carbonate rocks which may vary in shape from a pronounced mount or ridge (biohermal) to a broad sheet (biostromal). It is caused primarily by the accumulation in situ of the remains of sedentary colonial marine organisms, supplemented by chemical, biological and clastic deposits."

The Leduc Formation is a biohermal reef development and in the study area all the individual reefs (except Golden Spike) of the Rimbey-Meadowbrook trend belonging to this formation are completely dolomitized. Golden Spike and Redwater reefs also of Leduc age which lie on either side of the reef trend have not been dolomitized (Andrichuk, 1958b; Machel and Mountjoy, 1987). In the reefs the original lithologic texture and organic structures have been obliterated due to recrystallization associated with dolomitization. On account of a myriad of vugs, Leduc dolomite is characterized by excellent secondary porosity and permeability. McCourt (1953) has observed in the Leduc-Woodbend reef that the porosity and permeability of the Leduc and underlying Cooking Lake Formations are similar. This observation may be useful in conjunction with pressure-depth [p(d)] analysis to establish the hydraulic communication between these two formations. The Leduc reefs are the most promising hydrocarbon reservoirs in Central Alberta that are sourced by the adjacent bituminous shales of the Duvernay Formation.

The Leduc Formation type section is 184m thick in British American's Pyrcz well No.1 (12-25-050-26W4)(Imperial Oil Limited, 1950).

2.2.3 Duvernay Formation:

The Duvernay Formation is the basinal equivalent of the Leduc Formation. The Duvernay Formation is characterized by black to dark brown bituminous shales (calcareous) and argillaceous limestones as compared to the gray, green calcareous shales of the overlying Ireton Formation. The type section as described by Imperial Oil Limited (1950) is in the Anglo-Canadian's Beaverhill Lake well No.2 (11-11-050-17W4) where it is 53m thick. The Duvernay Formation may be distinguished from the Ireton Formation on the basis of its higher resistivity signature on electric logs.

2.2.4 Ireton Formation:

At the type section in British American's Pyrcz well No.1 (12-25-050-26W4) the Ireton Formation attains a thickness of 80m (Imperial Oil Limited, 1950) but can reach up to 250m in the off-reef regions of the study area. Downing and Cooke (1955) and McCrossan (1961) have made a tripartite division of the Ireton Formation reflecting three distinct depositional environments. The upper Ireton consists of fossiliferous shale and carbonate, the middle Ireton is mostly shale, and the lower Ireton consists of shale and limestones (Figure 2.5). The upper Ireton caps the Leduc reefal buildups in the study area.

The Ireton Formation is much thicker in the West Shale Basin (maximum thickness exceeding 350m) than in the East Shale Basin. Core analyses and drill-stem tests are generally restricted to geologic formations and areas that have some potential for economic value. There is a paucity of core analysis and drill-stem test data for the Ireton Formation (shale) which has a low economic value as compared to the hydrocarbon-rich reefs of the Leduc Formation.

2.2.5 Nisku Formation (D-2):

The Nisku Formation forms the base of the Winterburn Group and conformably overlies the Ireton Formation in the study area. The dominant lithology is dolomite with occasional anhydrite. According to Imperial Oil Limited (1950), this formation is 48m thick at its type section in British American's Pyrcz well No.1 (12-25-050-26W4). It is this formation where the first oil was struck in the Leduc-Woodbend field in 1948. The Nisku Formation subcrops at the Paleozoic unconformity near the Redwater reef where it is water-bearing (Imperial Oil Limited, 1950). The importance of this geologic feature in the context of hydraulics and hydrochemistry will be discussed in Chapter 5.

2.3 Topography

Apart from the geology, topography plays a major role in affecting the fluid potential distribution (Tóth, 1962, Hitchon, 1969a). The Rocky Mountains, Foothill Belt and western Alberta Plains are regions of elevations more than 1000m. In northern Alberta, drainage basins along the Peace River, Athabasca River and Slave River are regions of elevations lower than 500m. The present study area occupies parts of the Western and Eastern Alberta plains in the Alberta Basin with elevations ranging between 600-950m. Figure 2.6 indicates that the relief in the study area is relatively flat. The ground surface slopes gently to the northeast with a general slope of 0.1°.

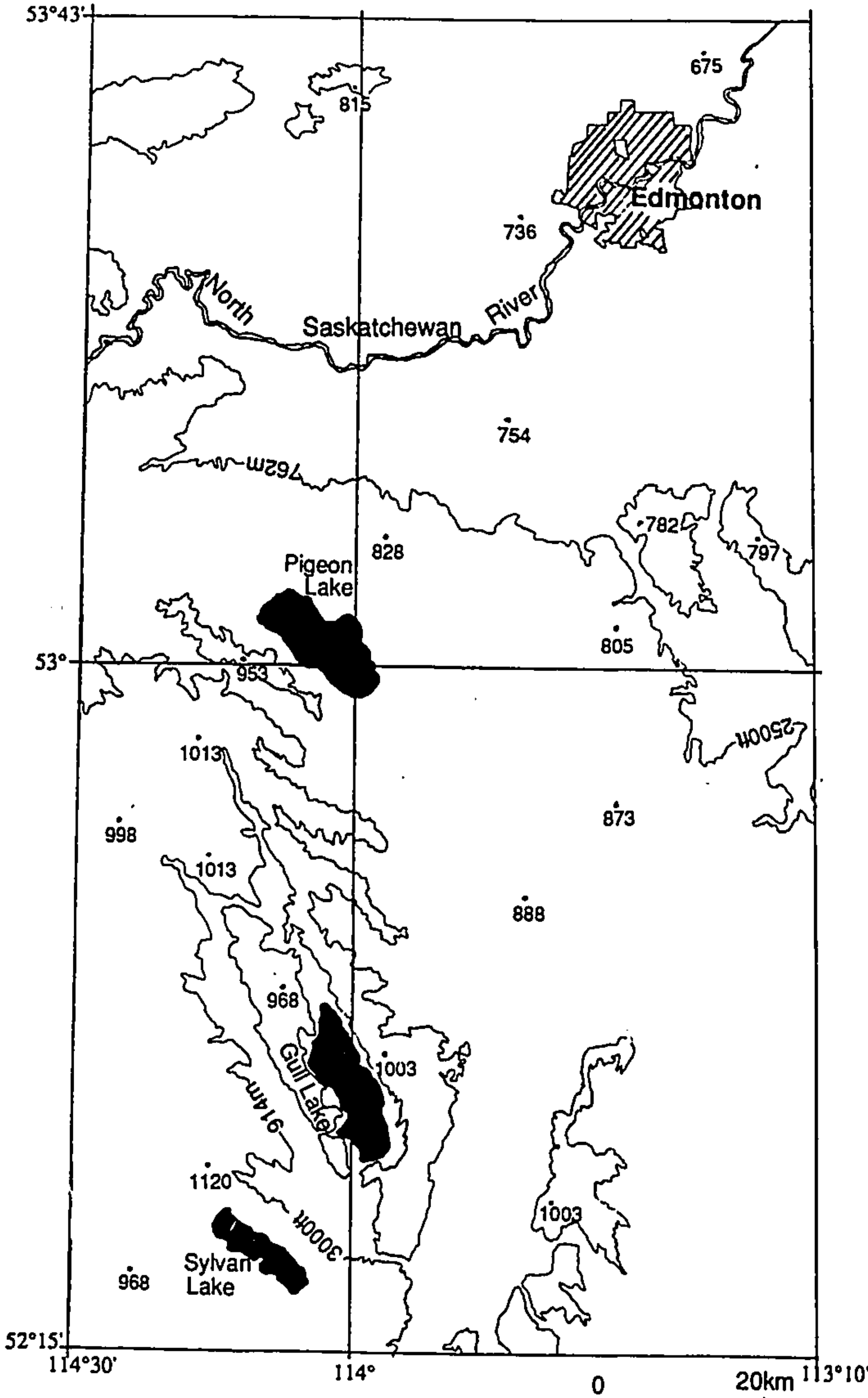

Figure 2.6 Topographic map of the study area

• 754 Elevation in meters

Chapter 3 Processing of hydrogeological data

3.1 Introduction

In any kind of study, ascertaining the validity and correctness of the database plays a significant role. It is imperative to process the raw data, using certain culling procedures, before any analysis or interpretation is done. How stringent the culling criteria are, depends on the nature of the problem at hand and on the practical feasibility and usefulness. This chapter is devoted entirely to the different types of data procured for the study and the culling criteria employed to ensure their validity and correctness.

3.2 Database

3.2.1 Permeability and Porosity data from core analyses

Lateral and vertical continuity of geologic formations play a significant role in controlling pathways for fluid flow. Recognizing continuity affects decisions related to different stages and modes of oil recovery from a reservoir. Therefore, the regional distribution of permeability and porosity which affect continuity in geologic formations, has to be carefully mapped.

It has always been a major concern for the exploration geologist to determine and map permeability and porosity with a fair degree of confidence using large amounts of data from core analysis. Particularly, permeability poses a problem due to its variable range, especially in geologic formations characterized by fractures and vugs.

Permeability can be evaluated directly from pressure-buildup curves and core analyses; and, depending on the rock type, it can be calculated indirectly from well logs (Schlumberger, 1989). Porosity can be determined from well logs and core analyses. Although there is no direct relationship between porosity and permeability (Lucia, 1986), empirical relations have often been used between values of permeability and porosity (Smith, 1971). Since, these relations are empirically derived for a given formation in a given area they do not serve general application and validity.

In the present study, core derived permeabilities and porosities provided by the Alberta Energy Resources Conservation Board (ERCB) have been used. Due to the biased nature of sampling, only the hydrocarbon producing zone, the Leduc Formation, had a large number of core analysis. Very few core analyses were recorded for the Ireton shales and the Cooking Lake Formation. Whole-core (full diameter) permeability and porosity values from 60 wells, chosen at random, in the Leduc Formation were evaluated. Even though the database was huge, the data sampling was unevenly distributed both areally and with depth.

A core analysis provides a maximum horizontal permeability k_{max}, a horizontal permeability measured orthogonally to k_{max} denoted as k_{90}, a vertical permeability k_v, porosity, grain density and oil saturation over a sampled interval. For the whole-core analysis the average sample length is 1 foot. Values of horizontal and vertical permeabilities and porosities used in this study were read from the reports provided by the ERCB. Certain reports contained the characteristic length of the sampled interval while others had only the sample interval limits. A sample length of 1 foot was assumed whenever the characteristic sampled length was not given. The reported characteristic sample length was used whenever it was recorded.

According to Cushman (1984), the core derived permeability and porosity values represent volume-averaged values corresponding to the sample size. To determine the spatial distribution of permeability and porosity, sequential scaling up of these parameters have to be performed from plug-scale (or whole-core) to well-scale and finally to the regional-scale because of the several orders of magnitude differences between the individual scales (Cushman, 1984).

During the scaling up process from the plug-scale to the well-scale it is assumed that the three-dimensional spatial distribution of core-derived permeability values are characterized by a certain randomness (Bachu and Underschultz, 1992). It is generally accepted as a tenet that variation in permeability of consolidated sediments is characterized by a lognormal distribution (Freeze, 1975). Thus, assuming a lognormal distribution for permeability, the geometric mean of the whole-core scale horizontal permeabilities (k_{max}) and vertical permeabilities (k_v) weighted over their sample thicknesses in each well is representative at the well-scale. Normal probability density function best describes the porosity distribution (Dagan, 1989). To scale up porosity from the whole-core scale to the well-scale, arithmetic mean weighted over the sample thickness was used. Table 2 shows the well-scale horizontal and vertical permeabilities and porosities for 60 wells within the Leduc Formation in the present study area. From among the 60 wells, those which fall within the boundaries of individual reefs geometric mean was used to represent the average horizontal and vertical permeabilities and arithmetic mean to represent the average porosity for that particular reef (Table 3).

No reasonable correlation between permeabilities and porosities could be obtained. This is probably because of the erratic distribution of the vugs and fractures within the extensively dolomitized Leduc Formation. The Leduc Formation has undergone complete dolomitization, mineral recrystallization and consolidation, whereby the original depositional textures have been destroyed (Andrichuk, 1958b) and secondary porosities simultaneously created.

It is not always true that permeability follows a lognormal distribution (Jensen et al., 1987). A statistical study of reservoir permeability by Jensen et al. (1987) suggested that permeability may not necessarily be log-normally distributed. In reality a range of probability density functions may represent permeability distributions in different locations and log-normal and normal distributions are simply two members in this range. Probability plots and histograms for well-scale permeabilities and porosities were generated (Figure 3.1 to 3.3).

The present study has shown that the averaged well-scale vertical permeabilities (n=57), which are scattered randomly along the Rimbey-Meadowbrook reef trend, are characterized by a log-normal distribution (Figures 3.1b, 3.3b). A set of random variables is considered to follow a normal or log-normal distribution if the

Normal Probability Plot

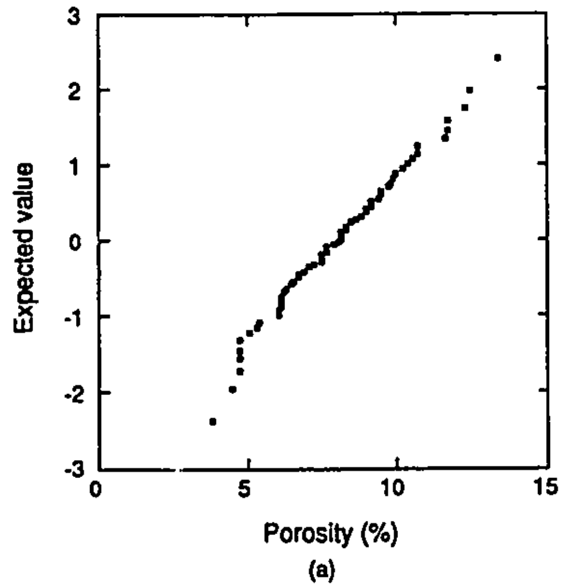

Lognormal Probability Plots

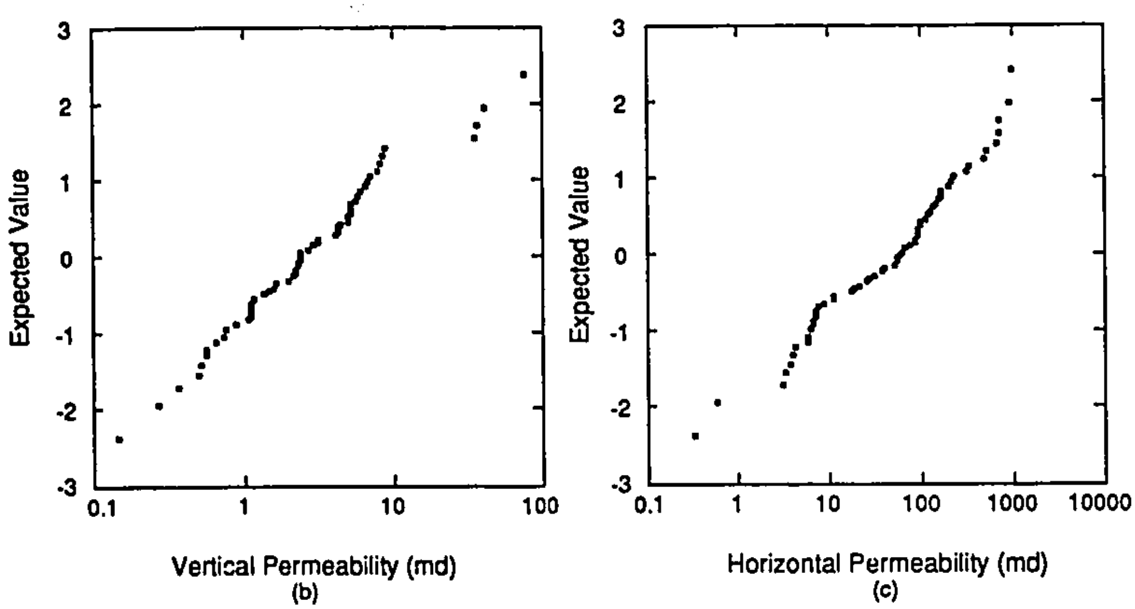

Figure 3.1 Probability plots of permeabilities and porosities from the Leduc Fm.

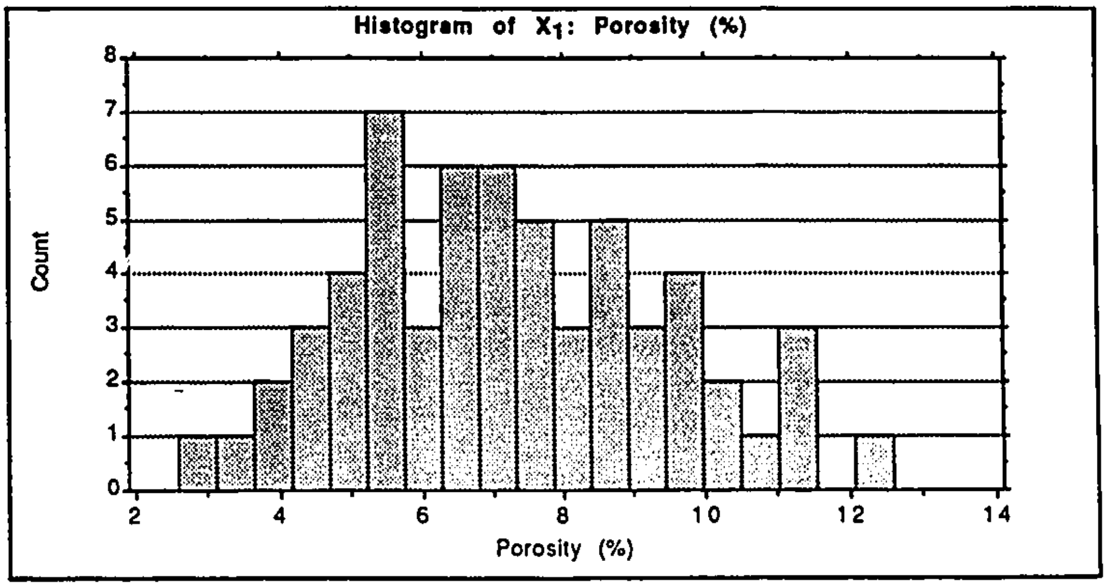

Figure 3.2 Histogram for averaged core porosities in the Leduc Formation

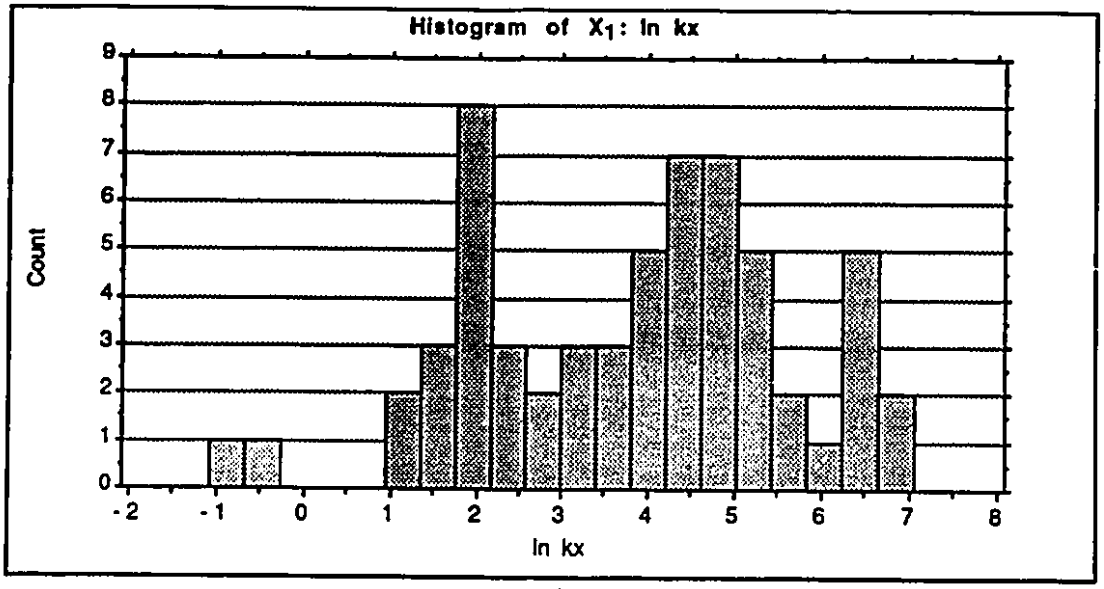

(a)

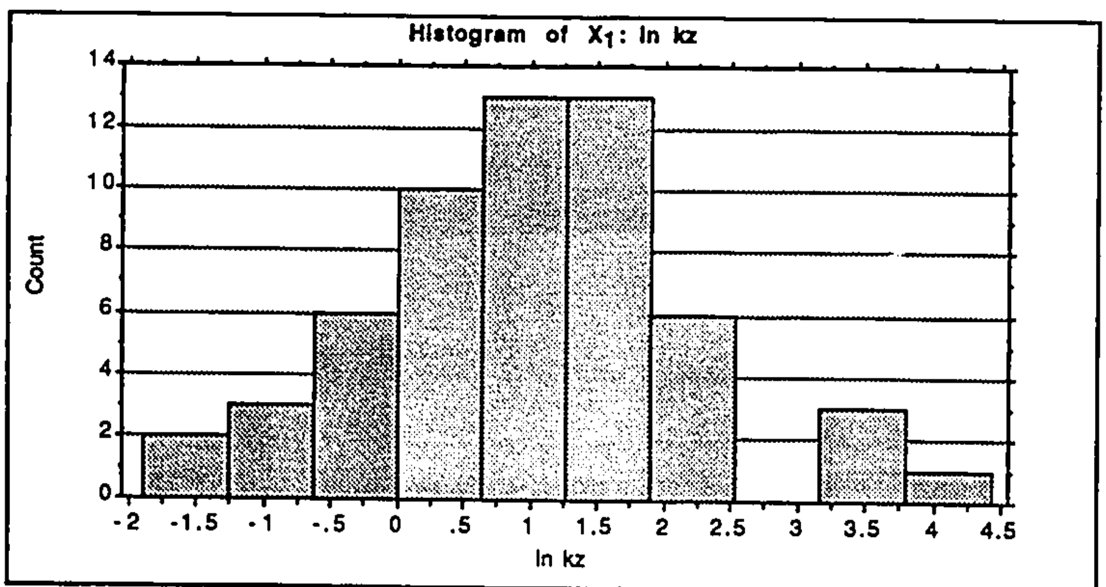

(b)

Figure 3.3 Histograms for averaged core log permeabilities in the Leduc Formation variables plot as a "more-or-less" straight line in a probability plot or show a bell-shaped curve when plotted against its frequency in a histogram. A statistical study conducted on the Westrose reef by McNamara and Wardlaw (1991) has also shown that the vertical permeability may be described by a log-normal distribution. Based on this statistical similarity in an individual Westrose reef and all the reefs together, it is assumed here that the vertical permeability in *any single reef* in this reef trend may be described by a log-normal distribution. In the present study the averaged well-scale horizontal permeability (n=60) *closely* follows log-normal distribution (Figure 3.1c) and its slight departure from lognormality is conspicuously depicted in its histogram (Figure 3.3a) where at least three populations of horizontal permeability can be recognized. Porosity, which can generally be characterized by a normal distribution shows a departure from this generalization. The histogram in Figure 3.2 illustrates that the averaged well-scale porosity (n=60) values are positively skewed (right handed tail) with a skewness of 0.3. The effect of skewness in the porosity data leads to a relatively poor linear correlation in its probability plot (Figure 3.1a); and hence, porosity, in this case, does not *strictly* follow a normal distribution. McNamara and Wardlaw (1991) have also shown in the Westrose reef, a deviation from lognormality and normality distribution for the horizontal permeability and porosity, respectively.

The horizontal permeabilities range between 0.4 - 1034md and has a variance of 27.4md. The vertical permeability, on the other hand, ranges between 0.2 - 77md and is characterized by a lower variance of 4.6md. The porosity ranges between 4 - 14% with a variance of 5%. The geometric mean of the horizontal and vertical permeabilities in Table 2 is 45md and 3md, respectively. It is noted that the mean horizontal permeability is an order of magnitude higher than the mean vertical permeability. McNamara and Wardlaw (1991) have observed that the horizontal permeability is ten times the vertical permeability in the Westrose reef. According to a study by Reitzel and Callow (1977), this relation reaches even up to fifty times in the Golden Spike reef. These differences in the permeabilities depend largely upon the averaging method employed and the inherent bias of the core measurement itself. The vertical permeability measurements may be influenced by horizontal permeability barriers which are continuous at the core scale but discontinuous at a regional scale, thereby resulting in unrealistically low vertical permeability measurements (McNamara and Wardlaw, 1991). Harmonic average results in the lowest value of the averaged variables, whereas arithmetic average provides the highest and geometric average an intermediate value.

3.2.2 Drill stem tests analyses

A drill-stem test (DST) is a temporary well completion conducted to gather information on the potential productivity of a geologic formation. Before money is invested to run casing, perform cementing and other completion operations, the commercial value of the well can be estimated by a DST. The Canadian Institute of Formation Evaluation (CIFE) is a service company specializing in DST analysis. CIFE ranks each DST with a code specifying the quality and reliability of a particular DST. Code A is the best quality DST which is mechanically sound with shut in pressures stabilized or near stabilization. Code B is a DST with near stabilizing pressures and slight mechanical difficulties which are insufficient to affect the test. Code C is a DST that has some mechanical difficulties evident on the chart, however, does not affect the pressure data. Code D is considered a questionable DST because it is not mechanically sound.

A total of 463 drill stem tests, of which 264 in the Nisku Formation and 199 in the Woodbend Group (Leduc, Ireton, Cooking Lake Fms. and their equivalents) were obtained from CIFE. Only the DST's with CIFE quality codes A, B and C were used for the Woodbend Group; whereas, DST's in the Nisku Formation included D quality also.

Differences in fluid potential drive fluid from one point to the other; which implies that the bottom-hole pressures used to compute the original, undisturbed potential field should unequivocally represent virgin or pre-production formation pressures. Further, virgin formation pressure forms the basis for subsequent hydrogeological analyses. Therefore, it is imperative that disturbed pressures that do not represent virgin conditions be removed from the database before any analyses using bottom hole pressures be done.

Horner (1951) derived the basic pressure build-up equation for a single well in an infinite reservoir as:

[1] $$p_w = p_o - 162.6\frac{Q\mu}{kb}\log\frac{t_o + \Delta t}{\Delta t} \qquad \text{........ Eq.(3.5)}$$

[1] The oil and gas industry still follow the American Imperial System of Units to express the variables in this equation. The given equation used in this form

where

p_w is the shut-in pressure (in well bore) in psi,
p_o is the reservoir (formation) pressure in psi,
Q is a constant rate of production in barrels/day,
μ is the fluid viscosity in centipoise,
k is the intrinsic formation permeability in darcy,
b is the reservoir (formation) thickness in feet,
t_o is the total flow time prior to a shut-in in minutes,
and Δt is the shut-in time in minutes.

A Horner plot is a graphical expression of Equation 3.5, where the shut-in pressures obtained from a DST are plotted against the dimensionless time ratio $\frac{t_o + \Delta t}{\Delta t}$. As Δt approaches infinity, in other words at infinite shut-in time, this ratio approaches 1. Since the logarithm of 1 equals zero the second term on the right hand side of Eq. 3.5 becomes zero yielding $p_w = p_o$. Therefore, the extrapolated or stabilized pressure from the Horner plot is considered to represent formation pressure.

All the 199 DST charts from the Woodbend Group were individually inspected for any mechanical failure/misrun, and stabilization of the shut-in pressures (buildups). If, by visual inspection of the charts, the shut-in pressure appears stable then no extrapolations were done and the stabilized pressures were accepted as formation pressures. Horner extrapolations were made for DST's in which the shut-in pressure had not stabilized. These extrapolated pressures were later incorporated into the database. If the extrapolated formation pressure was greater than the formation

---

alleviates the tedious conversion of the American to the SI units. The p_w calculated in psi can be converted into its SI unit of Pascal by multiplying psi by 6.89×10^3.

pressure provided by CIFE it was retained in the database. Using self-extrapolated and CIFE formation pressures, equivalent freshwater hydraulic heads were calculated from the relation:

$$h^* = z + \frac{p}{\rho_o g} \qquad \text{.................. Eq.(3.6)}$$

where,

h^* is the equivalent fresh water hydraulic head, z is elevation of the DST recorder, ρ_o is density of fresh water. p is stabilized formation pressure and g is acceleration due to gravity.

If the difference in the hydraulic head was <5m the extrapolated pressure was accepted. Otherwise the DST chart was rechecked for any error and omission. The extrapolated formation pressures were retained if there was no omission. This procedure is depicted in a simple logical flow chart (Figure 3.4). CIFE pressures were used only when no DST chart was available. Generally, the Horner extrapolations which were performed for DST's in the Woodbend Group yielded a stabilized pressure that accounted for a consistent difference of <10m of hydraulic head when compared to the hydraulic head obtained using CIFE's stabilized pressure. If a large contour interval is selected to construct potentiometric surface maps (contours of equal hydraulic head), a difference of <10m of hydraulic head is too small to affect the interpretation of these maps using either CIFE or my data. In this study CIFE extrapolated pressures were used for the Nisku Formation. The DST's were then divided into lithostratigraphic units comprising the

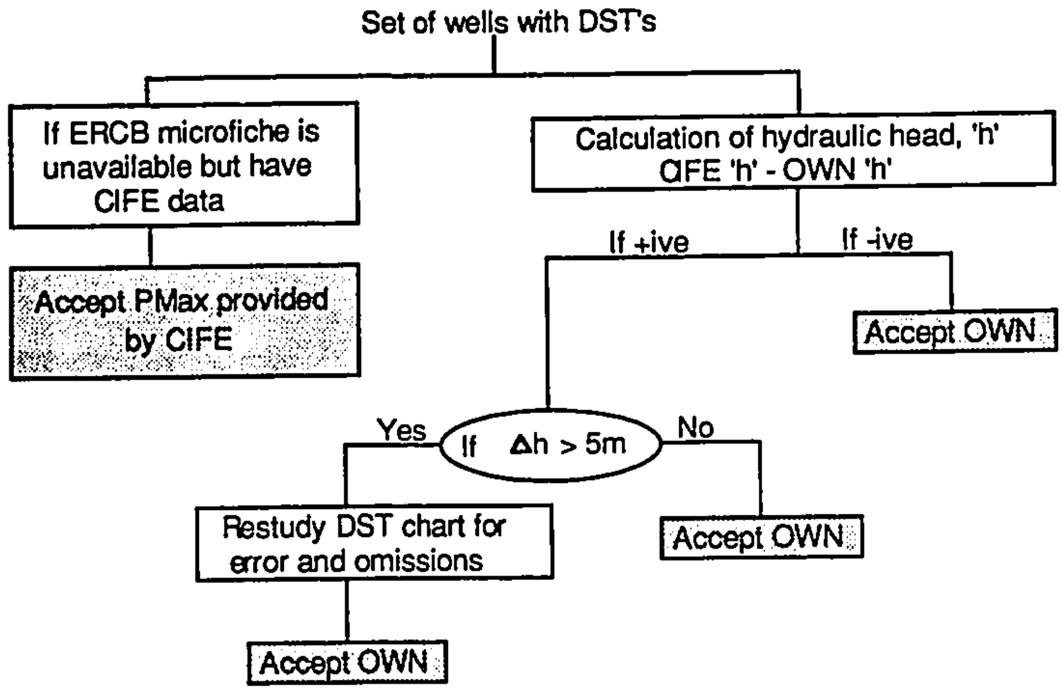

Figure 3.4 Flow chart depicting the steps undertaken to justify why stabilized formation pressures, used for computing OWN 'h', in the Leduc and Cooking Lake Formations were accepted in lieu of the CIFE 'h'

Nisku, Leduc, and Cooking Lake Formations. Because of stratigraphic equivalence, DST's in the Majeau Lake Member and Basal Reef Formation were combined with those in the Cooking Lake Formation while DST's in the Duvernay Formation were combined with those in the Leduc Formation. DST's in the Camrose Formation were grouped together with those conducted in the Nisku Formation.

The stabilized pressure obtained from a DST represents the formation pressure but it may not actually be the virgin, or undisturbed, formation pressure. Exploitation (production and/or injection) of a groundwater basin induces horizontal and vertical hydraulic gradients towards a well causing a decline/increase in the hydraulic heads in the aquifer (formation) around a well. Using the Jacob semilog method (Freeze and Cherry, 1979), production induced drawdown (s) can be computed as:

$$s = \frac{2.3Q}{4\pi T} \log \left(\frac{2.25Tt}{r^2S}\right) \qquad \text{............. Eq. (3.7)}$$

where

Q is the constant pumping rate in m^3/s,
T is the transmissivity in m^2/s,
t is the time elapsed since production started in seconds,
r is the distance between the production well and observation well in metres,
and S is the storativity.

From the above equation if Q, T, and S are assumed constant, production induced drawdown will depend on the distance 'r' and time 't'. Therefore, a comparison of the initial date of production to the DST date and the distance between the production and DST well should indicate whether a DST pressure measurement is disturbed or not.

Pressure-depth plots were made for the Nisku (Figure 3.5a), Leduc (Figure 3.6a) and Cooking Lake Formations (Figure 3.7a) using unculled DST pressure measurements. The majority of the data plot below the fresh water hydrostatic gradient, which indicates general (regional) underpressuring within individual formations (Tóth, 1978,1979). The unculled pressure measurements were also used to construct preliminary potentiometric surface maps of equivalent freshwater heads which revealed closed potentiometric lows aligned along the reef trend. The underpressuring indicated by both sub-hydrostatic pressure-depth plots and these closed potentiometric lows is undoubtably partly due to petroleum production. The reefs are prolific hydrocarbon reservoirs where production has continued since 1947.The Leduc-Woodbend was the first reef to start producing. The use of pressure-depth plots in conjunction with potentiometric surface plots to check the reliability of DST's and bottom hole pressures was applied by Akhter and Kreitler (1990). Production in most of the reefs other than Leduc-Woodbend had started by early 1950. In regions of such extensive production a stringent culling procedure must be adopted for proper interpretation of the fluid flow field.

To undertake this task, production/injection histories for all wells from the Leduc (D-3 pools) and Nisku (D-2 pools) Formations were obtained from the PUBCO CD-ROM (PUBCO, 1990). Pertinent data include the initial date, total hours and final date of production

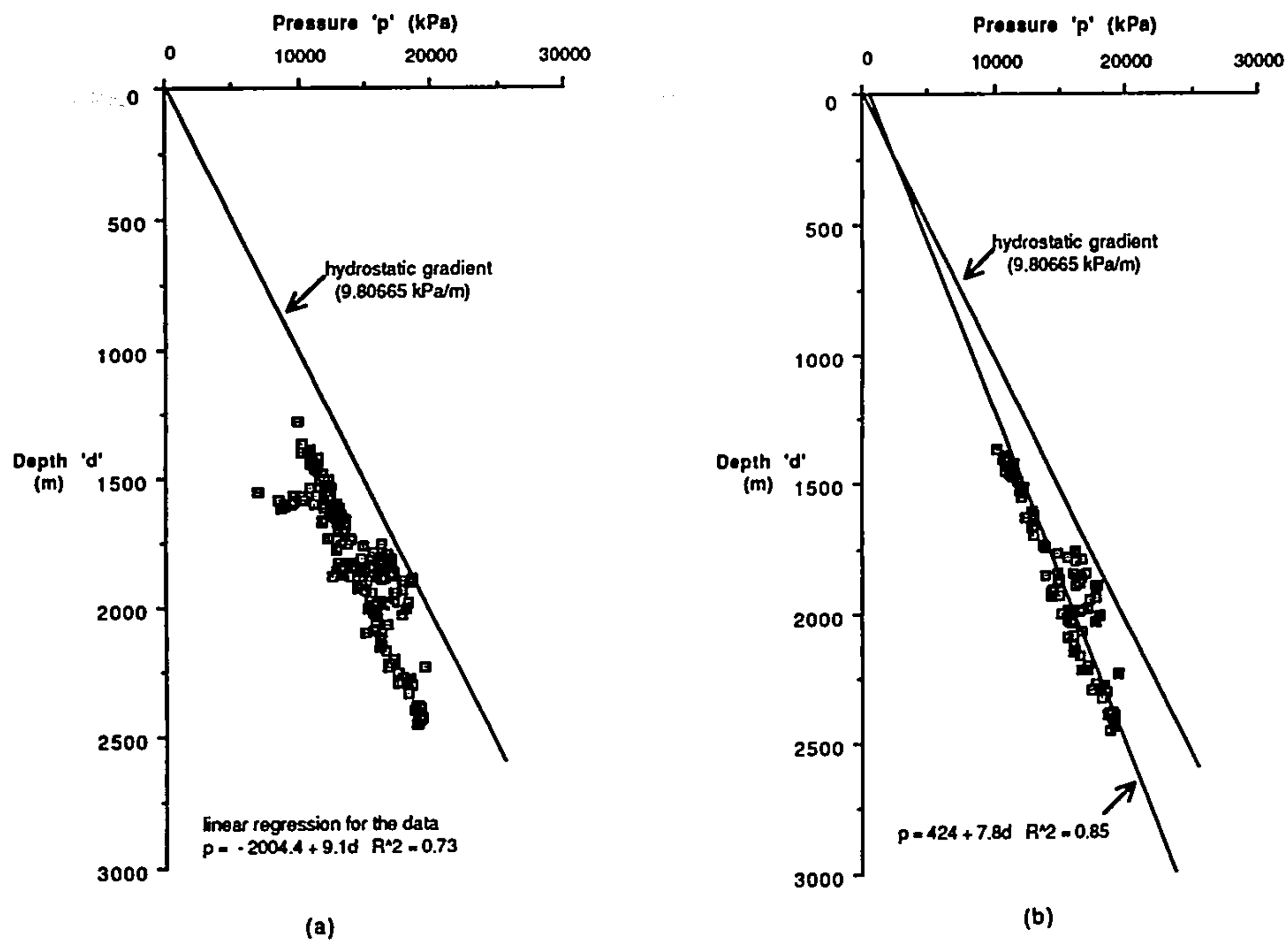

p(d) plot for Nisku (D-2) Fm. [unculled]

p(d) plot for Nisku (D-2) Fm. [culled]

Figure 3.5 Pressure-depth [p(d)] plots (unculled and culled) for the Nisku Formation

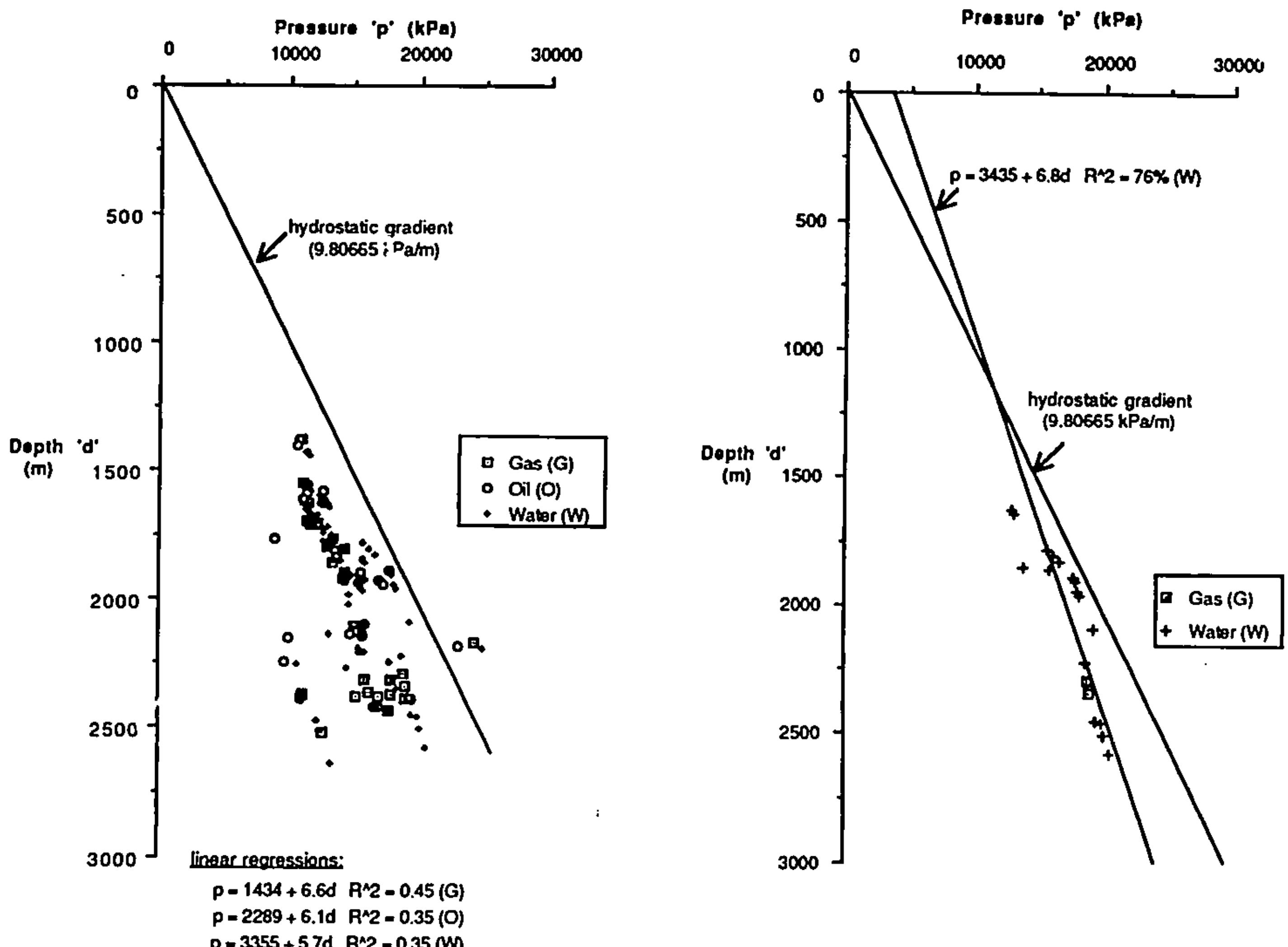

(a)
p(d) plot for Leduc(D-3) Fm. [unculled]

(b)
p(d) plot for Leduc (D-3) Fm. (culled)

Figure 3.6 Pressure-depth [p(d)] plots (unculled and culled) for the Leduc Formation

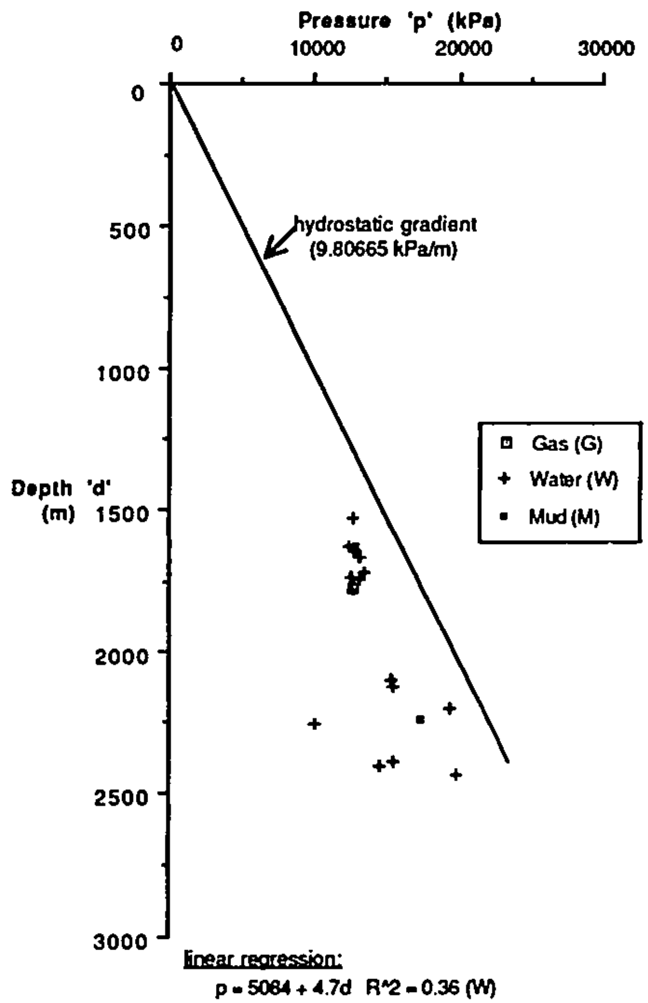

(a)

p(d) plot for Cooking Lake Fm. [unculled]

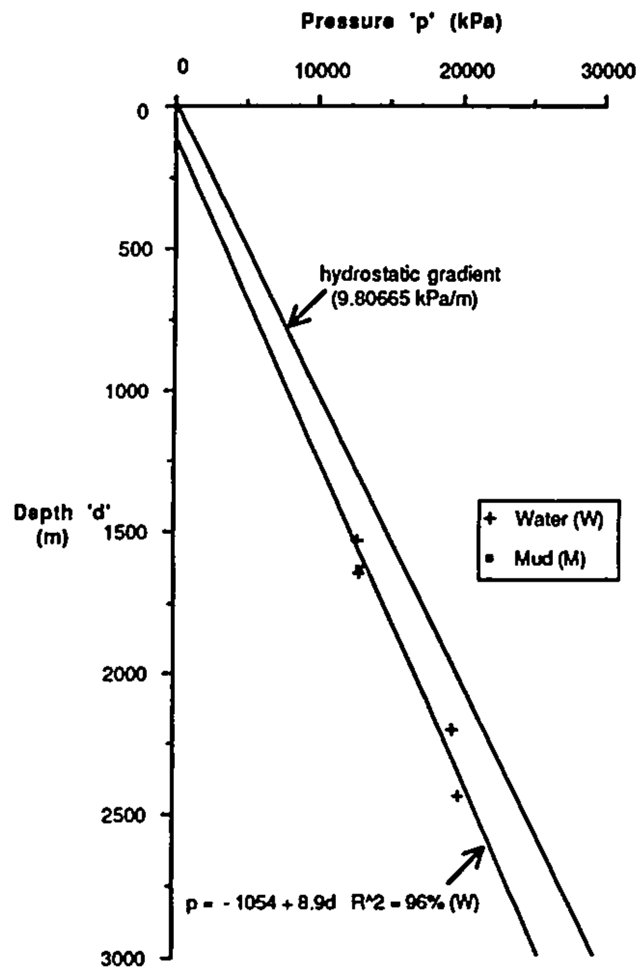

(b)

p(d) plot for Cooking Lake Fm. [culled]

Figure 3.7 Pressure-depth [p(d)] plots (unculled and culled) for the Cooking Lake Formation and/or injection, plus the cumulative volumes of gas, oil, water produced. Figures 3.8 and 3.9 show the distribution of the production and/or injection wells within D-2 and D-3 pools in the study area. Comparison of the DST pressure measurement date and the initial date of production within or between wells in a particular pool (D-2 or D-3) was the major criterion that was employed for culling production induced drawdowns. The two-stage manual culling procedure adopted in the present study is described below: *(note: D-2 and D-3 DST's were culled independently)*

(1) The first step was to cull DST's which were affected by prior production and/or injection in the DST well. Any DST that postdated initial production and/or injection in the same well was rejected. The second step was to evaluate if production and/or injection from nearby wells may have influenced a DST pressure measurement.

(2) The retained DST's were again scrutinized individually on the basis of their DST dates. Each DST date was compared with the initial date of production in wells that were present within the same and neighboring sections as the DST well. Again, if there was any production that predated a DST, that DST was removed from the database. Most of the DST's rejected were eliminated at this stage of culling. The DST's which passed this stage were retained for further "in depth inspection".

(3) Thus far, comparison of the DST and production (and/or injection) dates in wells were considered on a one to one basis. In fact however, drawdown effects are cumulative. Production wells

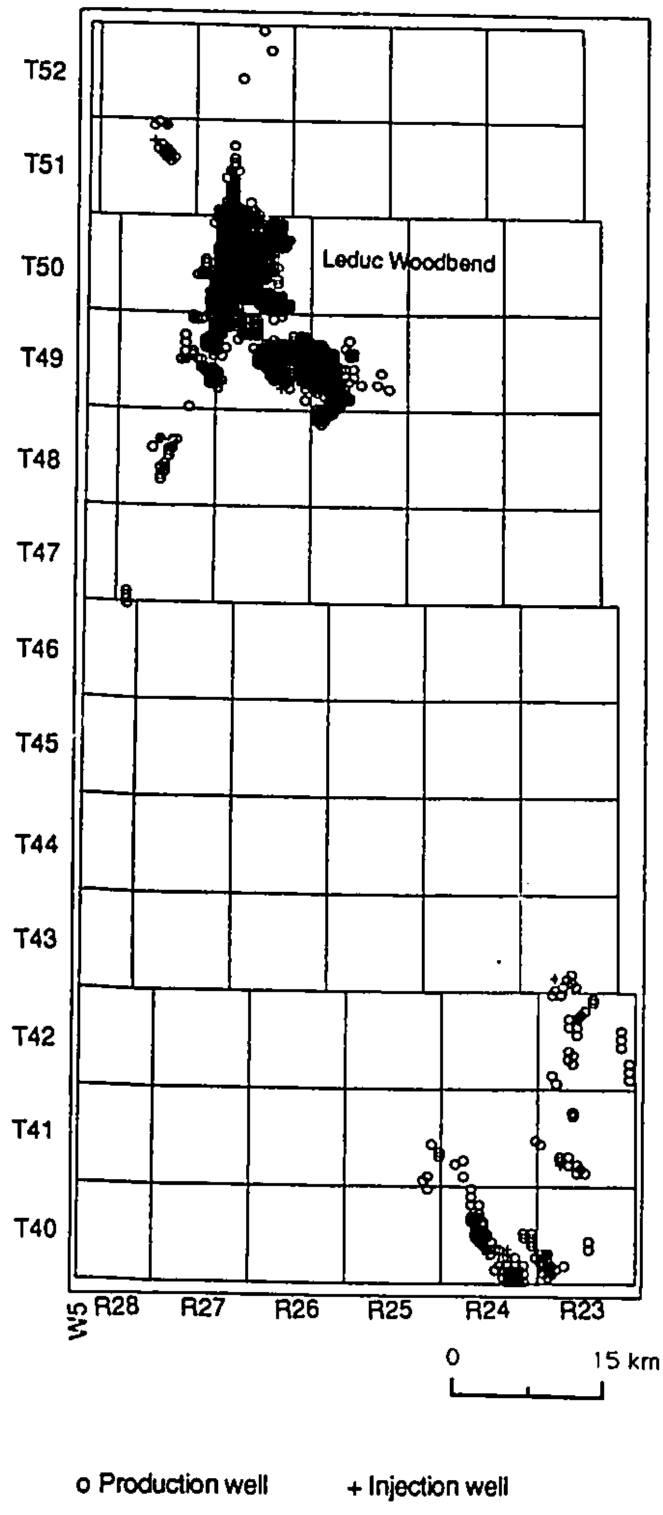

Figure 3.8 Production and injection wells in the Nisku (D-2) Formation.
High density of production wells in the Leduc-Woodbend field.

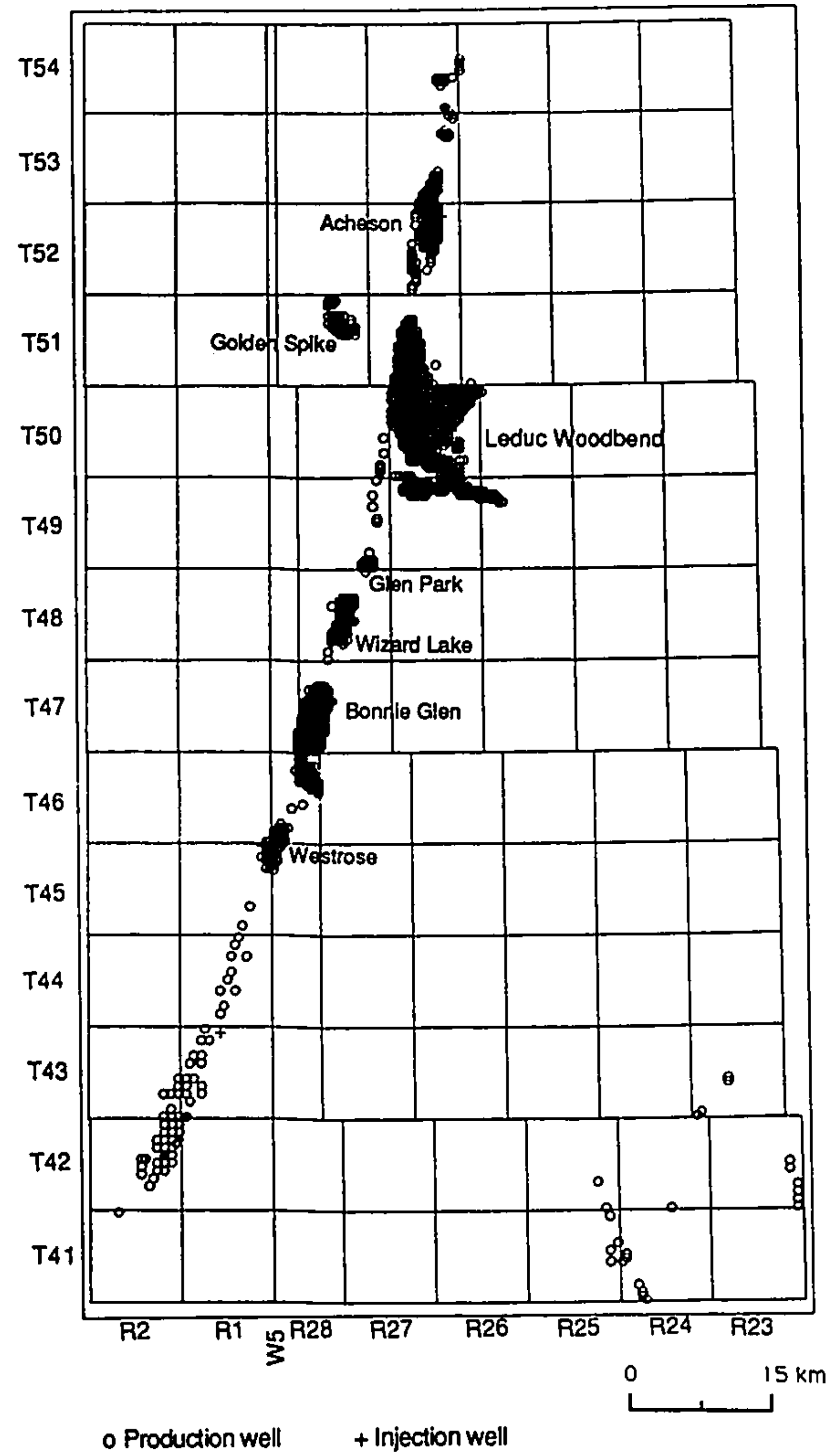

Figure 3.9 Production and injection wells in the Leduc (D-3) Formation
High density of production wells in Acheson, Golden Spike, Leduc-Woodbend, Glen Park, Wizard Lake, Bonnie Glen and Westrose reefs.

extract fluid from an aquifer. This reduces the hydraulic head locally, creating a depression on the potentiometric surface known as the cone of depression. Injection wells have an opposite effect creating a cone of impression. In an aquifer of constant transmissivity and storativity, the magnitude of the cone of depression around any single production well is directly proportional to the pumping rate and the pumping interval. Where production wells are closely spaced, their individual cones of depressions may overlap. Drawdowns within the zone of overlap are cumulative. Increasing the number of producing wells will therefore increase the drawdown at DST wells which are affected by multiple cones of depression. Individual DST dates for wells from Stage 2 were compared (as described previously) with the dates of producing (and/or injecting) wells active for more than ~30 yrs. within an increased zone of influence (approx. 10km radius). A DST was discarded if more than one production and/or injection well in this increased zone of influence was active long before the DST date.

Those DST's which passed all the above stages can be considered to be unaffected by production-induced drawdown and, therefore, safe for interpretative purposes. Tóth and Corbet (1986) used a culling criterion based on the value of log $\frac{t}{r^2}$ which they called the interference index (IN); where, r is the distance between a DST and a production well, and t is the production interval in years. All production and/or injection wells within a 4.8km radial distance of the DST well were considered. Tóth and Corbet used IN=0.7 as the threshold value of IN above which production induced drawdown affects were likely. In the present study IN values were calculated at two different stages - before and after the final stage of the culling procedure. It was found that the IN calculated for the DST's that passed the final stage of culling yielded an IN<0.7. However, for DST's not subjected to the final culling the IN varied around the threshold value. This implies that numerous DST's which were actually production affected would have been accepted as valid using Tóth and Corbet's threshold. Tóth and Corbet's IN failed because the cumulative drawdown induced by multiple production wells was never examined by them.

After every stage of culling the coefficient of determination (R^2) from the pressure-depth plots of the residual data improved. The final pressure-depth plot for the culled DST's in Nisku, Leduc and Cooking Lake Formations are provided in Figures 3.5b, 3.6b and 3.7b. Eventually, only 91 DST's in Nisku Fm. and 24 out of 199 in the Woodbend Group (19 in Leduc Fm., 5 in Cooking Lake Fm.) were used in this study. A list of these DST's are provided in Tables 4 to 6.

3.2.3 Formation water chemistry

The primary objective for considering formation-water chemistry in the present study was to discern possible patterns in the waters' chemical composition that may be causally linked with the hydrodynamics. Further, the fluid flow field may itself be affected by gravitational and buoyant forces related to variations in the density of formation waters in a dipping aquifer. It then becomes imperative to study the water chemistry because fluid density is a function of salinity and temperature.

Major ion analyses of formation water samples routinely recovered from drill-stem or production tests in oil wells form the basic data used in this section. Extreme care has to be taken before interpreting these water analyses because the water samples retrieved are often contaminated, usually by drilling mud, acid or fluids from other strata.

The formation water analyses in the study area were obtained on microfiche from the ERCB. Water samples obtained from the wellhead, after the well has produced for a while, are usually considered to be representative of the formation waters. These samples are less likely to be contaminated than samples from separators or tanks (Johnston, 1988). Therefore, production samples from wellheads were preferred. When wellhead water samples were unavailable, the next best samples are those taken from the separator (Johnston, 1988). If a water sample is obtained from a DST recovery, the location of the sample point is important. Mud contamination is usually less in a bottom sample than in samples from the top or middle of a DST recovery. The top sample is often pure mud filtrate because it is the first fluid to enter the drill collar when the drill-stem is opened; the middle sample is usually a mixture and the bottom sample is supposed to be formation water.

The following criteria were also considered before accepting any water analyses as being representative formation waters.

(1) Water analyses with a pH below 6 or above 8 were considered acid and mud contaminated respectively, and were discarded .

(2) If the DST recovery was solely mud then that water analysis was not used at all. Unless a water dominated DST recovery was obtained, the analysis was discarded.

(3) Mud filtrates are commonly solutions of NaOH, $NaHCO_3$ and/or $BaSO_4$. The average total dissolved solids content of mud filtrates is 3500 mg/l. Like most formation waters, mud filtrates show a high proportion of Na^+, the predominant anion of mud filtrate however is SO_4^{2-} whereas Cl^- dominates in formation waters. Thus, whenever a high concentration of SO_4^{2-} was observed, that analysis was further checked with respect to other enlisted criteria before accepting or discarding it. In addition, mud filtrates tend to show a high concentration of CO_3^{2-}. For water at 25°C, CO_3^{2-} will be found in solution only if the pH is greater than 8.3. The pH of mud filtrate is generally in the range of 8.5 to 9.0. The presence of any amount of CO_3^{2-} was therefore regarded as an indication of mud contamination.

(4) The final criterion (loosely implemented) related to the total dissolved solids (TDS) content. Most formation water samples in the study area exhibit a TDS content in the range of hundreds of grams per liter. A water analysis with a TDS which was an order of magnitude less was still accepted if it satisfied the first criterion ($6<pH<8$). This is because I did not want to exclude the possibility of any mixing from other relatively fresh water bearing geologic

units. On the other hand, the analysis was rejected if apart from having a low TDS the SO_4^{2-} concentration was higher than Cl^-. In such cases the water analysis most likely represented a mud filtrate.

The concentration of ions analyzed in water analysis may be plotted for graphical representations. Stiff diagram is one such graphical representation in which the major cation and anion concentrations, in milliequivalents per liter, are plotted to the left and right of a vertical line at zero concentration, respectively. In this study, stiff diagrams were generated for a quick graphical comparison of the individual water analyses in the Nisku, Leduc and Cooking Lake Formations. A distinctive graphical shape of the representative water for each of these geologic formations could be established. The Stiff diagrams facilitated recognition of any anomalous or misreported ionic concentration.

Once the water analyses had been culled, linear correlation between water density and the total dissolved solids in each of the Nisku, Leduc and Cooking Lake Formations (Figure 3.10) was examined. As expected, excellent linear correlations ($R^2 \approx$ 0.8-0.9) were obtained. The relation in each of the formations may be used to estimate either the density or TDS, provided one of the variables is known. In addition, the plots helped to identify any misreported density or TDS value in a given water analysis.

Plots between total dissolved solids and the depth of the sample point were constructed for the Nisku, Leduc and Cooking Lake Formations (Figure 3.11). The relatively shallow Nisku Formation waters have the lowest average salinity (TDS) followed by Cooking Lake and Leduc Formations. In the Nisku Formation the TDS

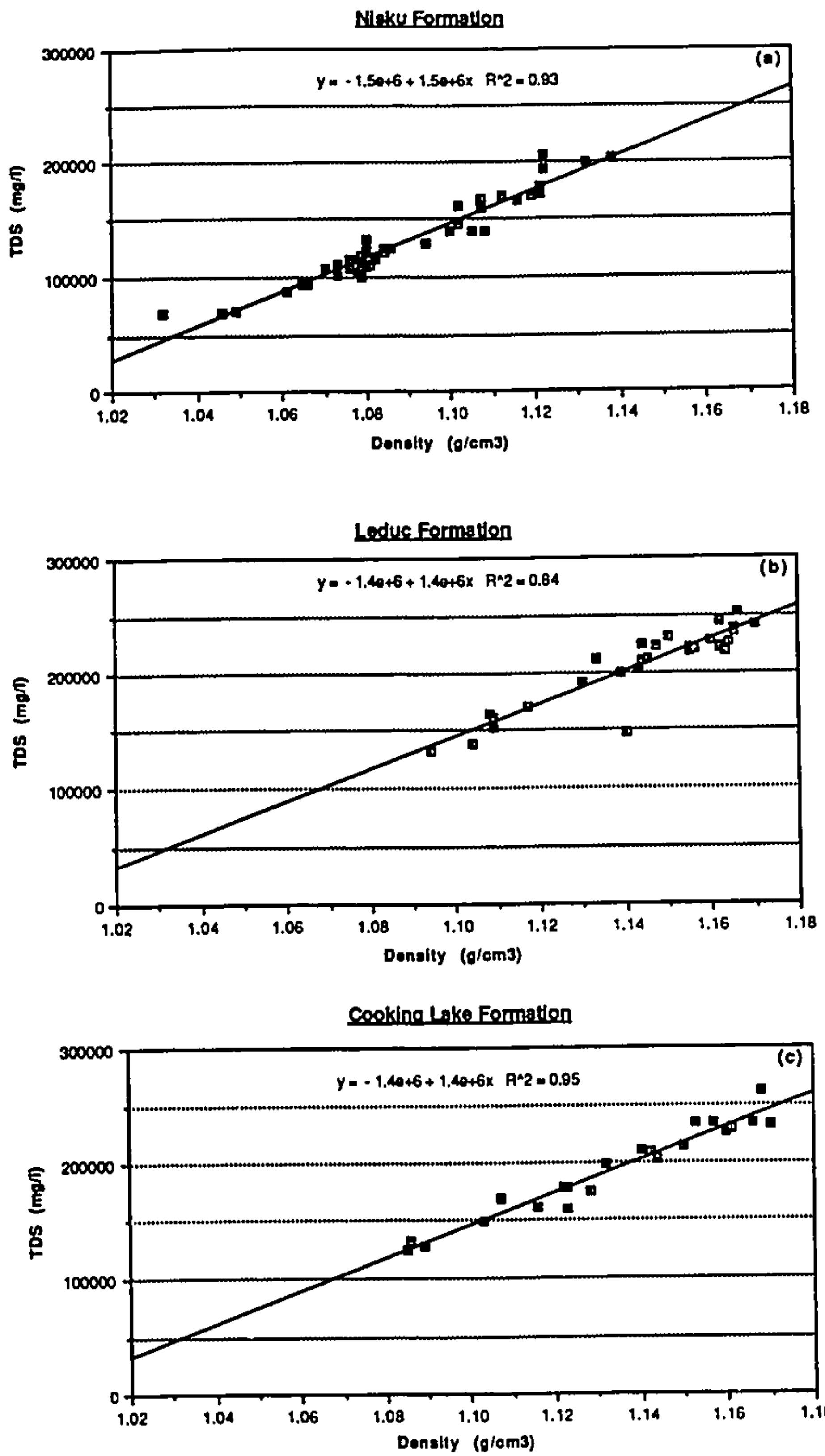

Figure 3.10 Relationship of salinity (TDS) to density of formation waters

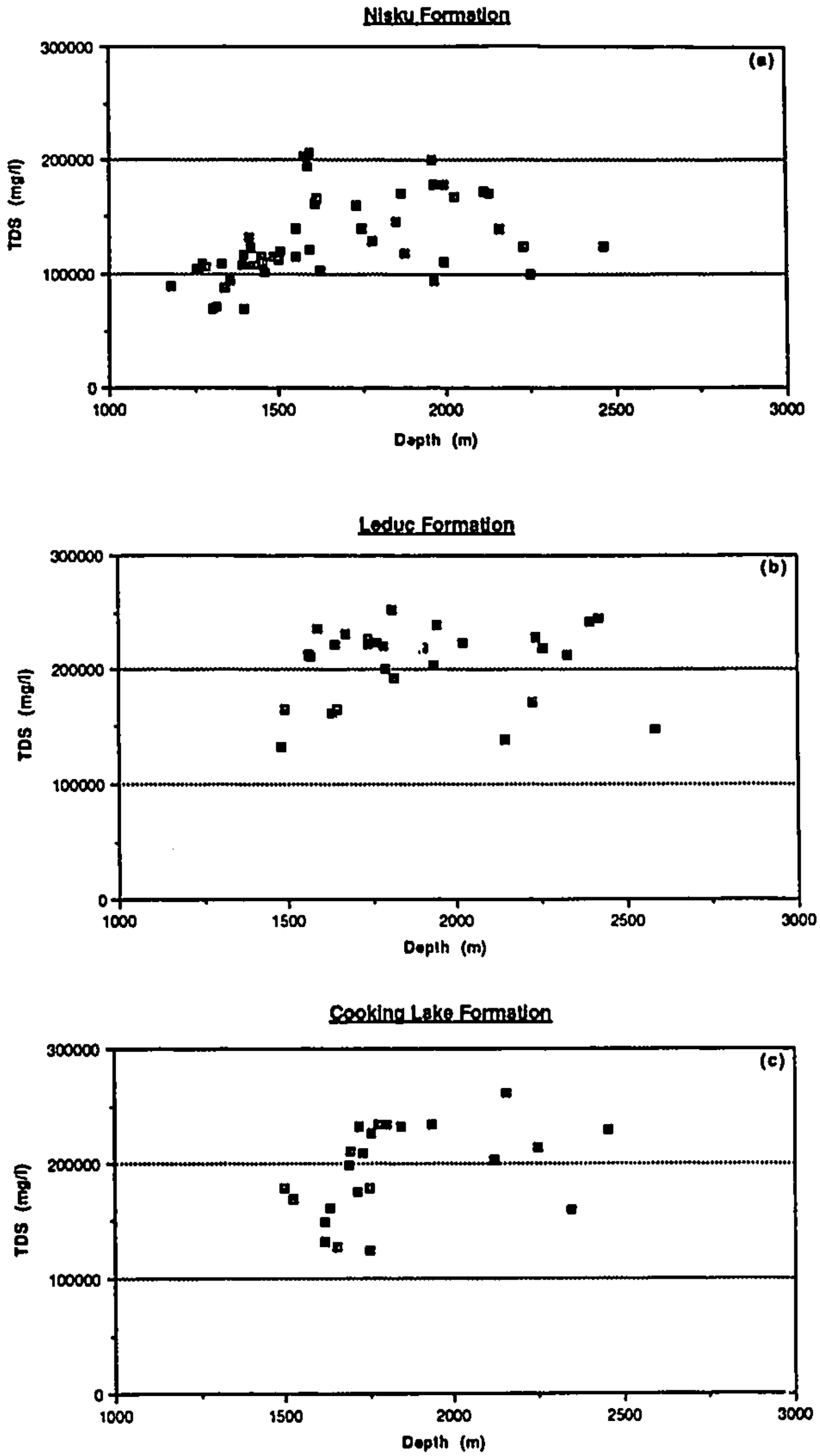

Figure 3.11 Scatter plots of salinity (TDS) vs. depth for formation waters

values range between 10^5 - $2x10^5$mg/l. Most waters in the Leduc Formation are more than $2x10^5$mg/l but less than $3x10^5$mg/l; and in the Cooking Lake Formation the TDS varies over a relatively greater range between 10^5 - $3x10^5$mg/l.

In Table 7, for each of the formations, the average interval density and computed vertical pressure gradient were tabulated which was subsequently used to assess the nominal hydrostatic gradient for interpreting the pressure-depth plots.

Chapter 4 Hydrogeological Analyses and Discussions

4.1 Introduction

The task of hydrogeological analyses would require validity and correctness of the database. The database set up in the previous chapter has been utilized to perform hydrogeological analyses within the study area.

The average well-scale permeabilities and porosities for the Leduc Formation provided the regional distribution of these hydraulic parameters. Permeability data was also employed for fluid flux (or flow intensity) calculations. The distribution of fluid potentials expressed in the form of equivalent fresh water (ρ_0=1000kg/m^3) heads were used to construct potentiometric surface maps (equivalent freshwater head) for the Leduc and Cooking Lake Formations and for the Nisku Formation. Potentiometric surface map analysis for lateral flow and pressure-depth analysis for vertical (or cross-formational) flow served as two vital hydrogeological tools to characterize the flow field.

The chemistry of groundwater may change both spatially and temporally along its flow path because of a variety of geochemical processes. Chebotarev (1955) concluded that groundwater tends to evolve chemically towards the composition of seawater and the dominant anions often exhibit a systematic change along the flow path. Trends in the distribution of various ion concentrations and of the total dissolved solids content of groundwater may aid in establishing flow directions which are established primarily from the fluid potential distribution.

4.2 Regional distribution of permeability and porosity in the Leduc Formation

Core analyses from 60 wells in the Leduc Formation along the Rimbey-Meadowbrook reef trend were used for the permeability and porosity studies (Figure 4.1). Values of horizontal permeability (k_x), vertical permeability (k_z) and porosity (ϕ) at each well were used for characterizing the regional distribution of these parameters (Figures 4.2, 4.3 and 4.4).

Figure 4.2 indicates that Big Lake, Acheson, Glen Park, Wizard Lake and Bonnie Glen reefs are characterized by relatively higher horizontal permeabilities in the order of 10^2 - 10^3 md as compared to the rest of the reefs. Among the reefs, Leduc-Woodbend and Wizard Lake reefs show the highest average vertical permeability in the range of 5 - 10 md (Figure 4.3). In the same figure, anomalously high vertical permeabilities of 37.4 and 76.4 md noted in the Leduc-Woodbend reef may accentuate vertical fluid flow within the reef. In the reef trend, Big Lake, Acheson, Wizard Lake and Bonnie Glen are the only reefs characterized by an average porosity greater than 9% (Figure 4.4). The southeast corner of the Leduc-Woodbend reef exhibits the highest porosity and permeability values obtained for the reef.

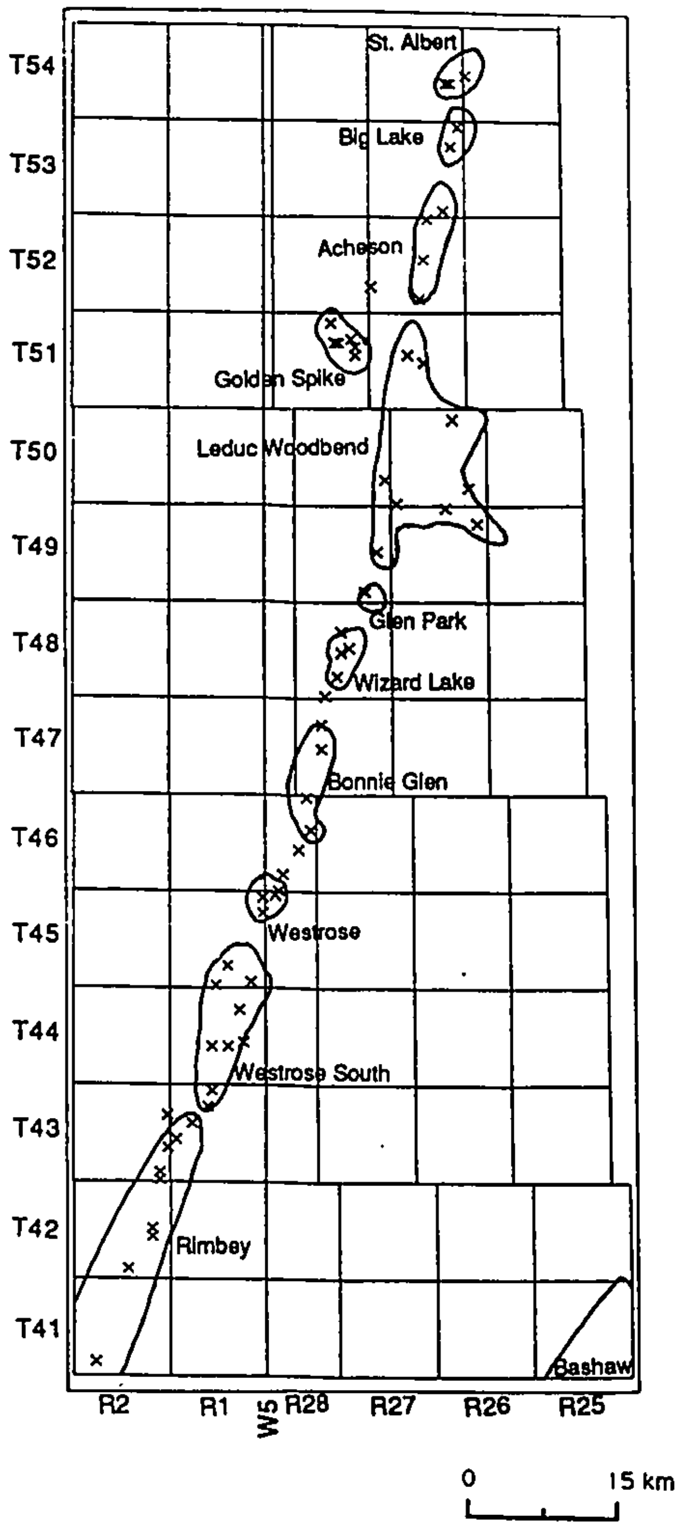

Figure 4.1 Well locations for core analyses
(with outline of the Leduc reefs)

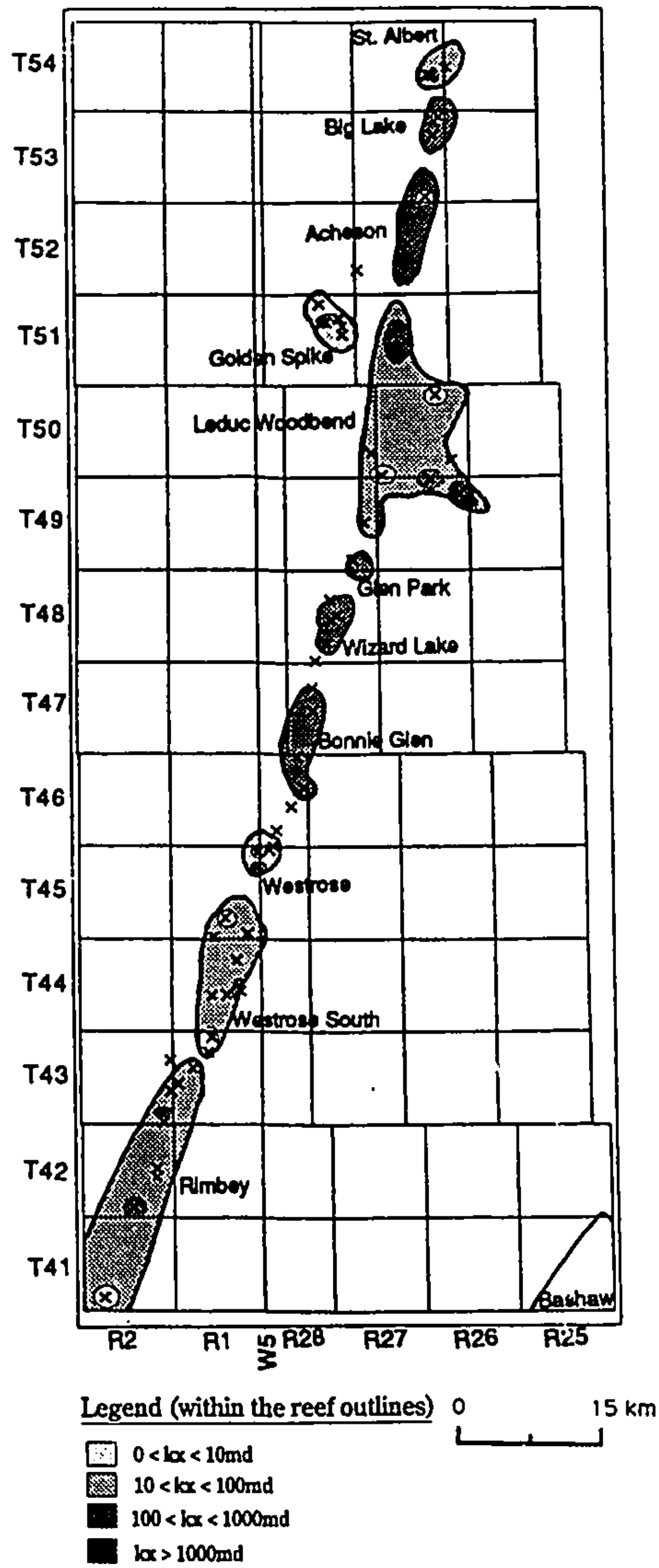

Figure 4.2 Well-scale horizontal permeability (k_x) distribution in the Leduc Formation

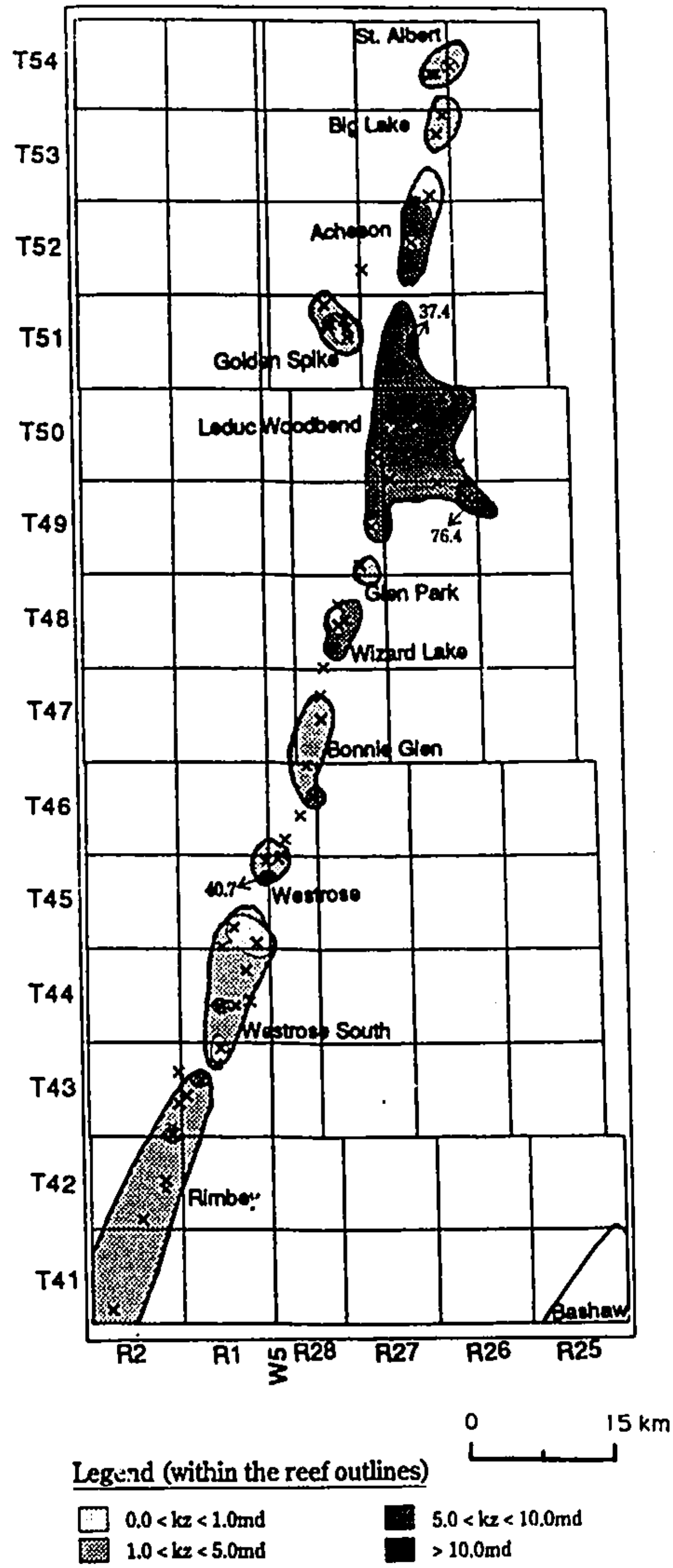

Figure 4.3 Well-scale vertical permeability (k_z) distribution in the Leduc Formation

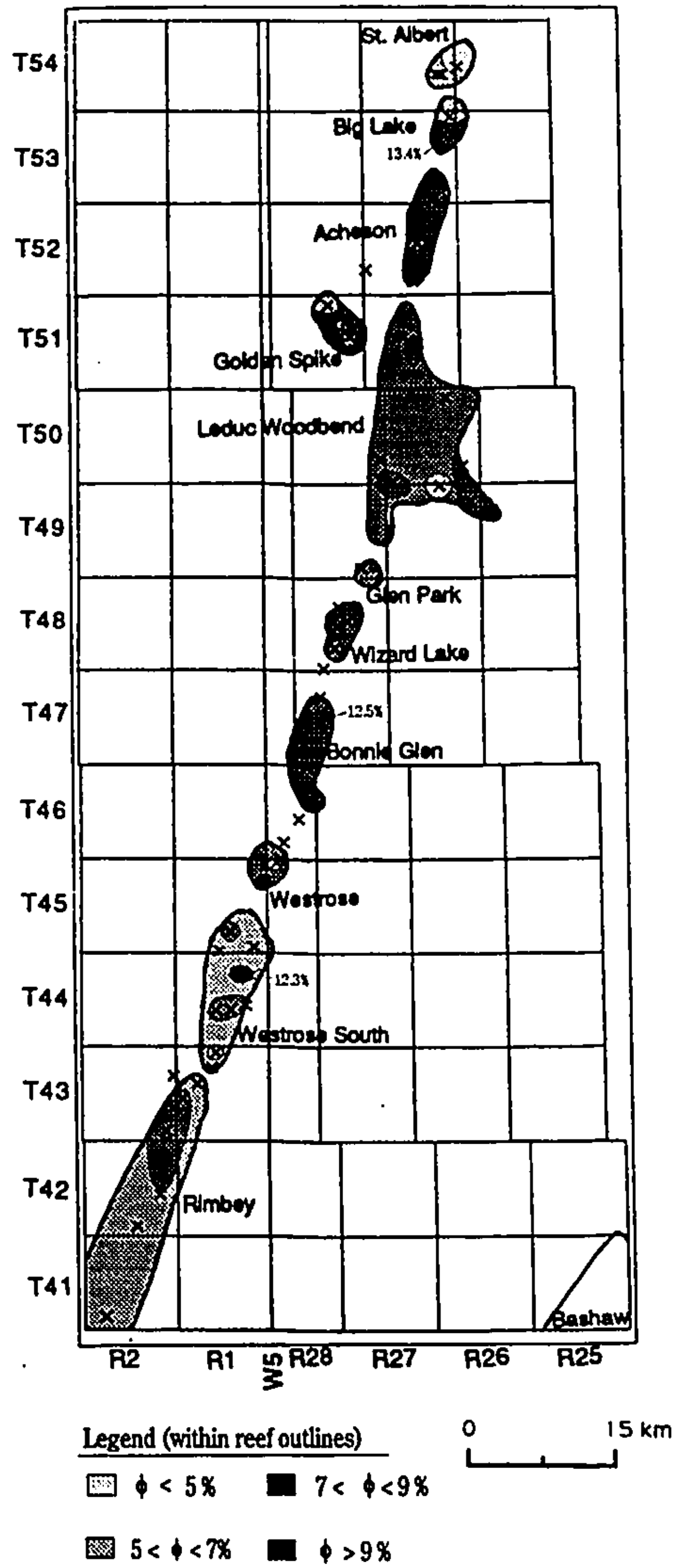

Figure 4.4 Well-scale porosity (ϕ) distribution in the Leduc Formation

4.3 Fluid flow patterns and its distribution

Fluid flow through a porous medium is a mechanical process and the direction of flow is governed by the potential gradient. Fluid flows from regions of higher to regions of lower fluid potential, regardless of the direction in space (Hubbert, 1940). The fluid potential,'Φ', (mechanical energy per unit mass of fluid) can be computed using its direct relationship to the hydraulic head,'h'

$$\Phi = gh \qquad \text{........................ Eq.(4.1)}$$

where, g is acceleration due to gravity.

The general Darcy equation for density-dependent flow is, according to Bear (1972) and de Marsily (1986)

$$q_i = -\frac{k_{ij}}{\mu} (\nabla p + \rho g \nabla z) \qquad \text{............................ Eq. (4.2)}$$

where,

q_i is fluid flux in the i-direction, $[LT^{-1}]$
k_{ij} is the permeability tensor, $[L^2]$
μ is the dynamic viscosity of the fluid, $[ML^{-1}T^{-1}]$
ρ is the density of the fluid, $[ML^{-3}]$
p is the formation pressure, $[ML^{-1}T^{-2}]$

and $\nabla z=1$ indicates the vertical direction while $\nabla z=0$ indicates the horizontal direction.

Note: Einstein's summation convention (or the double-index summation convention) is implied, and. i,j, = 1,2,3, or x,y,z, or x_1,y_1,z_1

Substituting, Eq. 3.6 into Eq. 4.2 and simplifying gives

$$q_i = -\frac{k_{ij}\rho_o g}{\mu} \left\{ \nabla h^* + \nabla z\left(\frac{\rho}{\rho_o} - 1\right) \right\}$$

or, $q_i = - K_{i,j} \{ \nabla h^* + \rho_r \nabla z \}$ .... Eq. (4.3)

where, ρ_r = relative density = $\frac{\rho}{\rho_o} - 1$

and $K_{i,j}$ = hydraulic conductivity = $\frac{k_{ij} \rho_o g}{\mu}$

Equation 4.3 is the Darcy equation in terms of equivalent fresh water head. This equation was used to calculate the fluid fluxes described in Appendix II.

In the present study, fresh water (ρ_o=1000kg/m^3) heads determined using Eq. 3.6 were used for interpreting lateral flow with the aid of potentiometric surface map analysis. Any interpretation of vertical flow, however, was based on the dynamic pressure increment estimated from pressure-depth 'p(d)' plots (Tóth, 1978, 1979).

4.3.1 Potentiometric surface maps

4.3.1.1 Theory

The concept of the potentiometric surface is strictly valid for horizontal flow in a horizontal aquifer (Freeze and Cherry, 1979). A two dimensional vertical projection of the elevation contours of this surface on a horizontal plane provides the most common hydrogeological tool, the potentiometric surface map. This map should be constructed separately for each hydrostratigraphic unit by contouring hydraulic heads that are computed using a constant fluid density.

The structural slope of the Cooking Lake Formation between townships 41-54 is very low (≈0.4°). The Cooking Lake Formation can, therefore, be considered approximately horizontal within the study area. Potentiometric surface maps have been constructed separately for the Leduc and Cooking Lake Formations and the Nisku Formation. No substantial spatial variation in fluid density gradient is observed within any of these formations, so density-related gravity effects are very small. A constant density fluid used for hydraulic head computation should, therefore, effectively characterize the flow. These two facts support the validity of the potentiometric surface maps that have been constructed.

However, should density-related gravity effects be significant Davies (1987) defined a dimensionless Driving-Force Ratio (DFR)

$$DFR = \frac{\Delta\rho \left|\nabla E\right|}{\rho_o \left|\nabla h^*\right|} \quad \text{.......................} \quad Eq.(4.4)$$

where $\Delta\rho$ is the fluid density difference in the aquifer, ρ_o is the density of fresh water, and $\left|\nabla E\right|$ and $\left|\nabla h^*\right|$ are the elevation gradient (i.e., aquifer slope) and the gradient of fresh water hydraulic head, respectively. Davies showed by numerical methods that DFR=0.5 is an approximate threshold at which density-related gravity effects may become significant. Using Table 7, the average formation water densities in the Leduc-Woodbend reef around Tp. 50 R26W4 and in the Rimbey reef around Tp.42 R2W5 were 1.150 and 1.162g/cm^3, respectively. Therefore, $\Delta\rho$ equals 0.012g/cm^3. A hydraulic gradient of $\nabla h^*=6.67\times10^{-4}$ is obtained using a hydraulic head difference of 50m over a 75km distance between the Leduc-Woodbend and Rimbey reefs (Figure 4.5). The slope of the Cooking Lake Formation represents the aquifer slope, ∇E which equals the tangent of 0.4° in this case. Having known all the variables in Equation 4.4, the DFR estimated between the Rimbey and Leduc-Woodbend reefs is 0.13. Because the estimated DFR < 0.5, density-related gravity effects on fluid flow are insignificant.

Davies illustrated that it is not the absolute magnitude of the density-related flow component, but the relative magnitude of this term versus the magnitude of the fresh water hydraulic head gradient term that determines whether the density-related gravity effects will be significant in a given situation.

4.3.1.2 Potentiometric surface map of the Leduc and Cooking Lake Formations:

The Leduc Formation reefs in the Rimbey-Meadowbrook chain trend NNE-SSW and are surrounded by shales on either side. Although there are many DST's in the Leduc Formation, most are affected by production which started as early as 1947. On the other hand, the Cooking Lake Formation is dominantly water bearing and since it has no direct economic value for the oil industry drill-stem tests are scarce.

Of the 199 DST's available for these formations culling (described in Chapter 3) removed the majority leaving only 19 DST's in the Leduc Fm. and 5 DST's in the Cooking Lake Fm. that were finally used for the hydrogeological analysis. Most of these DST's are clustered around the Bashaw and Westrose South reefs. The sparseness of control points makes contouring and interpretation problematic. For potentiometric surface map construction, the present DST database was supplemented by initial (or virgin) pool pressures obtained from the ERCB. The ERCB maintains a record of the initial pool pressures for all Canadian oil and gas fields. The ERCB also documents an average recorder elevation corresponding to the initial pool pressures. The average recorder elevation, which is the average elevation of the top and bottom of pools, is at different elevations within the Leduc reefs. The Leduc reefs reach a maximum thickness of about 200m in the study area. In order to obtain hydraulic heads, which are described at a point, and interpret horizontal flow from potentiometric surface maps standardization of the recorder elevations corresponding to the initial pool pressures was performed using pressure profiles for the reef trend and Bashaw Reef Complex. Hitchon (1984) provides relationships between the initial pool pressure (p) in kPa and recorder elevation (z) in metres for the Rimbey-Meadowbrook Reef Trend ($z=351-0.0949p$) and the Bashaw Reef Complex ($z=406-0.0839p$). These relationships were used to compute recorder elevations for the initial pool pressures obtained from the ERCB. Given the pressure and recorder elevations, equivalent freshwater hydraulic heads were calculated for each of the reefs in the study area. These hydraulic heads together with those obtained from the DST's were used for the potentiometric surface map construction (Figure 4.5). It should be noted that DST's in the Leduc Formation in 7-15-044-1W5, 7-16-044-1W5 and 7-10-045-1W5 were conducted in a gas pool of the Westrose South reef. A different procedure (described in Appendix

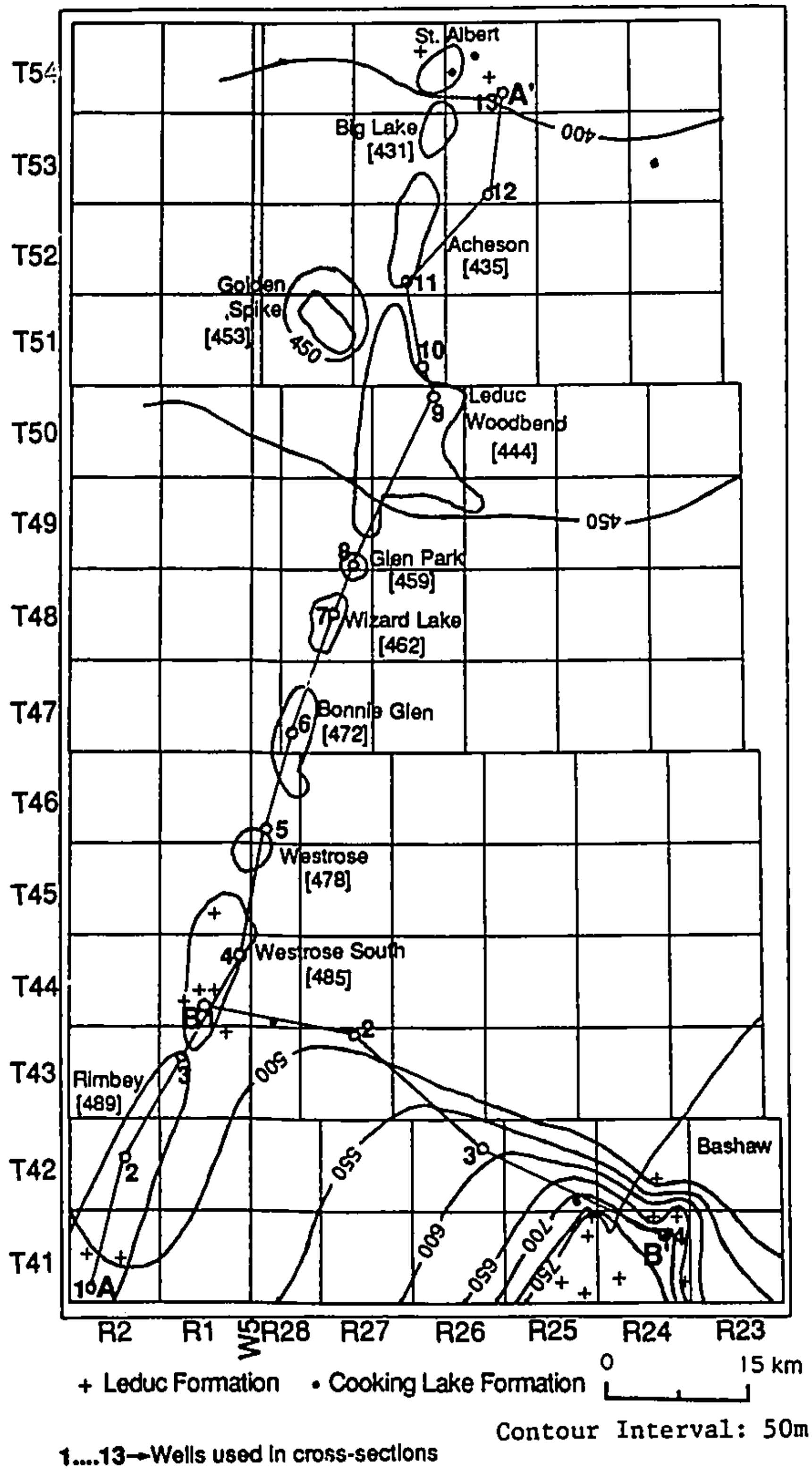

Figure 4.5 Potentiometric surface map (equivalent fresh water head) of the Leduc and Cooking Lake Formations [489]→Equivalent fresh water head (representative of the reef) calculated using the ERCB initial pool pressures (see text for details)

I) had to be employed to calculate equivalent fresh water hydraulic heads for these DST's.

The potentiometric surface map indicates a gradual decline in the hydraulic head towards the north (Figure 4.5). In the study area, fluid flow within the Rimbey-Meadowbrook reef trend is, therefore, directed north with a low hydraulic gradient of 0.001. Earlier studies in the reef trend by Hitchon (1969) and Hugo (1990) showed a similar uninterrupted fluid flow. The most striking observations made from the potentiometric surface map are: 1) the hydraulic heads in the Leduc and Cooking Lake Formations are similar in magnitude, 2) high fluid potentials are concentrated in the Bashaw reef with equivalent freshwater heads reaching more than 750m.

According to Tóth and Rakhit (1988) a high permeability lens embedded in a relatively low permeability matrix will cause negative and positive potentiometric anomalies in the upstream and downstream ends of the lens, respectively. The entire reef trend (analogous to the lens) may be visualized as a high permeability rock body embedded in the low permeability shale basins (Hugo, 1990). Therefore, U-shaped equipotential lines have been drawn between the Bashaw and Westrose South reefs (Figure 4.5).

4.3.1.3 Potentiometric surface map of the Nisku Formation:

The Nisku Formation, which conformably overlies the Ireton shales of the Woodbend Group, has a fluid potential maximum in the Bashaw reef similar to the underlying aquifers, the Leduc and Cooking Lake Fms. (Figure 4.6). The hydraulic heads in these

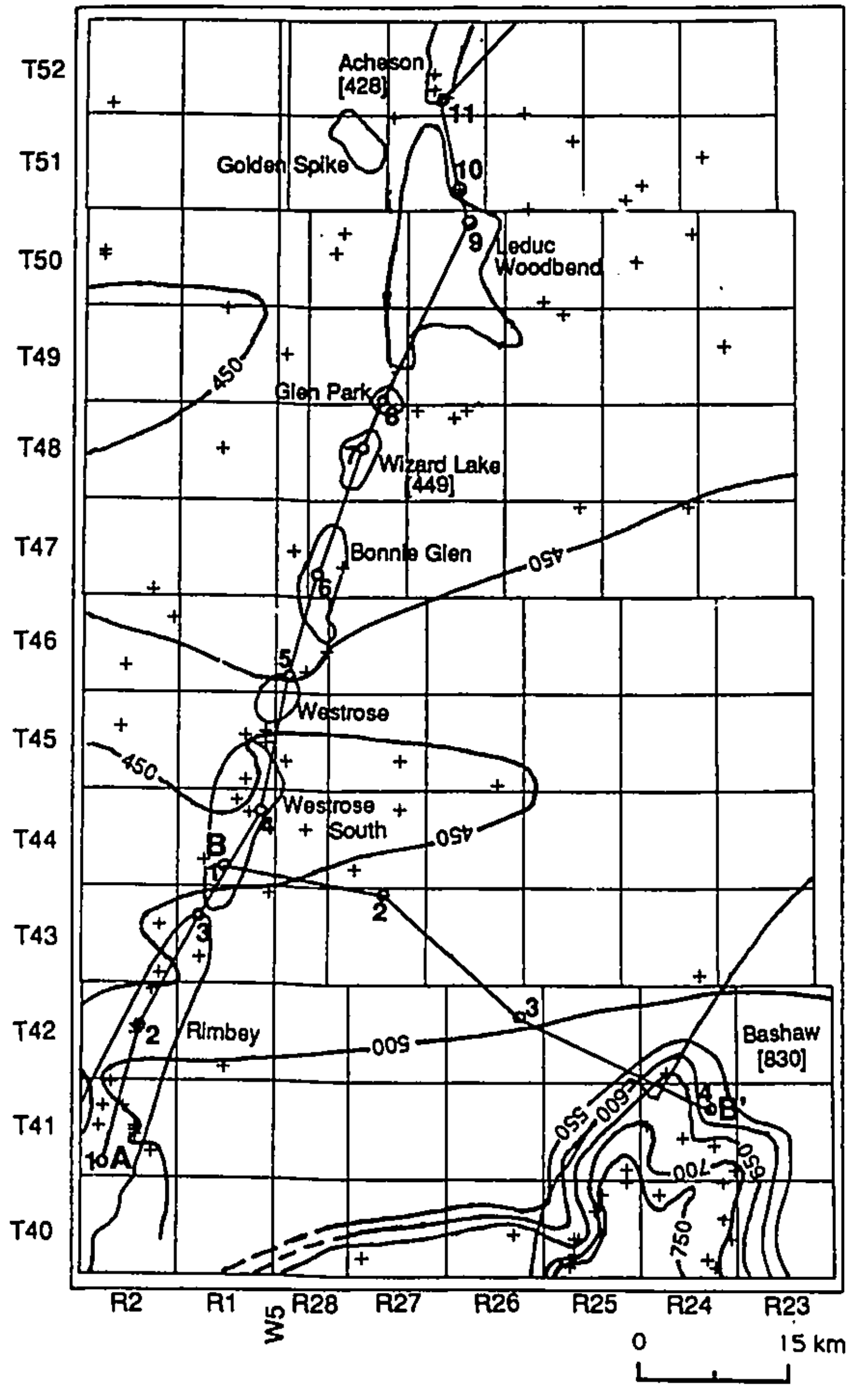

1....11 → Wells used in cross-sections

Contour Interval: 50m

Figure 4.6 Potentiometric surface map (equivalent fresh water head)of the Nisku Formation [449]→Equivalent fresh water head (representative of the reef) calculated using the ERCB initial pool pressures (see text for details) aquifers are of similar magnitude (up to 750m). Fluid flow is directed north from the Bashaw reef with a relatively strong hydraulic gradient of approximately 0.025 (25m/km); however, in general, the gradient is extremely low throughout the study area. The northward directed flow is deflected to the west between Tps.43-45 - a region occupied by the Westrose South reef in the underlying Woodbend Group. North of Tp.45 flow is dominantly northward.

4.3.2 Pressure-Depth [p(d)] plots

4.3.2.1 Theory

While a potentiometric surface may be employed for qualitative interpretation of horizontal groundwater flow directions, pressure-depth analyses disclose the pore-pressure conditions (super- or subhydrostatic), and whether there is any vertical flow component within and across geologic formations. Pressure-depth plots serve three major purposes in the present study. In the initial stages of the study, separate p(d) plots constructed for Nisku, Leduc and Cooking Lake Formations (Figures 3.5, 3.6 and 3.7) facilitated culling of the DST pressure measurements (as described in Chapter 3). Later the concept of dynamic pressure increment, was applied to determine vertical flow direction (Tóth, 1978, 1979). A qualitative evaluation of the effectiveness of the Ireton shales as a seal was also possible using p(d) analysis (discussed in Chapter 5). A theoretical review and the procedure undertaken for such an analysis is described in this section.

The dynamic pressure increment (Δp) at a given point in the subsurface may be defined as the difference between the real (measured) formation pressure and the nominal (static) hydrostatic value at that point.

$$\Delta p = p_{real} - p_{nominal} \qquad \text{.............. Eq.(4.5)}$$

According to Tóth (1978, 1979), if the formation pressures are measured in a hydraulically continuous flow regime any deviations from hydrostatic pressures are due to vertical fluid movement. The vertical sense of fluid movement may be inferred based on whether the deviation is positive or negative. Positive and negative Δp represent super- and subhydrostatic conditions with fluid flow ascending and descending, respectively, whereas a $\Delta p=0$ indicates lateral flow or no flow. When there is ascending flow the rate of pressure increase with depth (i.e., the measured pressure gradient) is greater than the rate at which the nominal pressure increases (nominal pressure gradient). However, when flow is descending the rate of pressure increase with depth is lower than the rate at which the nominal pressure increases. Hence, a comparison of the measured and nominal pressure gradients will indicate the vertical sense of fluid movement.

A number of factors influence accurate interpretation of pressure-depth plots. Poor data quality and distribution, effects of surface topography, structural dip of formation and potentiometric surface are some of the factors that may pose problems in such analysis (Orr and Kreitler, 1985). It may be misleading to analyze p(d) plots using sparse pressure measurements from large regions because not only will there be a scatter in the plots as a result of superimposed pressure-depth trends from different regions, a regression line through the entire data with a certain slope (measured gradient) and intercept will differ from a regression line through all the data from an individual well or from the appropriate hydrostatic gradient through individual data.

In this study the pressure-depth analyses have been performed in selected areas chosen separately for the Nisku Fm. and combined Leduc and Cooking Lake Formations. It is important to note that if the topography is complex a pressure-depth interpretation should always be done in conjunction with pressure-elevation [p(z)] analysis (Maccagno, 1991). Figure 2.6 indicates an even surface topography over the entire study area. The concept of dynamic pressure increment is, therefore, applied with the aid of pressure-depth plots for qualitative evaluation of any vertical fluid flow component.

Regions with a high density of pressure measurements spread over a relatively small area were chosen for the p(d) analyses. In such restricted geographic areas the variations of surface topography and structural dips of aquifers can be considered negligible. Further, the coefficient of determination (R^2) determined using the linear regression through the data provides the reader a feel for the reliability of p(d) interpretation. A relatively high R^2 value for a large data set should render the interpretation reliable and vice versa. In addition, the regression line through the data also provided the real (measured) pressure gradient. From Table 7, the average density within the depth interval in which the data points belonged was used to calculate the nominal (static) pressure gradient. Based on the concept of dynamic pressure increment, a comparison of the measured and nominal pressure gradients allowed determination of the vertical direction of flow (described below).

$$\gamma_{nominal} > \gamma_{measured} \Rightarrow \Delta p < 0 \quad \therefore \text{ indicating downward flow}$$

$$\gamma_{nominal} < \gamma_{measured} \Rightarrow \Delta p > 0 \quad \therefore \text{ indicating upward flow}$$

4.3.2.2 Pressure-depth [p(d)] analyses in the Nisku Formation

Pressure-depth analyses were performed for sites PDN1, PDN2, PDN3 and PDN4 (Figure 4.7). Figure 4.8 is a p(d) plot constructed for the Nisku Formation in the vicinity of the Bashaw reef (PDN1). Among the different types of recovery, mud recovery yielded the maximum R^2 value of 0.71. The nominal gradient of 10.8kPa/m, derived using density averaged over the depth interval 1727.6-2034.5m (Table 7) is comparable to the measured gradient of 10.5kPa/m (from the regression line for the mud recoveries). Dividing the difference between the nominal and measured gradients, 0.3kPa/m, by the acceleration due to gravity gives the vertical freshwater hydraulic gradient of 0.031. From the Figure 4.6, the estimated horizontal hydraulic gradient within the Nisku Fm. in the Bashaw reef region equals 0.033. Since the horizontal hydraulic gradient is greater than the vertical hydraulic gradient, horizontal

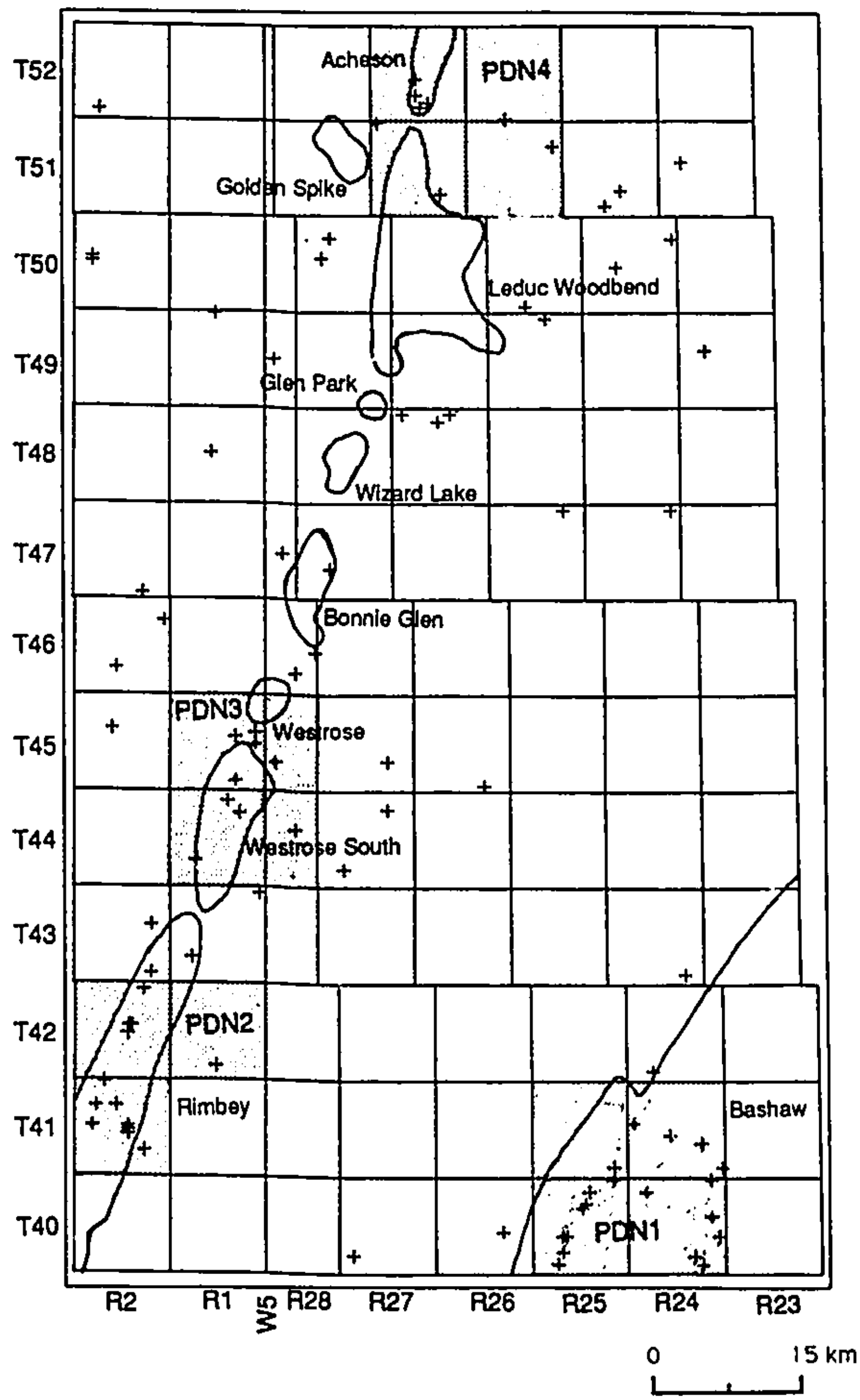

Figure 4.7 Sites for pressure-depth analyses in the Nisku Formation

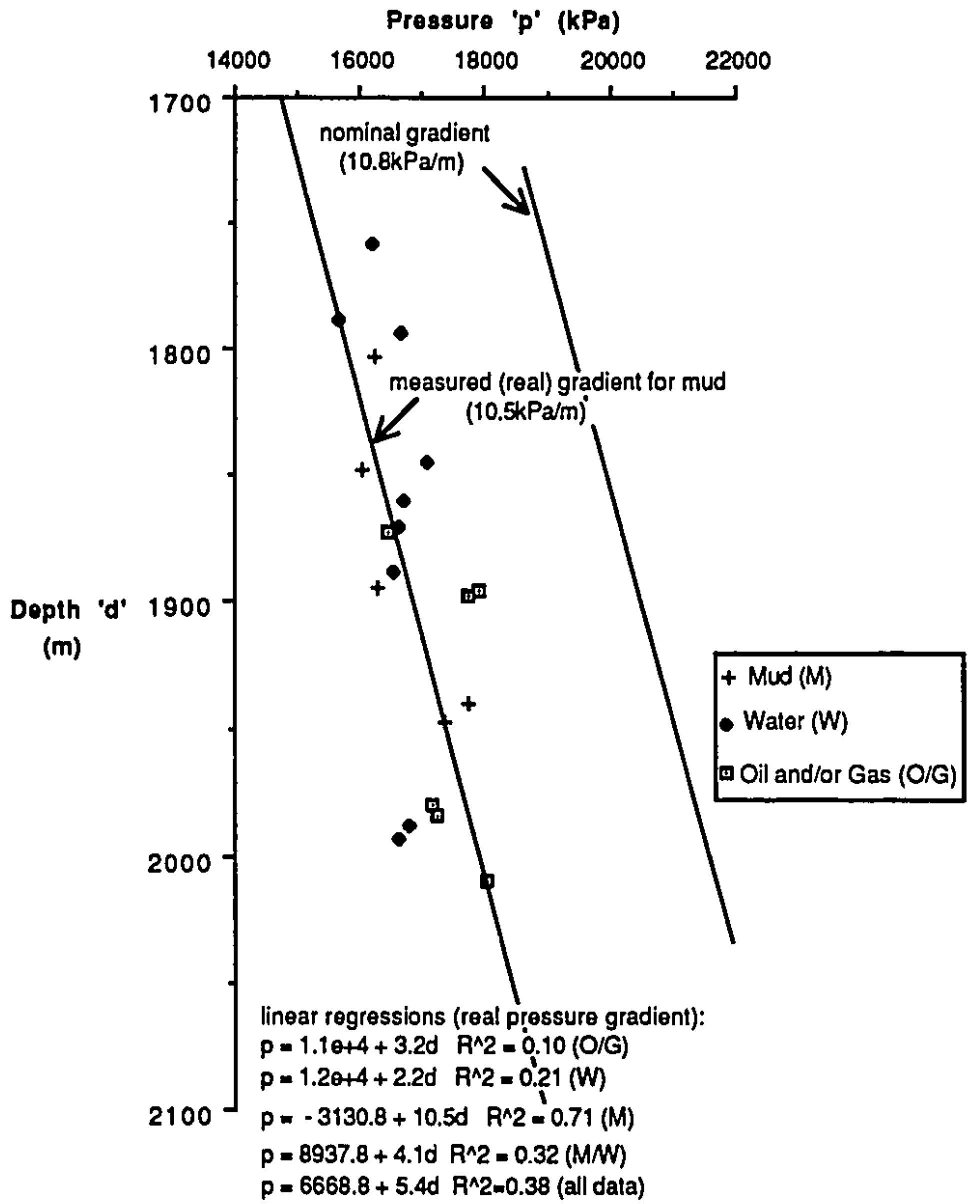

Figure 4.8 Pressure-depth plot in PDN1 [Nisku Fm.] [Bashaw reef region]

flow within the Nisku Fm. in the Bashaw reef region will be dominant.

Three regions were selected for p(d) analyses in the Nisku Formation that coincided with the positions of a few of the Leduc reefs. Pressure measurements in water recovery have been accepted for these p(d) analyses (Figures 4.9-4.11). For the p(d) plot near the Rimbey reef (PDN2) the nominal gradient, 10.6kPa/m computed using density averaged over the depth interval 2453.9-2473.1m, is higher than the measured gradient, 6.6kPa/m (Figure 4.9). The p(d) plot analyzed for a region near the Westrose South reef (PDN3) in Figure 4.10 also shows a higher nominal gradient, 10.9kPa/m (computed using density averaged over the depth interval 2006.8-2161.6m) than the measured gradient, 4.8kPa/m. The final p(d) plot covering part of the Leduc-Woodbend and Acheson reefs [PDN4](Figure 4.11) also has a nominal gradient 10.6kPa/m (using density averaged over the depth interval 1405.7-1490.5m) which is slightly higher than the measured gradient 9.5kPa/m.

In general, subhydrostatic conditions prevail within the Nisku Formation indicating a downward force component. However, the magnitude of the vertical flux (indicated by the difference between nominal and measured pressure gradients) varies along the Rimbey-Meadowbrook reef trend.

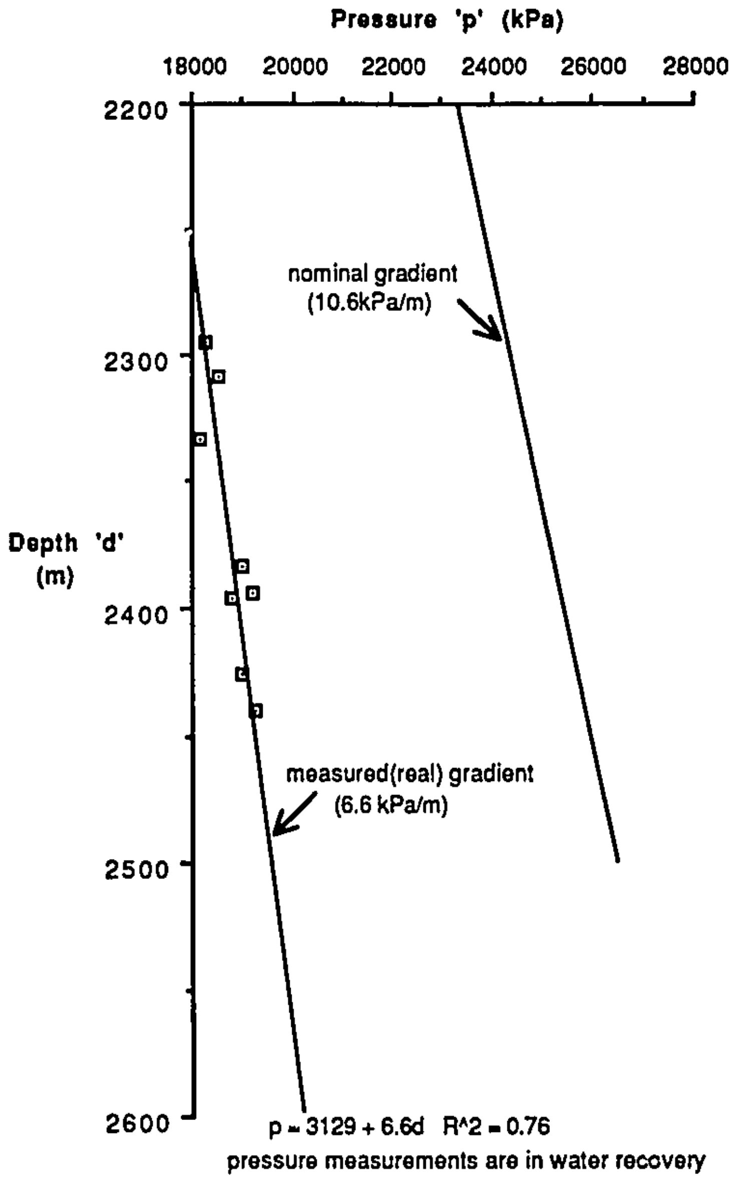

Figure 4.9 Pressure-depth plot in PDN2 [Nisku Fm.] [Rimbey reef region]

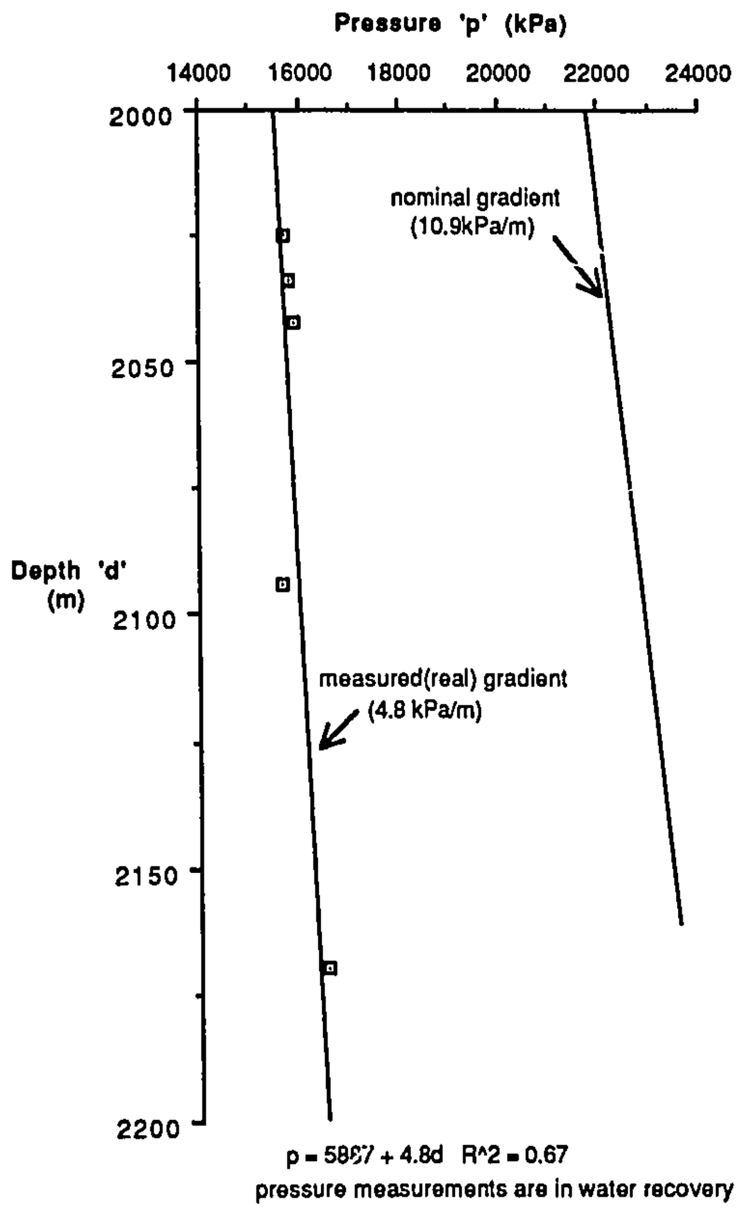

Figure 4.10 Pressure-depth plot in PDN3 [Nisku Fm.] [Westrose South reef region]

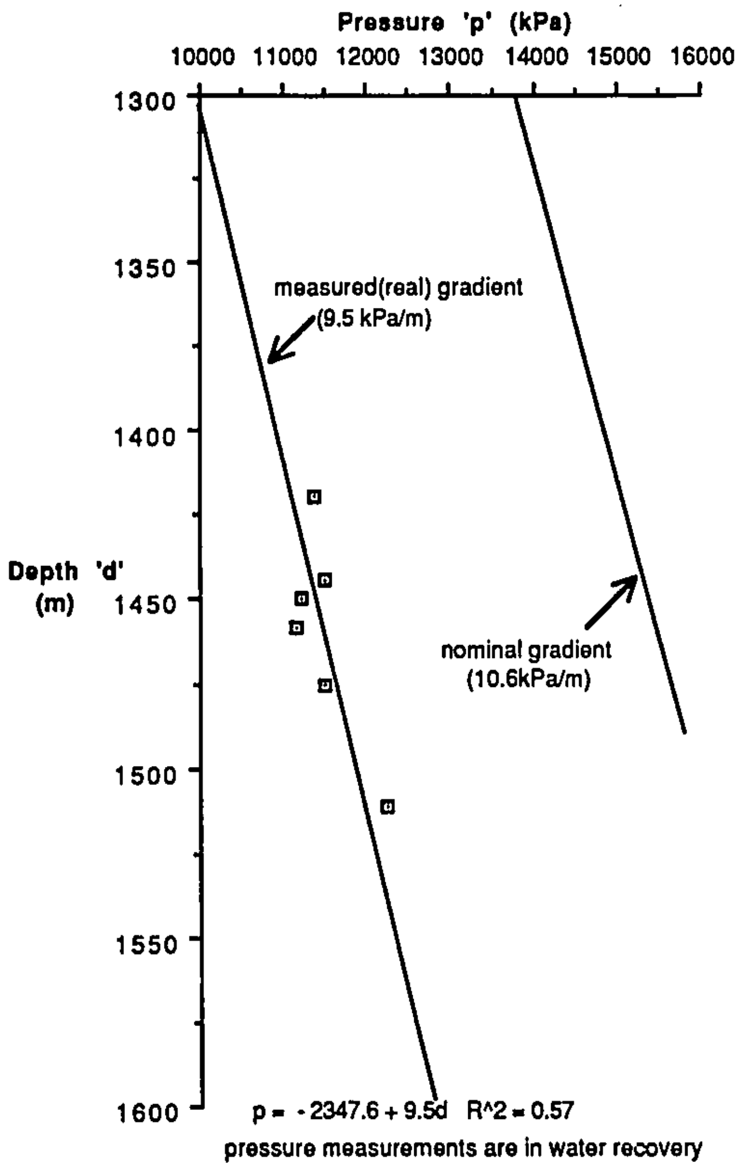

Figure 4.11 Pressure-depth plot in PDN4 [Nisku Fm.] [region of the Acheson and Leduc-Woodbend reefs]

4.3.2.3 Pressure-depth [p(d)] analyses in the Leduc and Cooking Lake Formations

Pressure-depth analyses were performed over two regions (PDLC1 and PDLC2) in the study area (Figure 4.12). Using pressure measurements in the Leduc Formation the p(d) plot in the Bashaw reef (PDLC1) exhibited a superhydrostatic gradient with a coefficient of determination (R^2) of 0.6 (Figure 4.13). The nominal gradient (11.2kPa/m) estimated using the density averaged over the depth interval 1780-2149.4m is less than the measured gradient (13.4kPa/m). Therefore, in the Bashaw reef (Leduc Formation) fluid flow is directed upward.

Data points that lie on the same hydrostatic gradient may be considered hydraulically continuous. However, a lateral shift of the lines representing the hydrostatic gradient could possibly indicate flow from regions of high to low hydraulic heads (Dahlberg, 1982). Alternatively the shift may indicate separate systems that are hydraulically discontinuous. Because of the paucity of pressure measurements, the northern end of the reef trend was the only other region (PDLC2) remaining where a pressure-depth analysis could be performed. Strictly speaking, hydrostatic gradients corresponding to the known density of the fluid must be drawn through individual points on a p(d) plot. However, where possible, fresh water hydrostatic gradients (9.80665kPa/m) were drawn through individual data points (Figure 4.14). A fresh water hydrostatic gradient was used because the data scatter is such that even using the actual gradient (which is slightly higher than that of

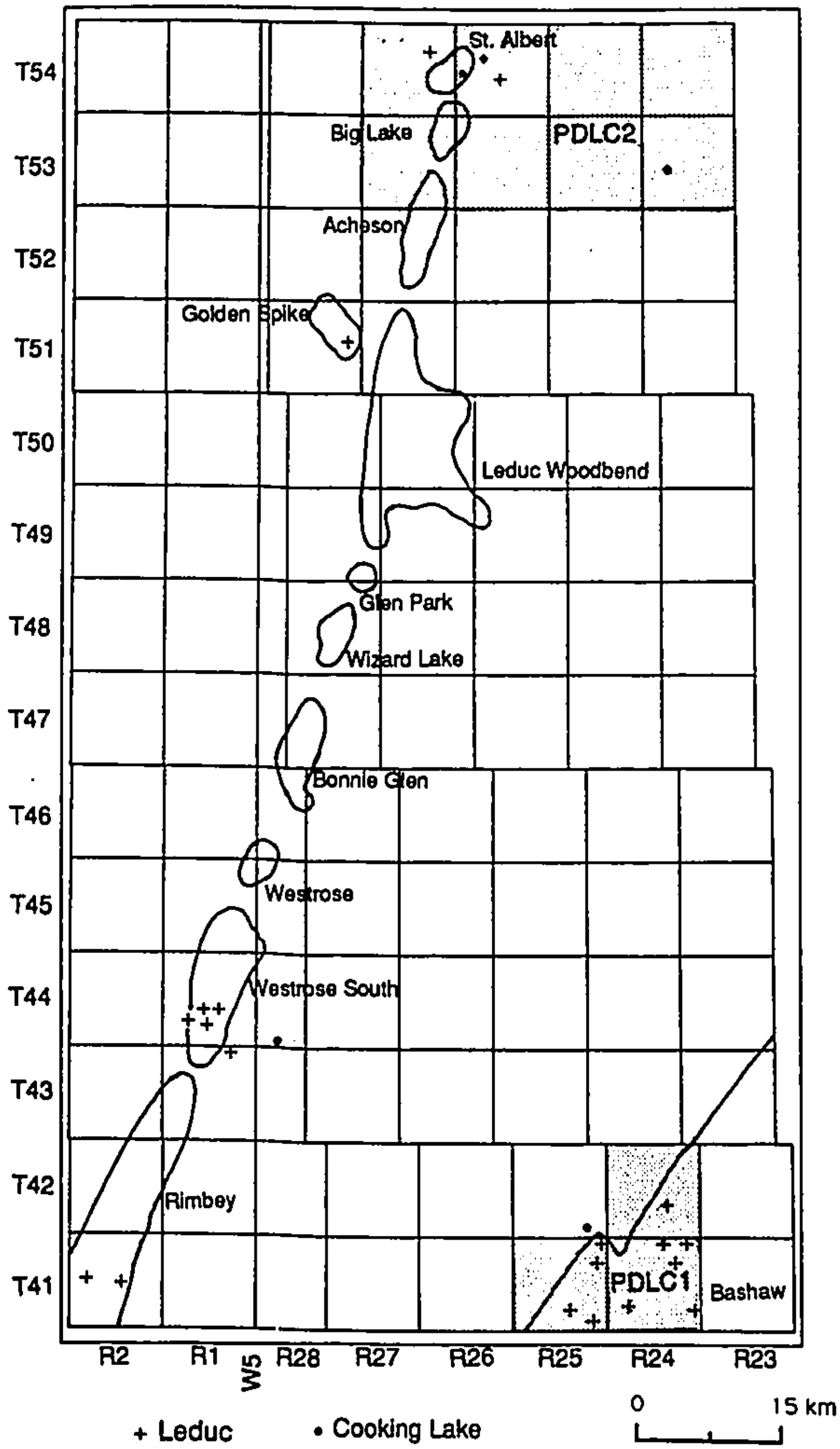

Figure 4.12 Sites for pressure-depth analyses in the Leduc and Cooking Lake Fms.

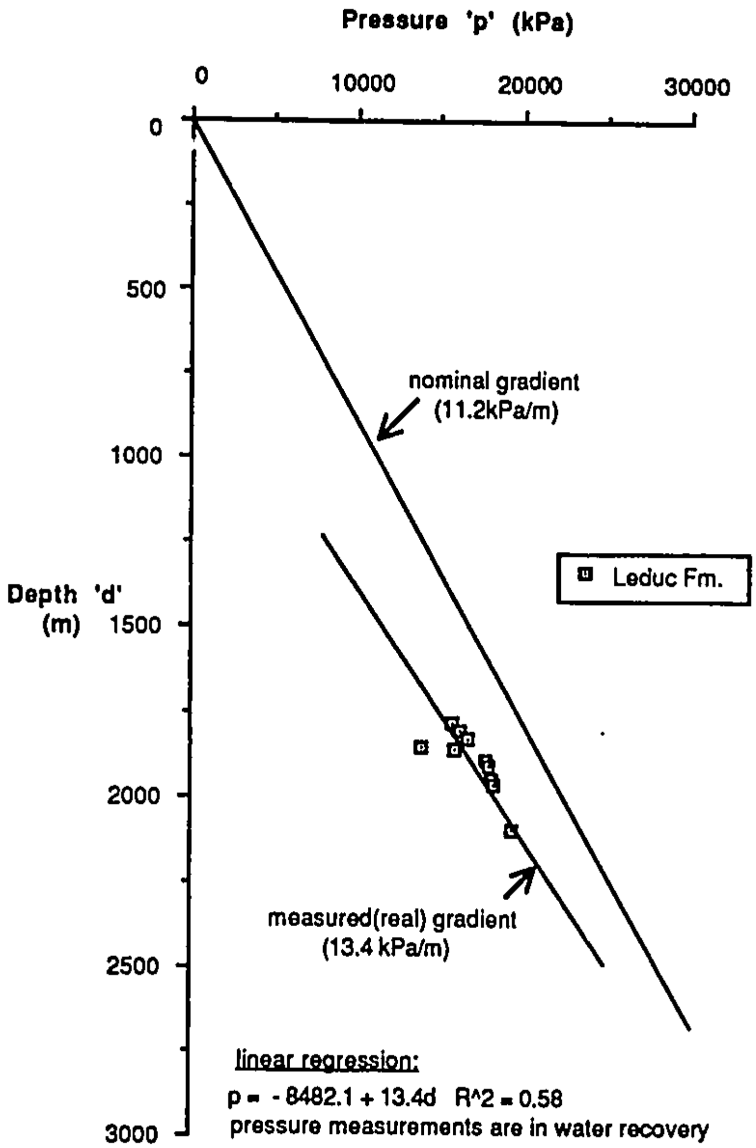

Figure 4.13 Pressure-depth plot in PDLC1 (Bashaw reef)

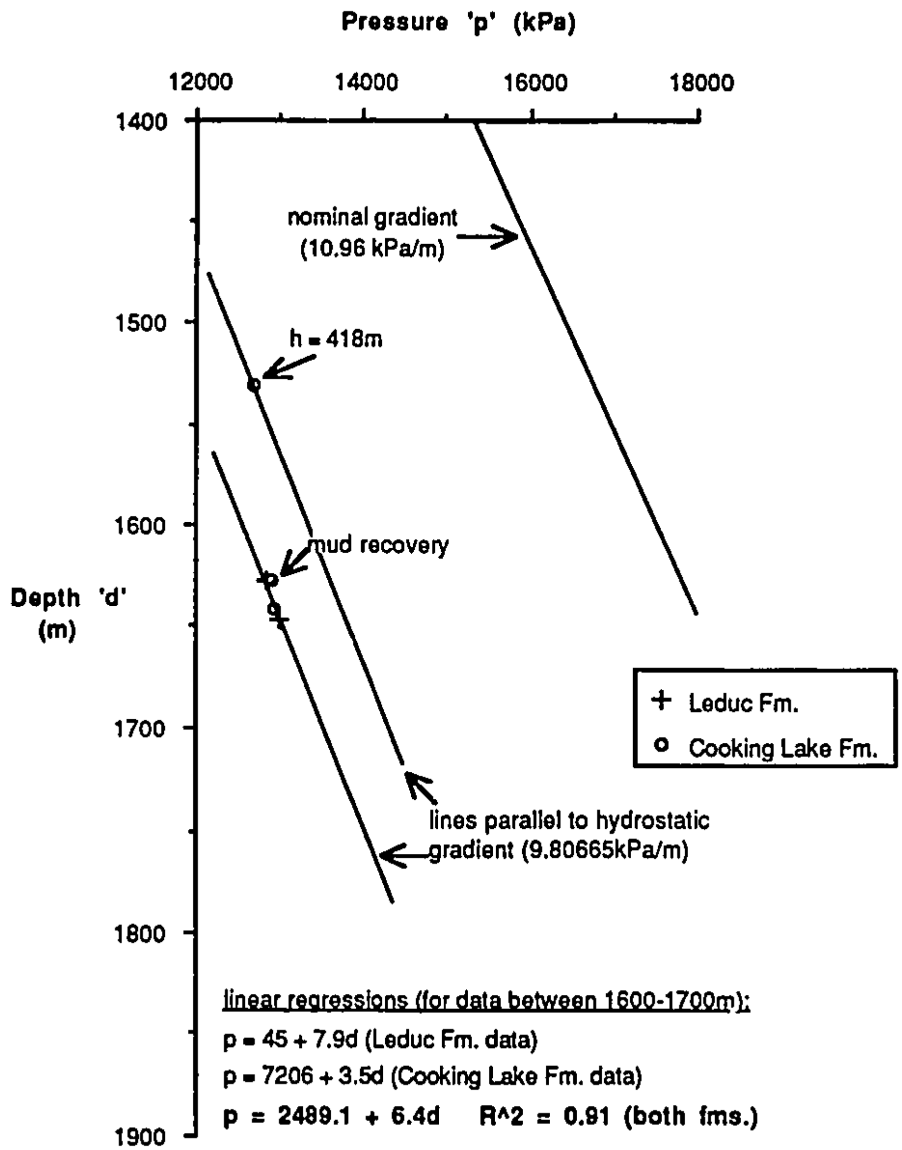

pressure measurements are in water recovery except where noted

Figure 4.14 Pressure-depth plot in PDLC2 [St. Albert reef region] fresh water) the interpretation of hydraulic continuity and flow direction remains unaffected.

The final p(d) analysis used data that encompassed a relatively large region (PDLC2). The surface topography over PDLC2 is almost flat. Figure 4.14 shows a cluster of four data points lying on the same hydrostatic gradient as that characteristic of the Leduc and Cooking Lake Formations. These data points lie in the region occupied by the St. Albert reef and, hydraulic communication between the two formations is inferred in that reef. A pressure measurement in the Cooking Lake Formation (at a shallower depth) with a hydraulic head of 418m has been indicated in this figure. It may be inferred that there is flow from the region where this particular pressure is measured to the region occupied by the cluster of the four data points (having hydraulic heads less than 418m). Knowing that only two pressure data are recorded, each in Leduc and Cooking Lake Fms., it may be erroneous to construct separate p(d) plots. The nominal gradient for the Leduc and Cooking Lake Fms. is 11kPa/m (Leduc and Cooking Lake Fms. densities were averaged over depth intervals of 1625.2-1647.4m and 1621.8-1640.1m, respectively). The nominal gradient is higher than the measured gradient 6.4kPa/m noted for the entire data (R^2=0.9). Comparison of these gradients indicate a negative dynamic pressure increment inducing fluids to move down.

4.3.3 Characterization and distribution of formation water chemistry

Formation water chemistry should form an integral part of any hydrogeological study. A hydrogeochemical study seeks to determine the origin of the chemical composition of groundwater and the relationship between water and rock chemistry, particularly as they relate to groundwater movement which plays a vital role as a transporting agent for subsurface mass and energy. When deciphering the groundwater flow direction, it must be realized that the spatial and temporal distribution of fluid potentials is the governing factor for flow; whereas, a hydrochemical study serves as a supplementary tool for its confirmation.

Water analyses in Nisku, Leduc and Cooking Lake Formations that passed the culling procedure (described in chapter 3) constituted the database for the hydrochemical study. The Nisku Formation was represented by the largest number of water analyses (49) followed by the Leduc (30) and Cooking Lake (23) Formations (Tables 8, 9 and 10). To visually inspect major groupings or trends in the data, Piper and Stiff diagrams were constructed for the three formations using only those water analyses which had a complete record of the ionic concentrations. For each of these formations, Stiff diagrams using the average ionic concentrations and their standard deviations have been presented in Figures 4.15 to 4.17. A Stiff diagram constructed using the average formation water chemistry data (Johnston, 1988) for the Basal Mannville Group of the Cretaceous period in Figure 4.18 will be discussed in Chapter 5. Based on the subdivision of the trilinear Piper diagram suggested by

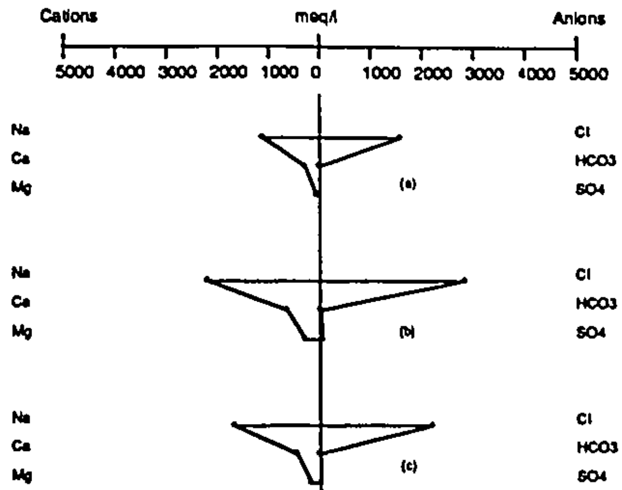

Figure 4.15 Stiff diagram for the Nisku Fm.

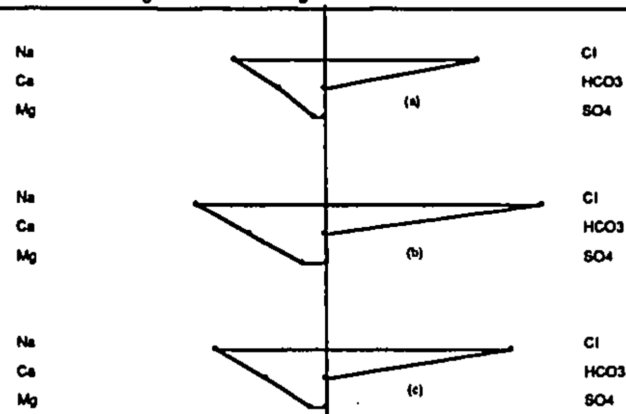

Figure 4.16 Stiff diagram for the Leduc Fm.

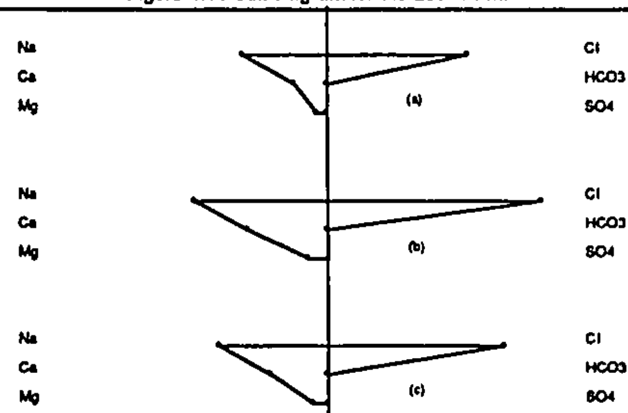

Figure 4.17 Stiff diagram for the Cooking Lake Fm.

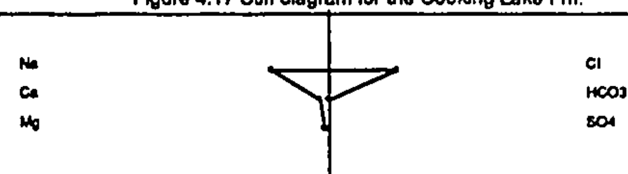

Figure 4.18 Stiff diagram for the Basal Mannville Gp.

Stiff diagrams for each formation
(a)- Average minus one standard deviation
(b)- Average plus one standard deviation
(c)- Average

Back (1961) and Back and Hanshaw (1965), the dominant cation and anion facies in each of the formations are sodium and chloride, respectively. However, careful inspection reveals that the Leduc and Cooking Lake Formations waters are almost identical. The waters from these formations are characterized by a slightly higher calcium and chloride content as compared to the Nisku Formation waters. Cl^- $+SO_4^{2-}$ type of water is present in all three formations. The Nisku Formation waters are dominated by sodium (60-90%meq/l) while Leduc and Cooking Lake Formations have sodium ranging between 40-80%meq/l. The Nisku Formation water is predominantly Na-Cl brine while the Leduc and Cooking Lake Formations waters are Ca-Na-Cl to Na-Cl brines.

Relationship of salinity (TDS) to individual ions in the three formations was examined (Figures 4.19 to 4.21). For each one of these figures a linear regression analysis was performed. Again the R^2 values will determine the confidence with which one can infer an increase or decrease in the concentration of a particular ion with TDS. In general, there is a increase in Na^+, Ca^{2+}, Mg^{2+}, and Cl^- with an increase in the salinity in each of the formations. However, Cl^- shows a consistent increase ($R^2 \approx 1.0$) in each of the formations while the proportion of Na^+ increase is relatively uniform ($R^2=0.8$) in the Nisku Formation (Figure 4.19) as compared to its increase in the Leduc and Cooking Lake Formations ($R^2=0.6$ and 0.7) (Figures 4.20 and 4.21).

There is a decrease in the SO_4^{2-} content with increased salinity in the Leduc and Cooking Lake Formations. In the Nisku Formation, there is a large scatter ($R^2=0.0$) of the SO_4^{2-} field, and

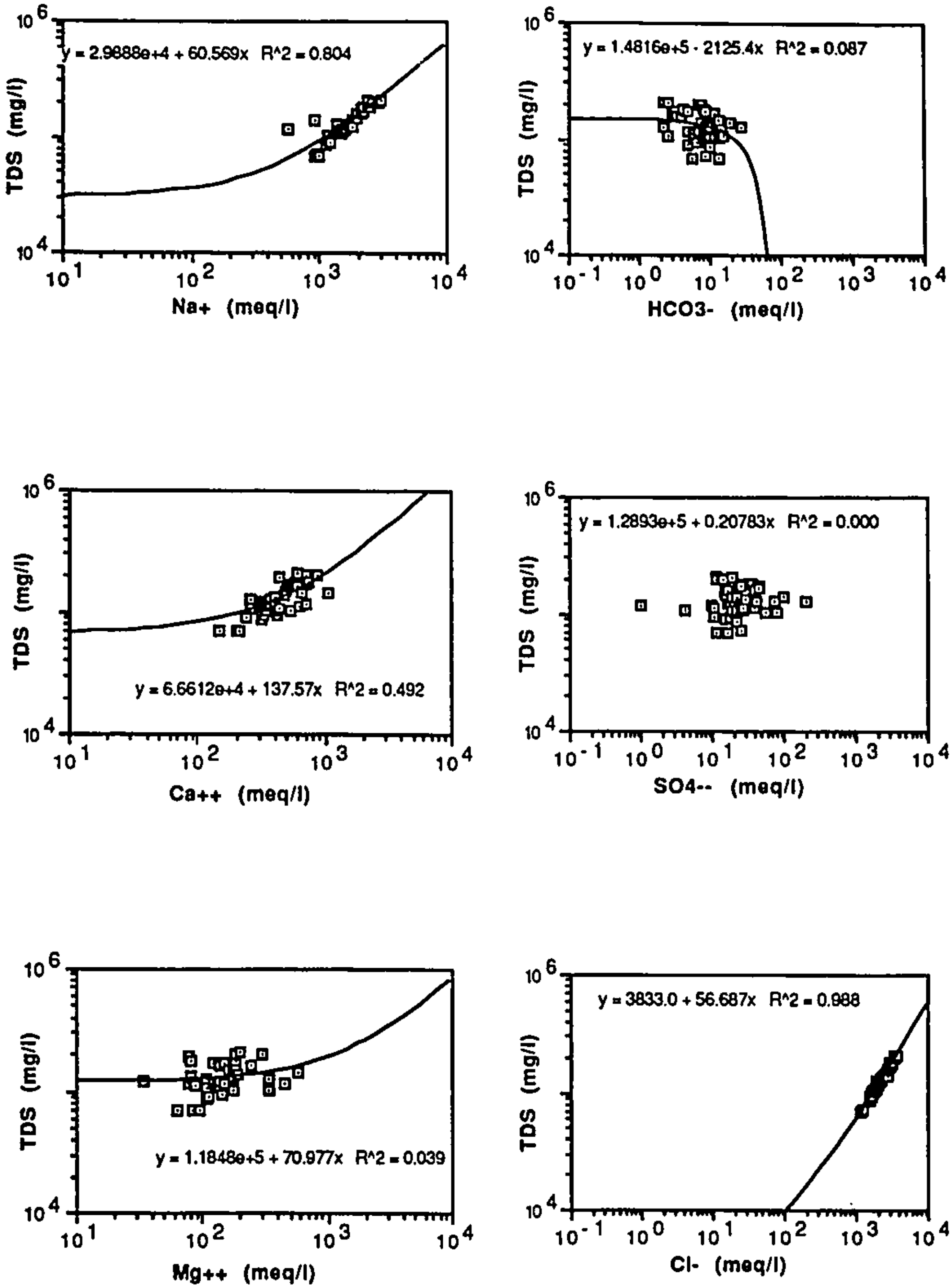

Figure 4.19 Relationship of salinity (TDS) to individual ions in the Nisku Formation

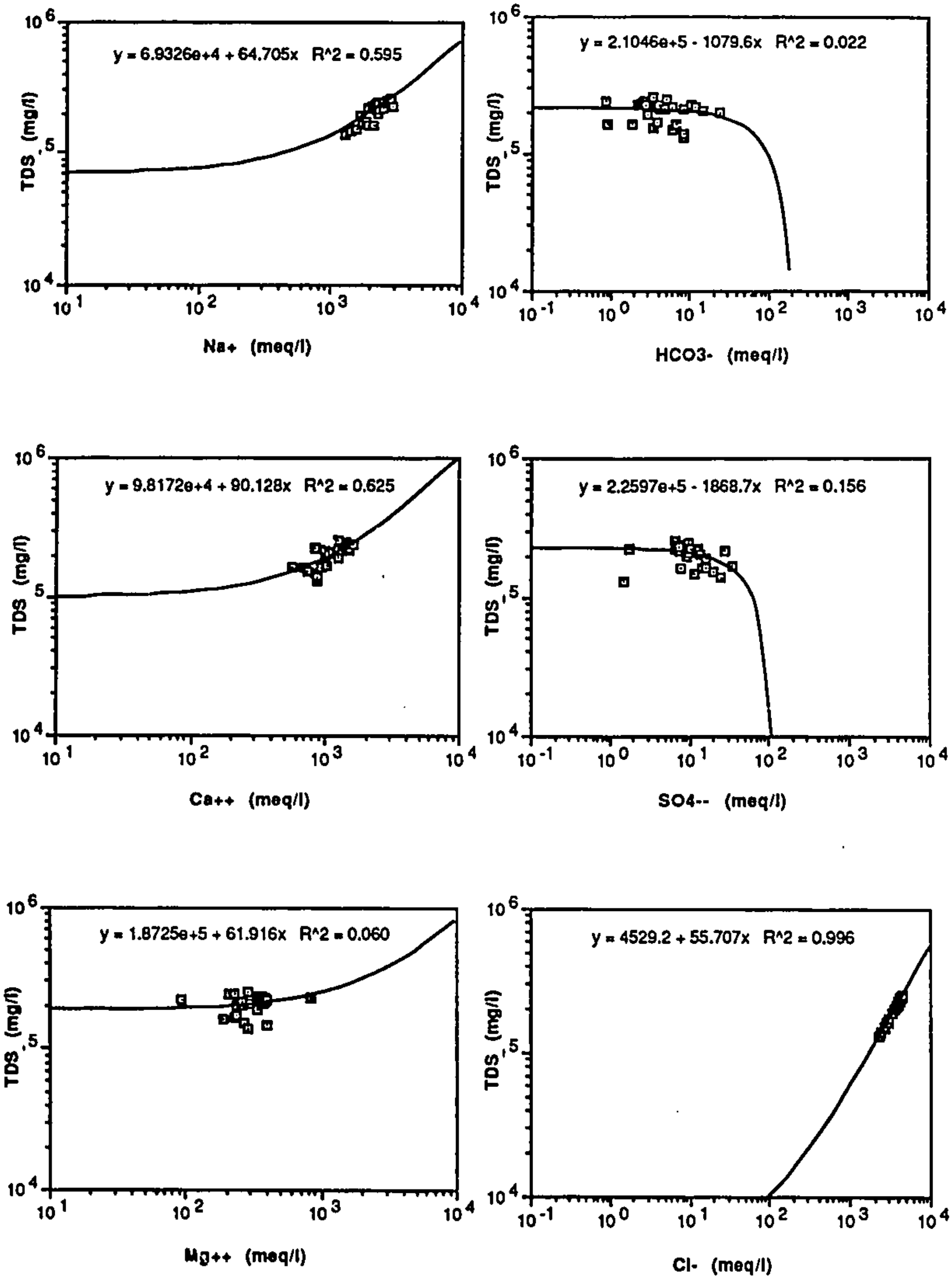

Figure 4.20 Relationship of salinity (TDS) to individual ions in the Leduc Formation

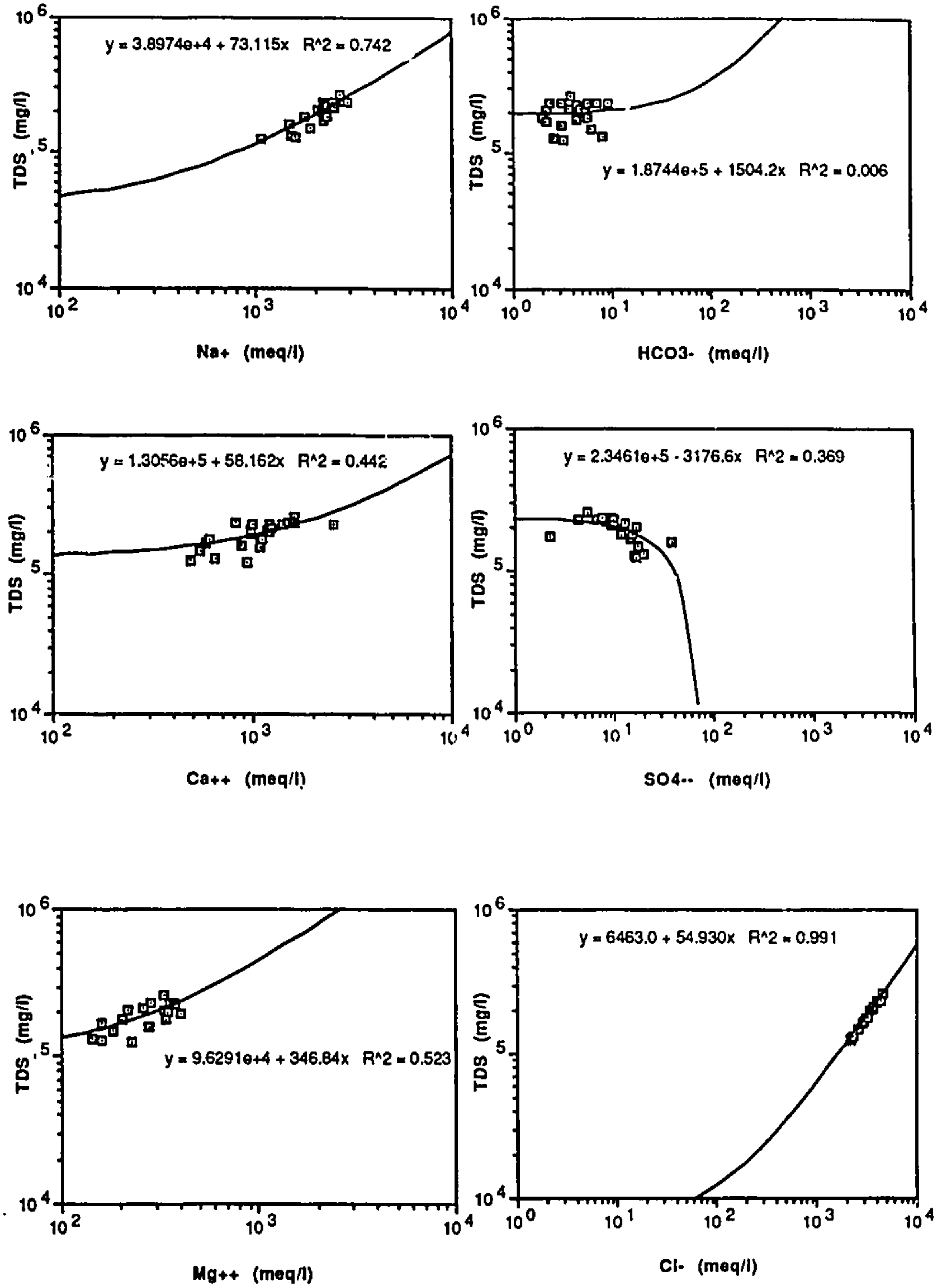

Figure 4.21 Relationship of salinity (TDS) to individual ions in the Cooking Lake Formation

the indicated positive slope may be erroneous. A plausible explanation for SO_4^{2-} depletion is the process of dolomitization The release of calcium ion as a by-product of the dolomitization of limestone may trigger the precipitation of sulfate minerals like gypsum and/or anhydrite thereby, reducing the SO_4^{2-} concentration. The most general chemical reaction for this process is given below -

$$2CaCO_3 + Mg^{2+} \Leftrightarrow CaMg(CO_3)_2 + Ca^{2+}$$

Despite the fact that HCO_3^- concentrations show a wide scatter in each of the formations, HCO_3^- concentration decreases (negative slopes in Nisku and Leduc Fms.) with increasing salinity. Precipitation of carbonate minerals (calcite and/or aragonite) is a possible explanation for this phenomenon. Generally, precipitation of carbonate minerals causes a simultaneous decrease in the Ca^{2+} concentrations (Jankowski and Jacobson, 1989). However, especially in the Nisku and Leduc Formations, the proportion of Ca^{2+} increases with increasing salinity implying that the carbonate minerals (calcite and/or aragonite) may not be the *dominant phase* to precipitate.

Although, the above reaction is commonly used to depict the replacement of calcite by dolomite (process of dolomitization), it does not imply necessarily, a resulting volume gain, preservation, or loss. According to Machel and Mountjoy (1986), if both kinetic and thermodynamic factors are considered conditions conducive to dolomitization would be favoured by fluids with: (i) high Mg/Ca ratios, (ii) low Ca/CO_3 (or Ca/HCO_3) ratios, (iii) high temperatures, at any salinity.

On the basis of thermodynamic considerations, higher temperatures will favour dolomitization. Pakhomov and Kissin (1973) have examined the relationship between molar Ca-Mg concentration ratio ($\log\frac{rCa}{rMg}$) and temperature (Figure 4.22). From CIFE's DST data, the average bottom-hole temperature for the Leduc and Cooking Lake Formations is 66°C. Using the graphical relation in Figure 4.22, the $\log\frac{rCa}{rMg}$ at 66°C is 0.43 (i.e., a molar Mg-Ca concentration ratio of 0.37). Because both magnesium and calcium have the same valence their concentration ratios expressed in molar concentration and equivalent mass (meq/l) are alike. Corresponding to the temperature range of 81-51°C, along the reef trend, the molar Mg-Ca concentration ratio varies between 0.32-0.41. A plot of salinity vs. Mg/Ca ratio in Figure 4.23 shows the boundaries for the calcite-dolomite equilibrium constructed at temperatures of 51°C, 66°C and 81°C. In the Nisku Formation the boundary between the calcite-dolomite equilibrium is drawn at a Mg/Ca ratio of 0.37, a value obtained using the average bottom-hole temperature for the Leduc and Cooking Lake Formations. The spread of the data points over the calcite and dolomite fields in Figure 4.23 suggests that the formation water has not yet attained equilibrium with respect to either of these phases.

Figures 4.24 and 4.25 depict the average ion and ratios of the average ion concentration in the individual formations. Based on the similar characteristics of the Nisku, Leduc and Cooking Lake Fms. water, it may be inferred that waters in these formations have the same source. However, the Nisku Formation is characterized by

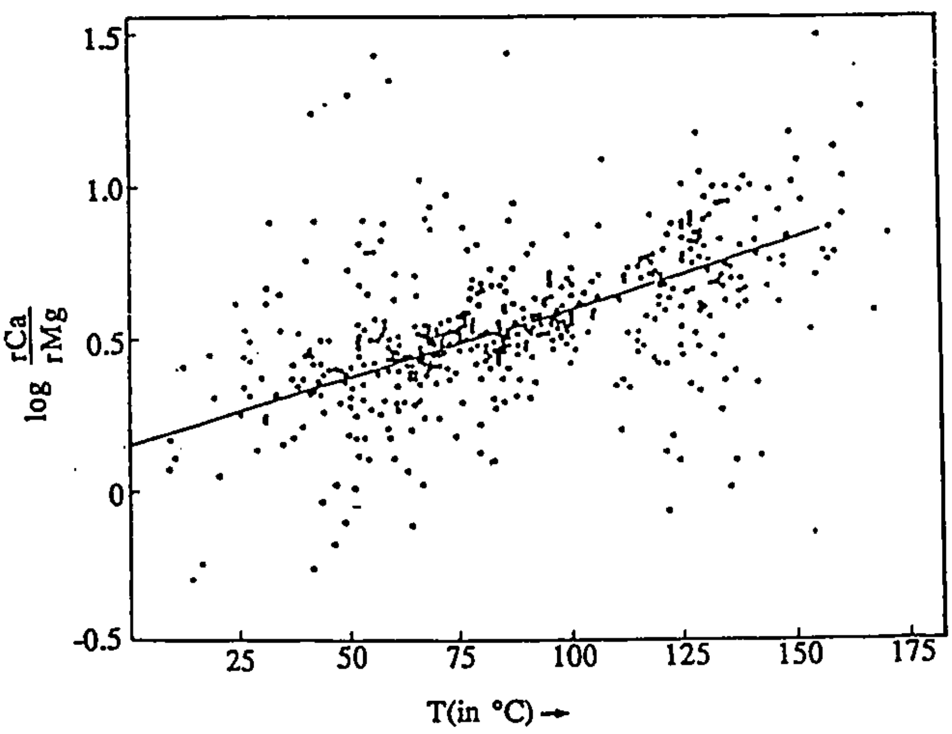

Figure 4.22 Relationship of molar Ca/Mg ratio to subsurface formation water temperature (after Pakhomov and Kissin, 1973)

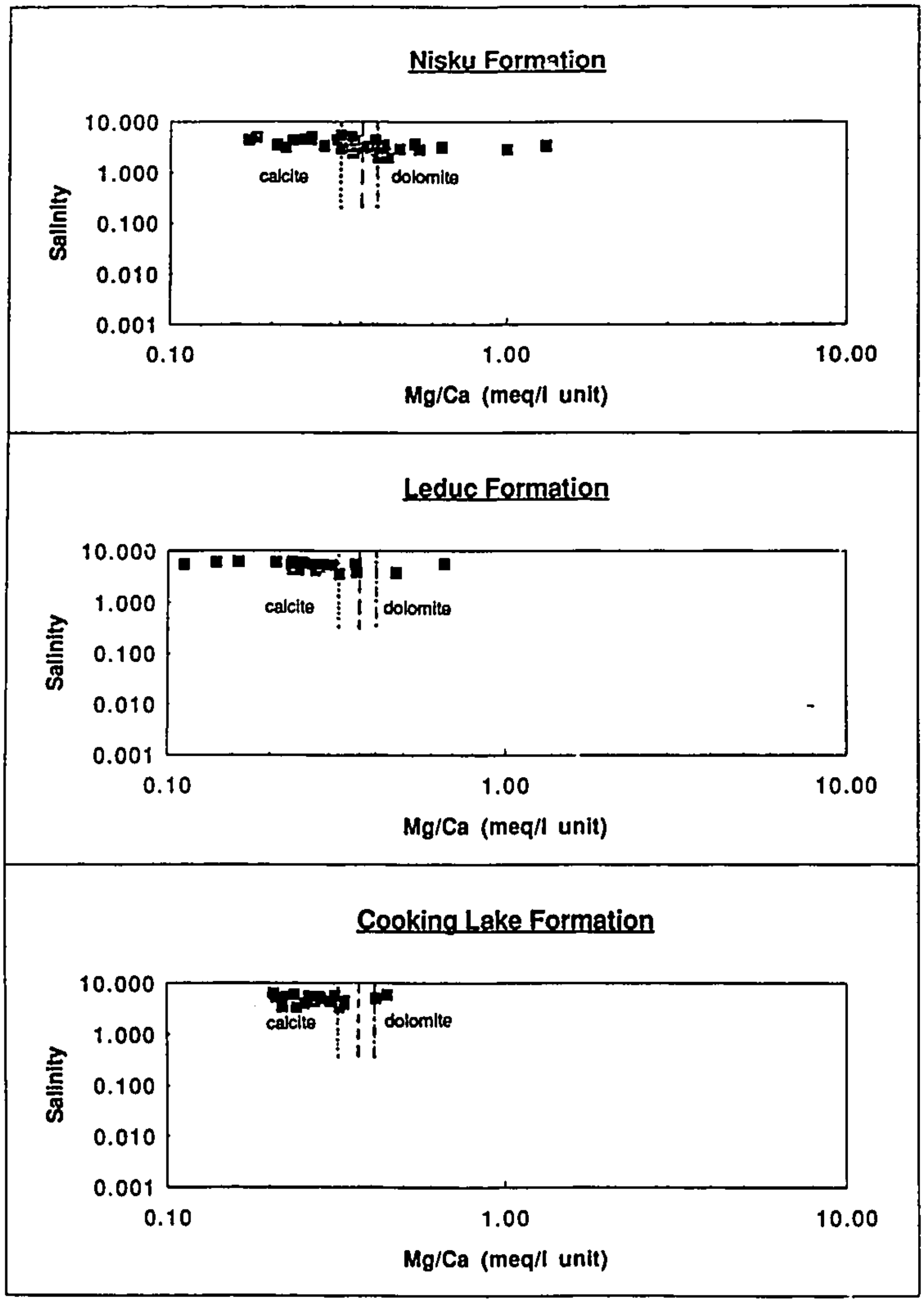

Figure 4.23 Plots of salinity vs. Mg/Ca ratios in the Nisku, Leduc and Cooking Lake Fms.

········· Boundary between calcite and dolomite at 81°C for which Mg/Ca is 0.32

------ Boundary between calcite and dolomite at 66°C for which Mg/Ca is 0.37

-·-·-·-· Boundary between calcite and dolomite at 51°C for which Mg/Ca is 0.41

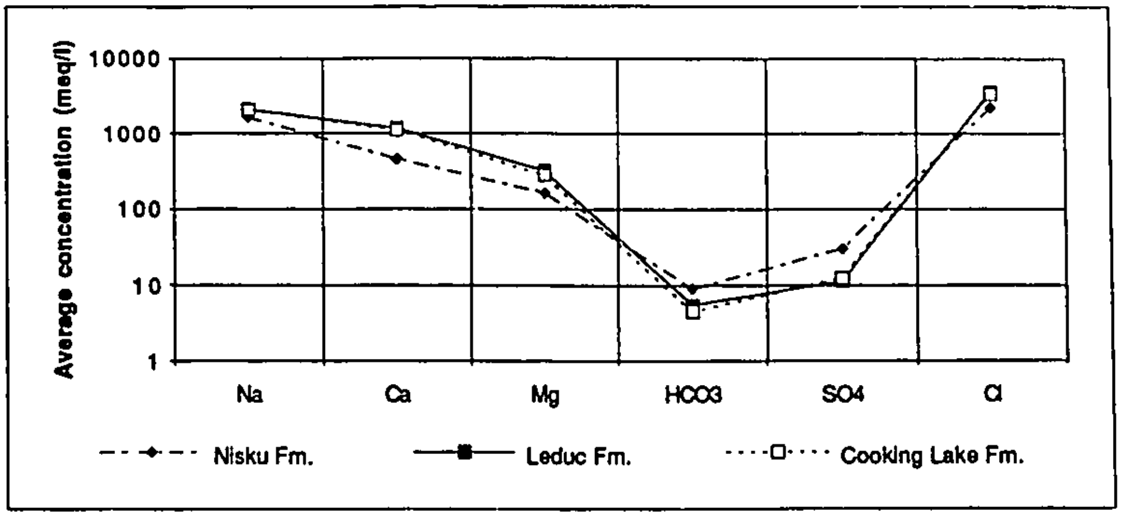

Figure 4.24 Plot of average ion concentration in the Nisku, Leduc and Cooking Lake Fms.

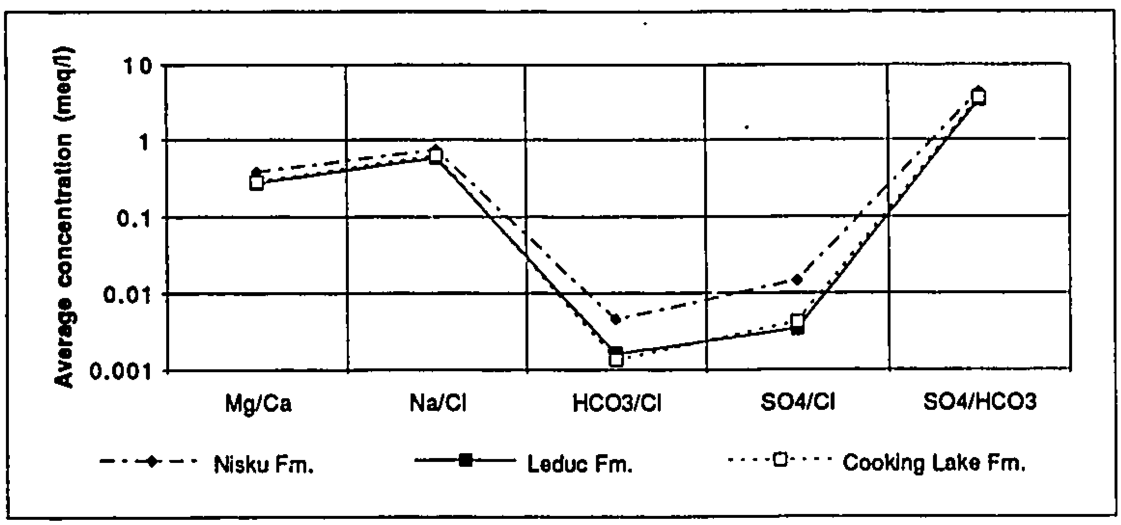

Figure 4.25 Plot of the ratio of average ion concentration in the Nisku, Leduc and Cooking Lake Fms.

fresher waters compared to the other two formations. Chebotarev (1955) observed an anion-evolution sequence (described below) that depends on the mineral availability and mineral solubility.

Direction of flow path and increasing age →

$HCO_3^- \rightarrow HCO_3^- + SO_4^{2-} \rightarrow SO_4^{2-} + HCO_3^- \rightarrow$

$SO_4^{2-} + Cl^- \rightarrow Cl^- + SO_4^{2-} \rightarrow Cl^-$

For most deep groundwater or groundwater that has moved long distances in sedimentary basins, the dominant anion is generally Cl^- and its proportion to total anions generally increases with salinity and depth (White, 1965). A plausible explanation for the higher HCO_3^- and SO_4^{2-} and lower Cl^- concentrations in the Nisku as compared to Leduc and Cooking Lake Formations may be based on the anion-evolution sequence and the stratigraphic level (depth) of each formation (Figure 2.1). As expected, SO_4^{2-} exceeds HCO_3^- within each formation.

Of the cations, Na^+, which is dominant in chloride waters, tends to increase in the flow direction because of its weak adsorption affinity. The divalent ions normally have stronger adsorption affinity than the monovalent ions. Further, ions that have the same valence but higher atomic number have a greater tendency to be adsorbed. For example, Ca^{2+} will be adsorbed in preference to Mg^{2+}. It is important to note that cation exchange does not depend solely upon the adsorption affinity but also on the ratio of the adsorbed mole fractions at the initial condition and on the concentration ratio of the two ions in solution (Freeze and Cherry, 1979). The sequence of cations following the cation exchange phenomenon is not always observed along the flow paths. Changing lithologies and cross-formational mixing may reverse not only the cation but also the anion-evolutionary sequence along flow paths. White (1965) also noted that among the cations the relative proportion of Ca^{2+} increases with increasing salinity and commonly increases with depth and age of the rocks. Even Mg^{2+} concentrations increase with depth but not as rapidly as Ca^{2+}. Figure 4.24 does show a increase of Ca^{2+} over Mg^{2+} in the deeper Leduc and Cooking Lake Fms.

Figure 4.25 illustrates that the ratios of average Mg/Ca, Na/Cl and SO_4/HCO_3 are almost identical in the Nisku, Leduc and Cooking Lake Formations. Generally, Mg/Ca and SO_4/HCO_3 ratios prove to be important indicators of the groundwater evolutionary process. Jankowski and Jacobson (1989), showed that ratios of Mg/Ca and SO_4/HCO_3 increase while HCO_3/Cl and SO_4/Cl decrease with increasing salinity and in the direction of flow.

The salinity (TDS) distributions in the Nisku Fm. and the Leduc and Cooking Lake Fms. have been hand contoured in Figures 4.26 and 4.27. With the aid of potentiometric surface maps and salinity distributions for these individual formations, trends of groundwater evolution with respect to major ion concentrations and total dissolved solids (TDS) content along the flow path were made.

The salinity distribution in the Nisku Formation (Figure 4.26) shows that fresher waters (80-120g/l) occur north of Tp. 46. The edge of this fresh water zone trends roughly NW-SE in the northern half of the study area. In this region, it is noted that there is a TDS decrease in the direction of flow. The highest salinities (160 to

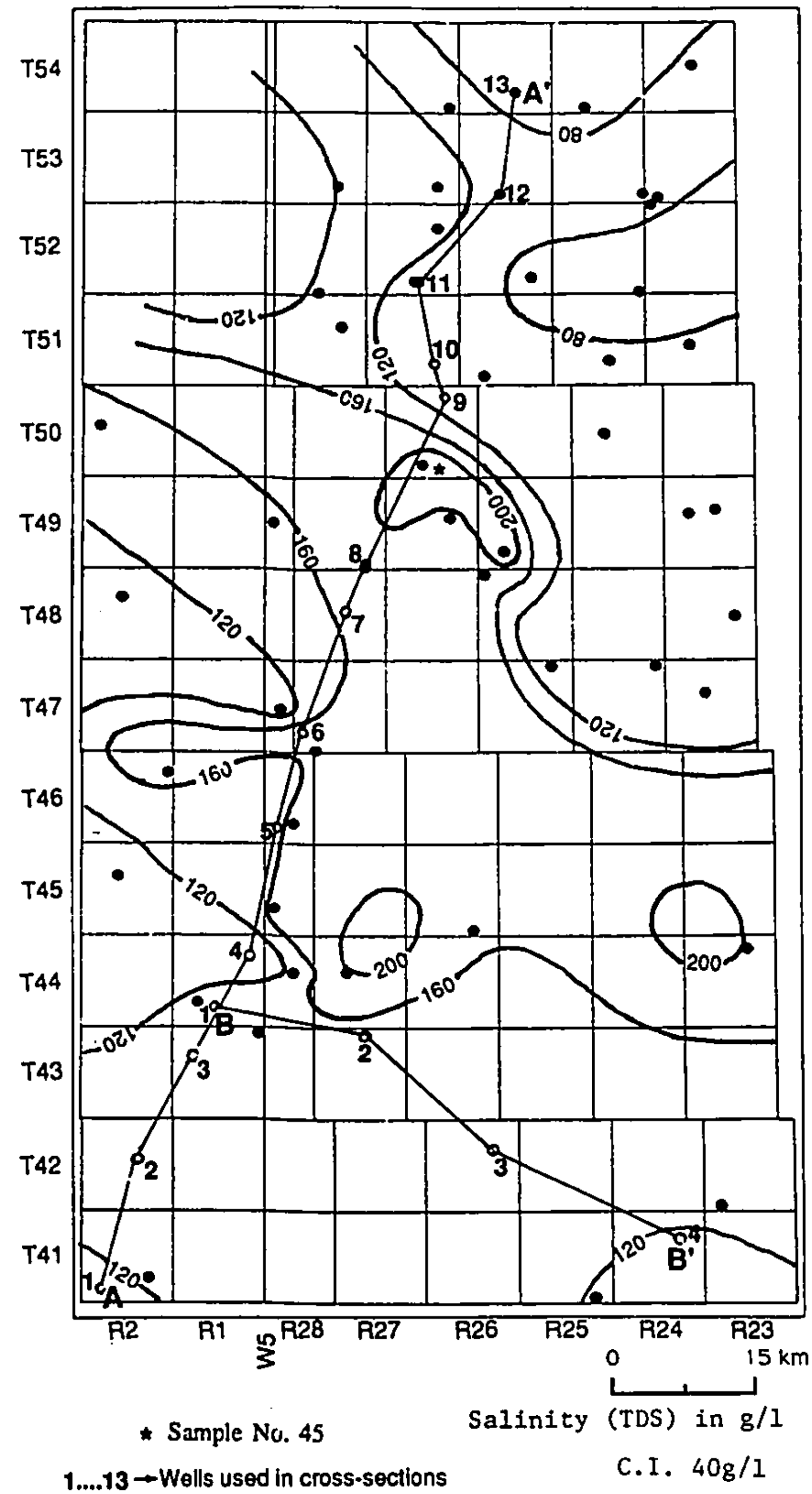

Figure 4.26 Isosalinity map of the Nisku Formation

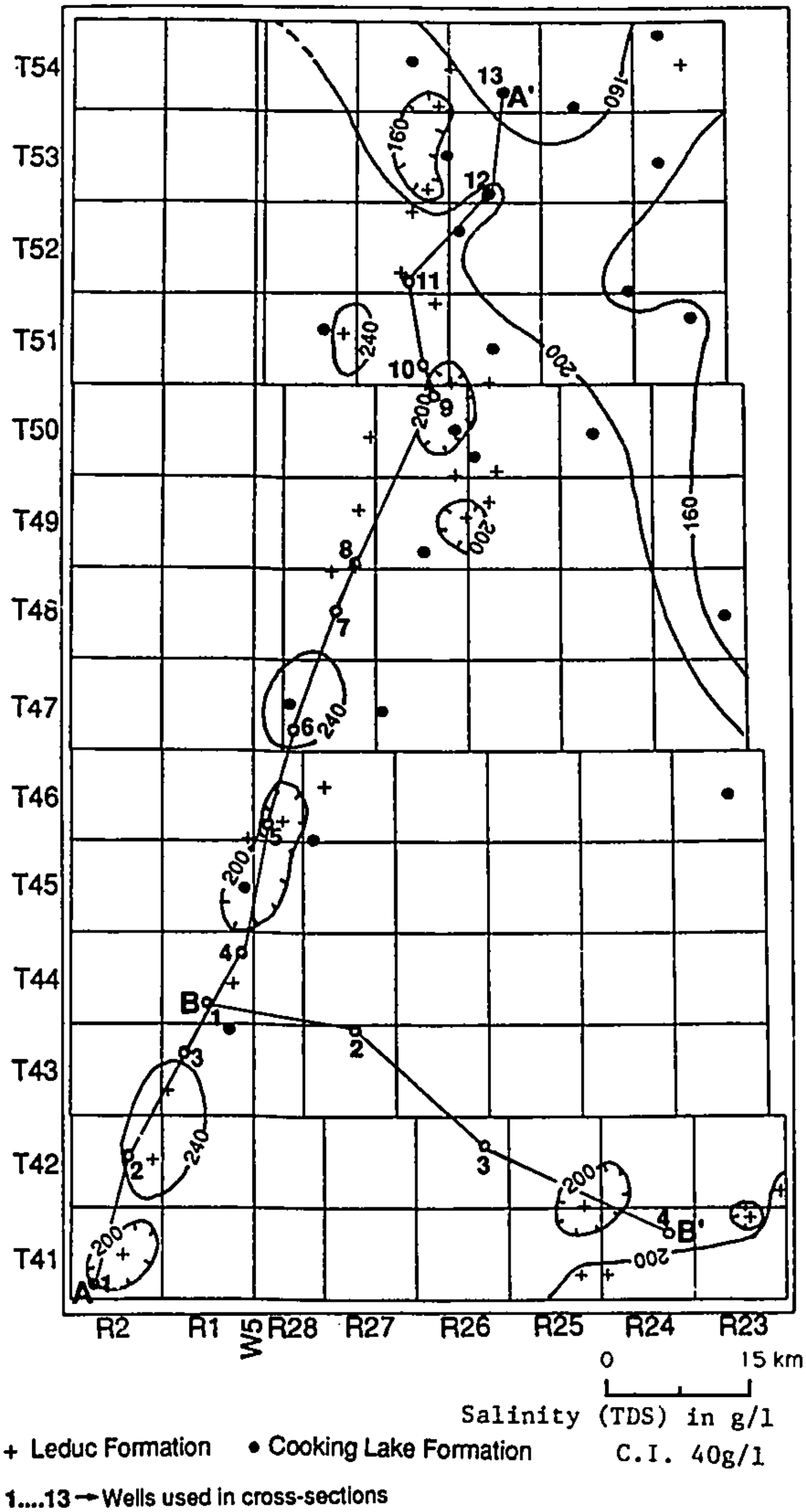

Figure 4.27 Isosalinity map of the Leduc and Cooking Lake Fms.

>200g/l) occur in the center of the study area with three prominent closed highs (TDS>200g/l). The closed TDS high near Tp.49 R.26 is the site occupied by the southern end of the underlying Leduc-Woodbend reef. Apparently, the underlying Leduc reefs influence the salinity distribution in the Nisku Formation. South of Tp.44 an increase in TDS in the direction of flow is conspicuous.

The salinity distribution map of the Leduc and Cooking Lake Fms. indicates the highest salinity zones (200->240g/l) restricted to the Rimbey-Meadowbrook reef trend (indicated as closed contours)(Figure 4.27). Similar to the Nisku Fm., fresher waters (160-200g/l) in the Leduc and Cooking Lake Fms. occur in the northeastern half of the study area; and, consequently a decrease in salinity is encountered in the flow direction. A disagreement regarding the general notion of TDS content increase in the flow direction warns a researcher the underlying danger of inferring fluid flow directions based exclusively on hydrochemical studies.

Chapter 5 Hydrogeological Synthesis and Discussion

Fluid-flow pattern and distribution in the study area

The gradient of fluid potential at points in the subsurface governs the direction of fluid flow between them. Therefore, the spatial and temporal distribution of fluid potential enables evaluation of the flow pattern.

Lateral fluid flow

The study area occupies a region of intermediate ground level elevations (600-950m) within the Alberta Basin. The land surface gently slopes (0.1°) towards the north. As indicated by the potentiometric surface maps (Figures 4.5 and 4.6) the present-day flow direction within the Leduc and Cooking Lake Formations and the Nisku Formation is in the direction of the regional slope of the land surface (Figure 2.6). Equivalent fresh water hydraulic heads within these formations are subdued when compared to the topography. These maps indicate hydraulic heads in the Bashaw reef are anomalously higher than those in the Rimbey-Meadowbrook reef trend. In the Bashaw reef the laterally surrounding Ireton shales are effective aquitards; therefore, fluid pressures do not dissipate readily (Hitchon, 1984). A high energy difference is required to move fluids across a low permeability rock framework. In other words, a high hydraulic gradient is required. The congestion of the equipotentials along the edge of the Bashaw reef indicates the high hydraulic gradient required to force the fluids laterally into the Ireton shales. On the other hand, Hitchon (1969a) had earlier recognized the Rimbey-Meadowbrook reef trend as a low fluid-potential drain channeling fluids from the Alberta Basin towards the Athabasca oil sands in the north. It is noted from Figure 4.5 that fluid flow within the Rimbey-Meadowbrook reef trend is northward with a low hydraulic gradient of 0.001.

The present study has confirmed the regional pattern of uninterrupted northward flow within the Rimbey-Meadowbrook reef trend found by Hitchon (1969) and Hugo (1990). Fluid flow is concentrated within the Cooking Lake Formation, as shown by the relative magnitudes of fluid fluxes[2] (flow intensity) computed within this formation and between reefs and the intervening Ireton shales. The horizontal flux within the Cooking Lake Formation is about 500 times the flux between two consecutive reefs with intervening shales. The Rimbey and Westrose South reefs were chosen as an example. In the Cooking Lake Fm., the estimated horizontal flux is 5.4×10^{-9}m/s (≈0.5mm/day), whereas an estimated horizontal flux of 1.3×10^{-11}m/s (≈0.001mm/day) was computed for flow between the reefs. The shale hydraulic conductivity of 1.7×10^{-9}m/s and 2×10^{-6}m/s for the Cooking Lake obtained from Hugo (1990) were used in the flux calculations.

At this point it should be mentioned that understanding the concept of hydraulic continuity is indispensable for correct evaluation of groundwater flow-patterns. Hydraulic continuity is

---

[2] refer Appendix II for fluid flux calculations in the study.

quantitatively characterized as the ratio of an induced change in hydraulic head, or pore pressure, at a point of observation to an inducing change of head (pressure) at a point of origin (Tóth, 1990). Pore pressure responses at various points in the subsurface to an inducing pressure change may take longer than the time span of observation, causing the rock body to appear impermeable. Consequently, hydraulic continuity is a function of both space and time. Based on production history records, Hnatiuk and Martinelli (1967) and Barfoot and Ko (1987) conducted studies on the degree of pressure communication between the reefs in the Rimbey-Meadowbrook trend. Their results indicated groups of hydraulically disconnected reefs implying impermeable barriers between them. Since oil and gas production in the reef trend started less than 50 years ago, this time framework may not be long enough to reflect the changes in the pore pressure conditions at each reef. Thereby, leading to believe impermeable barriers in the reef trend. Judiciously applying the concept of hydraulic continuity it will be erroneous to incorporate Hnatiuk and Martinelli (1967) and Barfoot and Ko (1987) studies for the assessment of regional flow patterns within the reef trend on a geologic time scale.

Cross-formational fluid flow

In general, the potentiometric surface for the Nisku Formation is lower than that for the Leduc and Cooking Lake Formations. However, in the vicinity of the Bashaw reef the potentiometric surfaces in these formations are similar. In the Bashaw reef region the Ireton shale capping the reef is an ineffective aquitard; the similarity between the potentiometric surfaces is due to hydraulic communication between the Nisku Formation and the underlying Leduc and Cooking Lake Formations. The Ireton shale isopach in Figure 5.1 reveals that the shales are thinnest (0-50m) on top of the Bashaw reef complex (around Tps.41-42 R23-24W4). The thinning shales, therefore, explains the close correspondence of the hydraulic heads in these formations.

The pressure-depth plot [PDLC1] (Figure 4.13) in the Bashaw reef indicates a positive dynamic pressure increment that forces fluids to move upwards. The vertical fluid flux (flow intensity) is 1.49×10^{-8}m/s ($\approx$1.3mm/day). Since excellent vertical hydraulic communication between these geologic formations exists, fluids from the Leduc Formation will move upward into the overlying Nisku Formation.

The extent to which there is vertical hydraulic communication across aquitards may be assessed qualitatively by examining pressure-depth gradients. Within a homogeneous saturated porous medium, pressure increases with depth at a constant rate. If the rate of pressure increase is constant across an aquitard, it indicates that the aquitard is an ineffective barrier to flow, implying hydraulic communication across the aquitard. However, changing pressure-depth gradients indicate the effectiveness of the aquitard as a barrier to flow because of the lack of hydraulic communication.

Pressure-depth analyses for the region Tp.41 R.2W5 and in well 10-08-044-01W5 (Figures 5.2 and 5.3) show that pressure measurements across the Ireton shale (thickness less than 50m) can

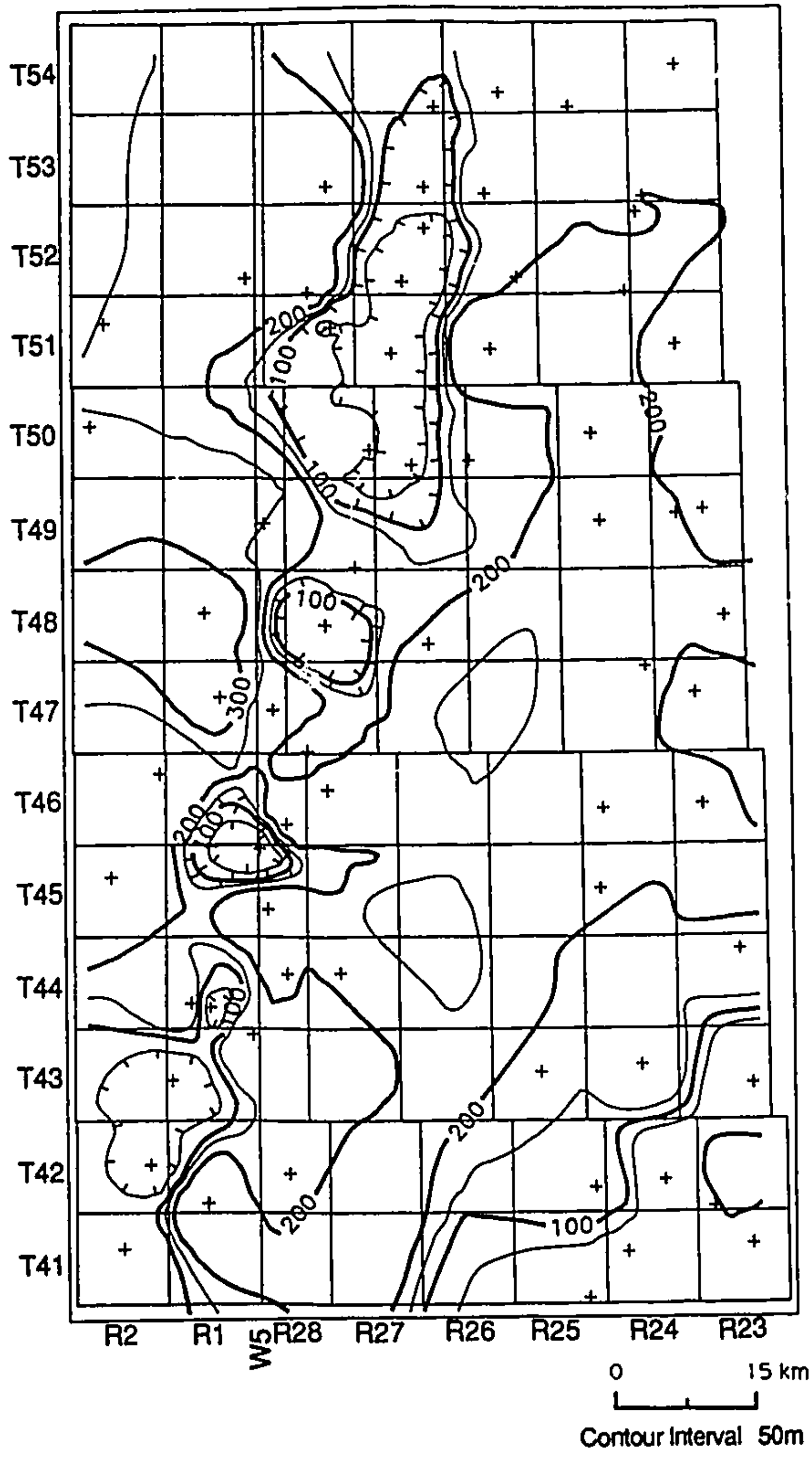

Figure 5.1 Ireton (shale) isopach in the study area

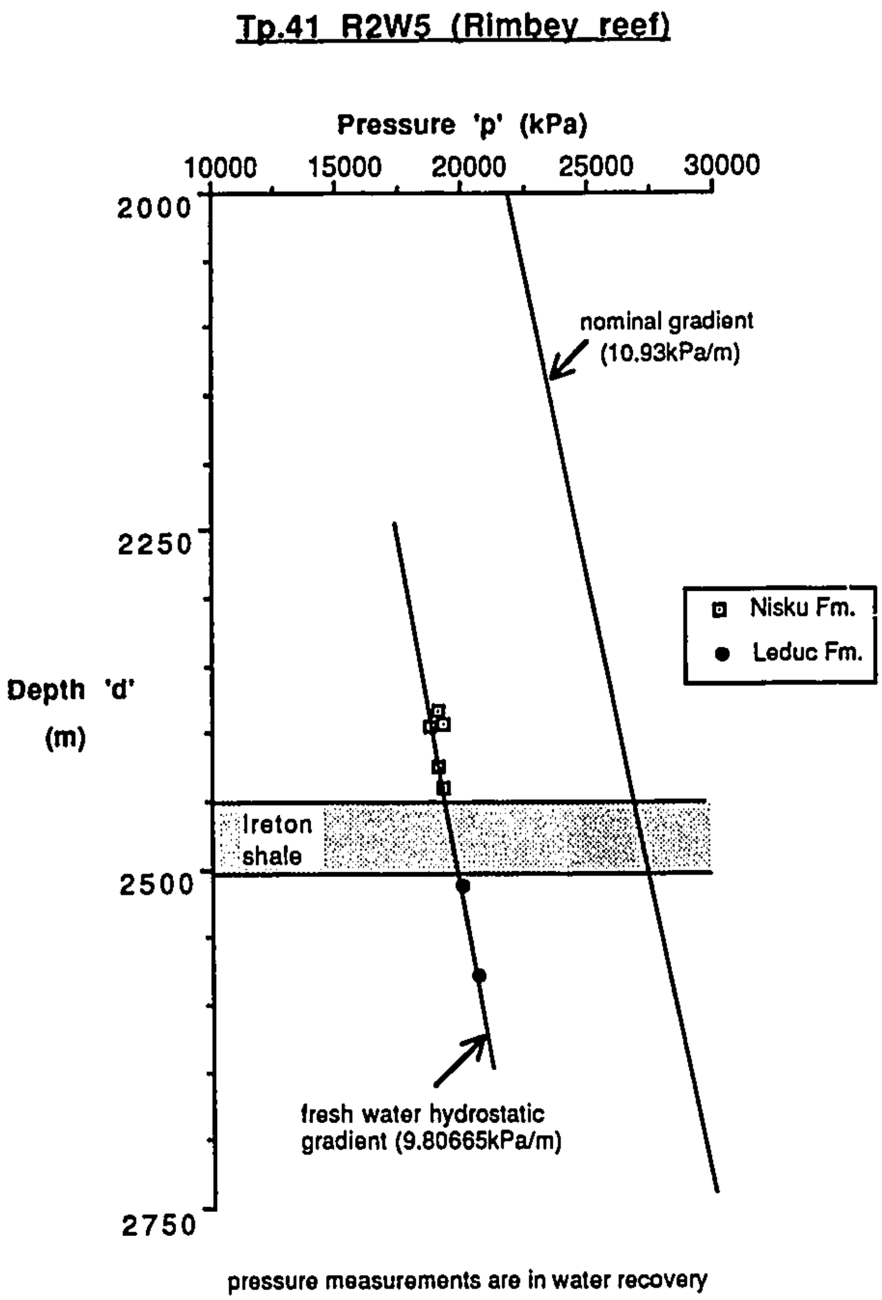

Figure 5.2 Pressure-depth plot in Tp.41 R2W5

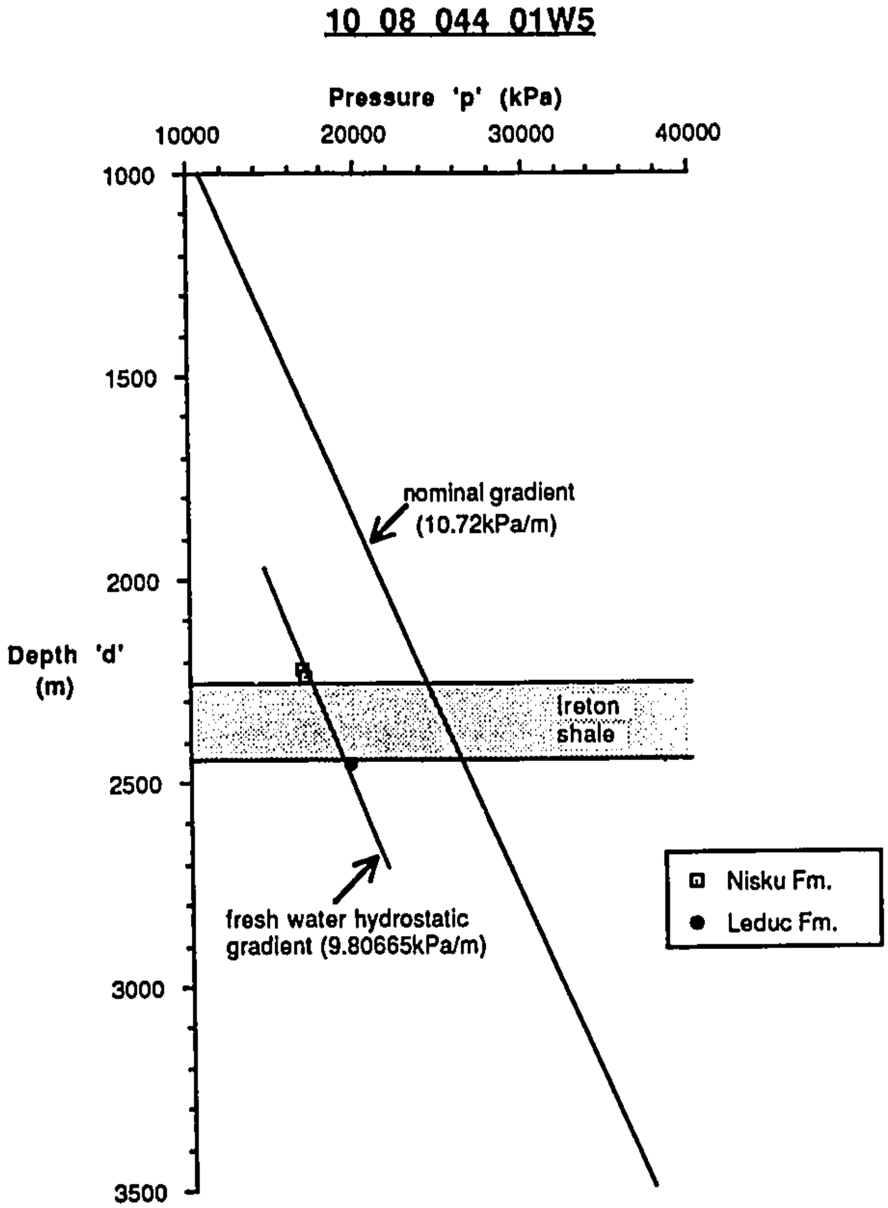

Figure 5.3 Pressure-depth plot in 10-08-044-01W5

be represented by a single gradient (fresh water hydrostatic gradient), implying weak aquitard characteristics for these shales.

Similarity in salinity distributions within geologic formations across an aquitard may be an additional indicator of cross-formational flow. In Figure 4.26 the closed high salinity contour of 200g/l around Tps.49-50, which is an anomaly for the Nisku Formation, corresponds to the salinity distribution of the underlying Leduc and Cooking Lake Formations (Figure 4.27). Further, the Stiff diagram for the Nisku Formation water sample no. 45 (located in this closed contour) has chemical characteristics, especially high Ca^{2+} concentration, similar to the Leduc Formation water. At this sample site the Ireton shale is only 40m thick. Therefore, the anomalously high salinity in the Nisku Formation may be explained if the Leduc Formation waters moved up and across the thin Ireton shale cap into this formation.

Discussions related to fluid flow

All pressure-depth analyses along the reef trend indicate negative dynamic pressure increments that would force fluids to move down within the Nisku, Leduc and Cooking Lake Formations. This observation refutes the upward movement of fluids invoked to explain the correspondence of the salinity distribution between the Nisku and Leduc Formations. This apparent contradiction in flow direction can be resolved if the present-day observed vertical flow-field is not the same as that which existed during the time of oil migration and accumulation within the reefs. A plausible explanation for such an observation is provided in the ensuing paragraphs.

According to Deroo et al (1977), the principal phase of crude oil generation in the Alberta Basin took place during the Late Cretaceous. At the same time the first minor pulse of the Laramide Orogeny caused uplift of the Canadian Cordillera. Consequently, thick clastic sequences were deposited during the Paleocene in the Foothills and across the Alberta Plains. The second major orogenic pulse began in the early Eocene - a period when most of the clastic sequence was eroded and subaerial topographic relief was at its maximum (land surface sloping northeastward in the central part of the Alberta province).

Compaction flow during the time of oil generation (Late Cretaceous) and gravity-driven flow (early Tertiary) were ascending and updip from the Foothills in the west to the basin's easternmost limit (Hitchon, 1984). The compacting Woodbend shales expelled approximately 8×10^6 m^3/km^2 of feedstock fluids laterally through the Duvernay shales into the reefs (Hugo, 1990). On the other hand, gravity-driven ascending flow must have aided in filling the reefs with the feedstock fluids.

The average pore diameter in shales estimated by Tissot and Welte (1978) is around 1nm (10^{-9}m or 10°A) at a depth of 4000m, whereas the effective diameter of a water molecule is ≈0.3nm. This implies that the Ireton shale capping the reefs acted as a barrier for the hydrocarbons (smallest pore diameter >1nm) while allowing ascending waters from the Leduc Formation to move across and into the Nisku Formation.

According to Tóth (1978), subaerial exposure of the pre-Cretaceous unconformity in northeastern Alberta resulted in the subaerial exposure of the highly permeable Devonian strata. Tóth identifies this as a relatively recent event (<4m.y. B.P.) which, by dramatically changing the boundary conditions in the basin, led to the development of the low fluid-potential drain within the Devonian strata.

The pre-Cretaceous unconformity breaches the Nisku Formation at the Redwater reef (~Long. 113° W, Lat. 54° N); while, further to the north, the pre-Cretaceous subcrop of the Grosmont complex is around Lat. 57°N. The Cooking Lake-Beaverhill Lake system subcrops at the same unconformity, close to the Alberta-Saskatchewan border. Excellent hydraulic continuity along the 600km Devonian Rimbey-Meadowbrook/Grosmont carbonate complex with its outcrop at Fort McMurray has been suggested by Hitchon (1984). Fluids would discharge by flowing along bedding planes to the unconformity's outcrops at low elevations beyond the boundaries of the study area. Approximately 350km north of the study area the Leduc Formation outcrops at an elevation of 270m. The outcrop elevation would be the maximum hydraulic head for the Leduc Formation in that area and with 400m of hydraulic head in the northern end of the study area, an average lateral hydraulic gradient of 0.0004 is computed between the present study area and the outcrop area in northern Alberta. It may, therefore, be possible that the rate at which energy of the Devonian system is dissipated by lateral flow along the unconformity to the outcrop area, exceeds the rate of regeneration of recharge; thereby, causing the pressure-depth plots to indicate negative dynamic pressure increments that force fluids to move down.

Fluids in the Nisku Formation can access the unconformity (at the Redwater reef) before fluids in the Leduc and Cooking Lake Formations (near the Alberta-Saskatchewan border). This implies that energy dissipation along the unconformity towards its outcrop would be faster for the Nisku Formation than for the Leduc and Cooking Lake Formations. This may be the mechanism that causes the potentiometric surface of the Nisku Formation to be subdued when compared to that of the Leduc and Cooking Lake Formations. Further, using a hydraulic conductivity of 2×10^{-5}m/s for the Nisku Fm. obtained from Hugo (1990), the horizontal flux (flow intensity) estimated in this formation is 1.36×10^{-8}m/s ($\approx$1.2mm/day) which is almost twice the flux within the Cooking Lake Formation.

A note on the dolomitization of the Nisku Formation

Compactional flow and regional topography (gravity) driven flow may prove effective mechanisms for subsurface dolomitization. Machel and Mountjoy (1986) believe that the Nisku Formation exemplifies dolomitization induced by burial compaction. Their observations indicate that the Nisku Formation has undergone massive post-depositional dolomitization only in the structural down-dip regions. The areal extent of massive dolomitization is necessarily limited if compaction flow is the sole mechanism for supplying dolomitizing fluids (Land, 1985), as seen in the Nisku Formation.

Fluid flow in a geologically mature basin, where compaction has ceased to exist, is governed by gravity-driven cross-formational flow (Tóth, 1980). In a gravity-driven flow, meteoric waters infiltrate to great depths in upland areas, migrate laterally under regions of medium elevations, and are discharged in lowland areas. Hitchon (1969, 1984) and Hugo (1990) have observed decreasing fluid potentials in the structurally updip regions of the Alberta Basin which is indicative of lateral gravity-driven fluid flow in the basin. In the structurally downdip regions of the study area near the Bashaw reef, gravity-driven cross-formational flow should be considered in addition to compactional flow as a cause for dolomitization of the Nisku Formation. It is possible that fluids which dolomitized the Leduc reefs of the underlying Woodbend Group also migrated up cross-formationally to the Nisku Formation via the Bashaw reef as indicated by the positive dynamic pressure increment in a pressure-depth plot (Figure 4.13) and earlier discussions.

Discussions related to the regional salinity distributions

According to Hitchon (1984), the Rimbey-Meadowbrook reef trend exhibits good hydraulic connection with the warmer, more saline deeper fluids at its southwestern end. During the early evolutionary history of the Alberta Basin, when fluid movement was upward and updip in the stratigraphic section, high salinity waters from lower formations may have moved up and into the reef trend at its southern end. Also, in southern and southeastern Alberta, the shallow water and local evaporitic deposition of the Leduc

Formation (Burrowes and Krause, 1987) must have contributed, in part, to the relatively high salinity patterns observed today.

Increase in the total dissolved solids content (TDS) within the Nisku, Leduc and Cooking Lake Formations in the northeastward regional flow direction is not conspicuous (Figures 4.26 and 4.27). Instead, a zone of lower total dissolved solids content is encountered in the northeastern half of the study area.

Unlike most minerals, the solubilities of calcite and dolomite decrease at higher temperatures because CO_2 is less soluble at higher temperatures. Therefore, in a carbonate terrain, like the present study area, low TDS content in the flow direction is not unusual (Freeze and Cherry, 1979). However, this argument fails to explain the low TDS content in the northeastern (updip) half of the study area, where lower formation temperatures would increase the solubilities of these minerals and consequently the total dissolved solids.

Mixing of lower salinity waters from geologic formations with those from the Nisku, Leduc and Cooking Lake Formations waters was another process that could have created the low salinity zones. Mixing as described by Hitchon and Friedman (1969) is *"a slow percolation of water through the basin, carrying with it the dissolved salts, and simultaneously changing both the composition of the inflowing water and the water in the basin"*.

The Nisku Formation waters with TDS<160g/l occupying the low salinity zone in the northeastern portion of Figure 4.26 were represented by the Stiff diagram constructed using the average ionic concentrations minus one standard deviation (Figure 4.15a). A visual comparison of the Stiff diagrams (Figures 4.15a and 4.18) indicates that the water analyses in this zone are similar to those of the average Basal Mannville waters of Cretaceous age. The Basal Mannville Formations overlie the pre-Cretaceous unconformity. A sequence of carbonate strata is present between the top of the Nisku Formation and the pre-Cretaceous unconformity. An isopach between the top of the Nisku Formation to the pre-Cretaceous unconformity shows a general thinning of these carbonate strata towards the northeast with contours running NW-SE (Figure 5.4). The NW-SE orientation of these contours is roughly similar to the orientation of the low salinity zone boundary in the northeast portion of Figure 4.26. Downward leaking of the Cretaceous Formation waters through the thin carbonate sequence, which have relatively higher permeabilities compared to other rock types, may facilitate mixing in the northeast portions of the study area. The Nisku Formation that subcrops at the unconformity near the Redwater reef is the locus of initial mixing with the Cretaceous waters (Figure 5.5). It is, therefore, concluded that the unconformity has played an important role in controlling the pattern of mixing of the Cretaceous with the Nisku waters.

A similar low salinity zone, but with a smaller areal extent is noted in the isosalinity map of the Leduc and Cooking Lake Formations (Figure 4.27). Again, a similar argument has been invoked to explain this observation. The Stiff diagrams for the water analyses in this zone are similar to Cretaceous Formation waters but with a relatively higher calcium content. The Leduc and Cooking Lake Formations subcrop at the pre-Cretaceous unconformity close

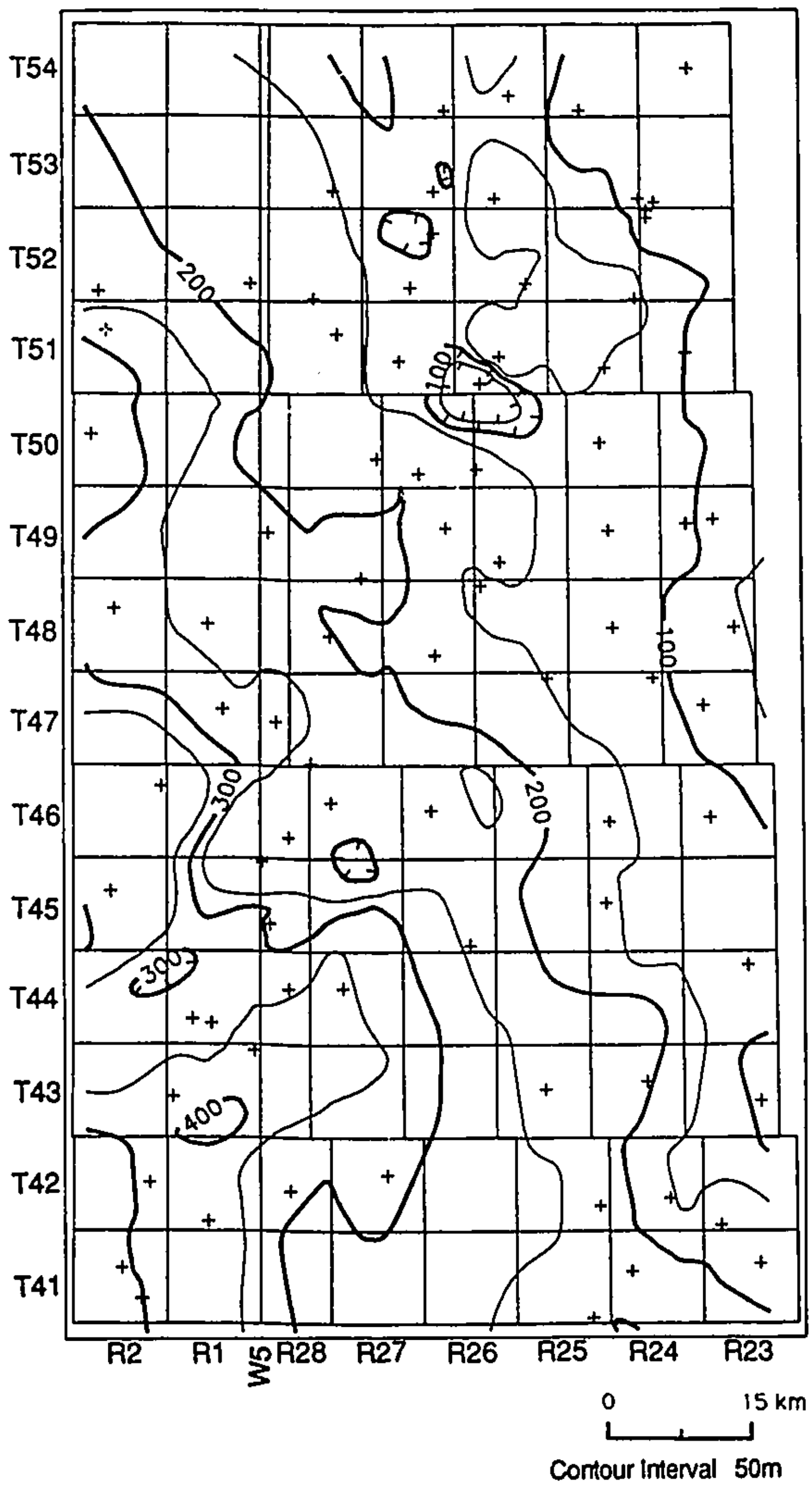

Figure 5.4 Isopach of the top of the Nisku Fm. to the pre-Cretaceous unconformity

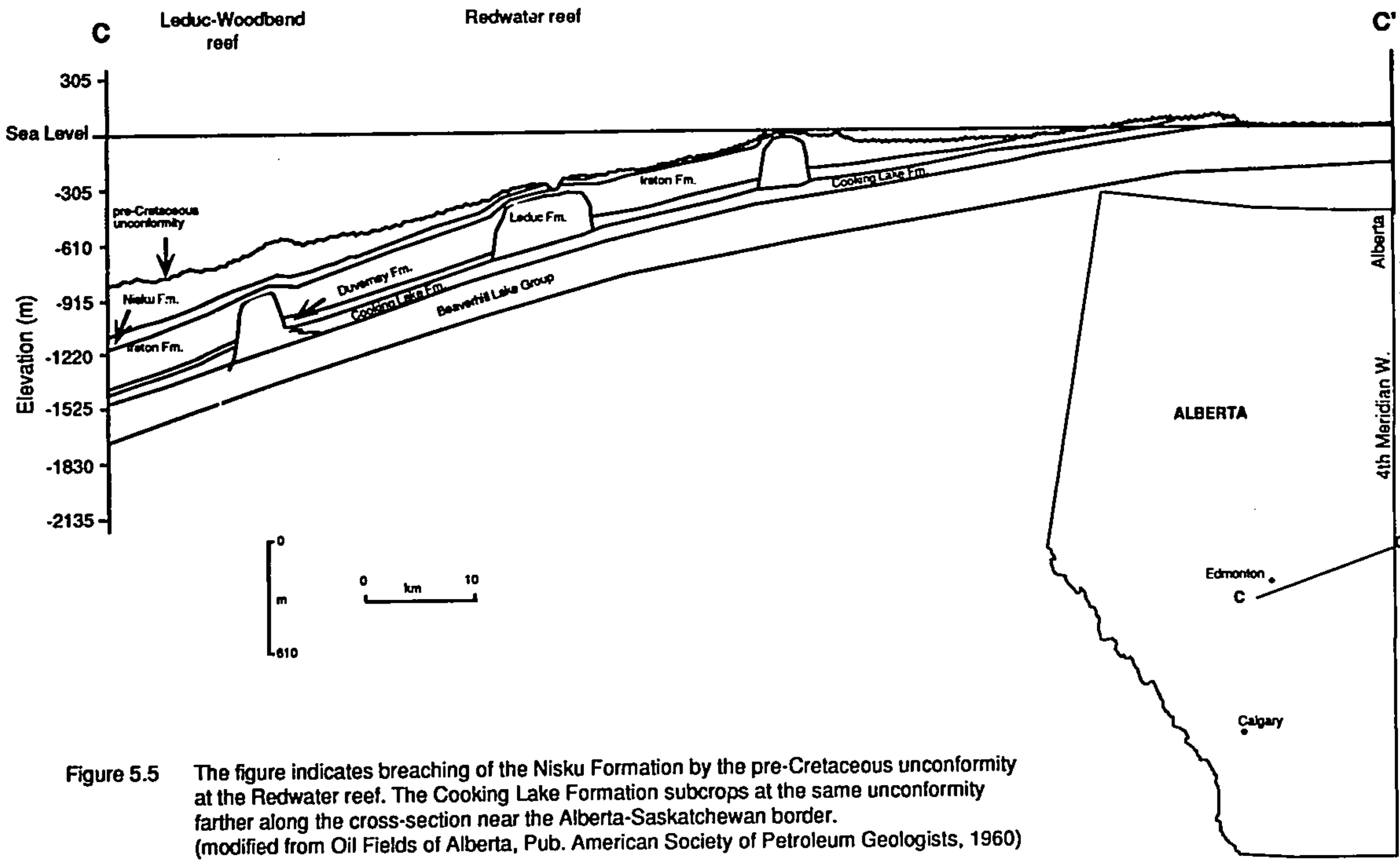

Figure 5.5 The figure indicates breaching of the Nisku Formation by the pre-Cretaceous unconformity at the Redwater reef. The Cooking Lake Formation subcrops at the same unconformity farther along the cross-section near the Alberta-Saskatchewan border.
(modified from Oil Fields of Alberta, Pub. American Society of Petroleum Geologists, 1960)

to the Alberta-Saskatchewan border (Figure 5.5). Therefore, dilution in these formations by the Cretaceous Formation waters must have taken place farther away from the Redwater reef, to the northeast.

Cross-sections showing the distribution of salinity (TDS) and the freshwater hydraulic heads have been presented to summarize the observations regarding fluid flow directions and its relation to salinity (Figures 5.6 to 5.9).

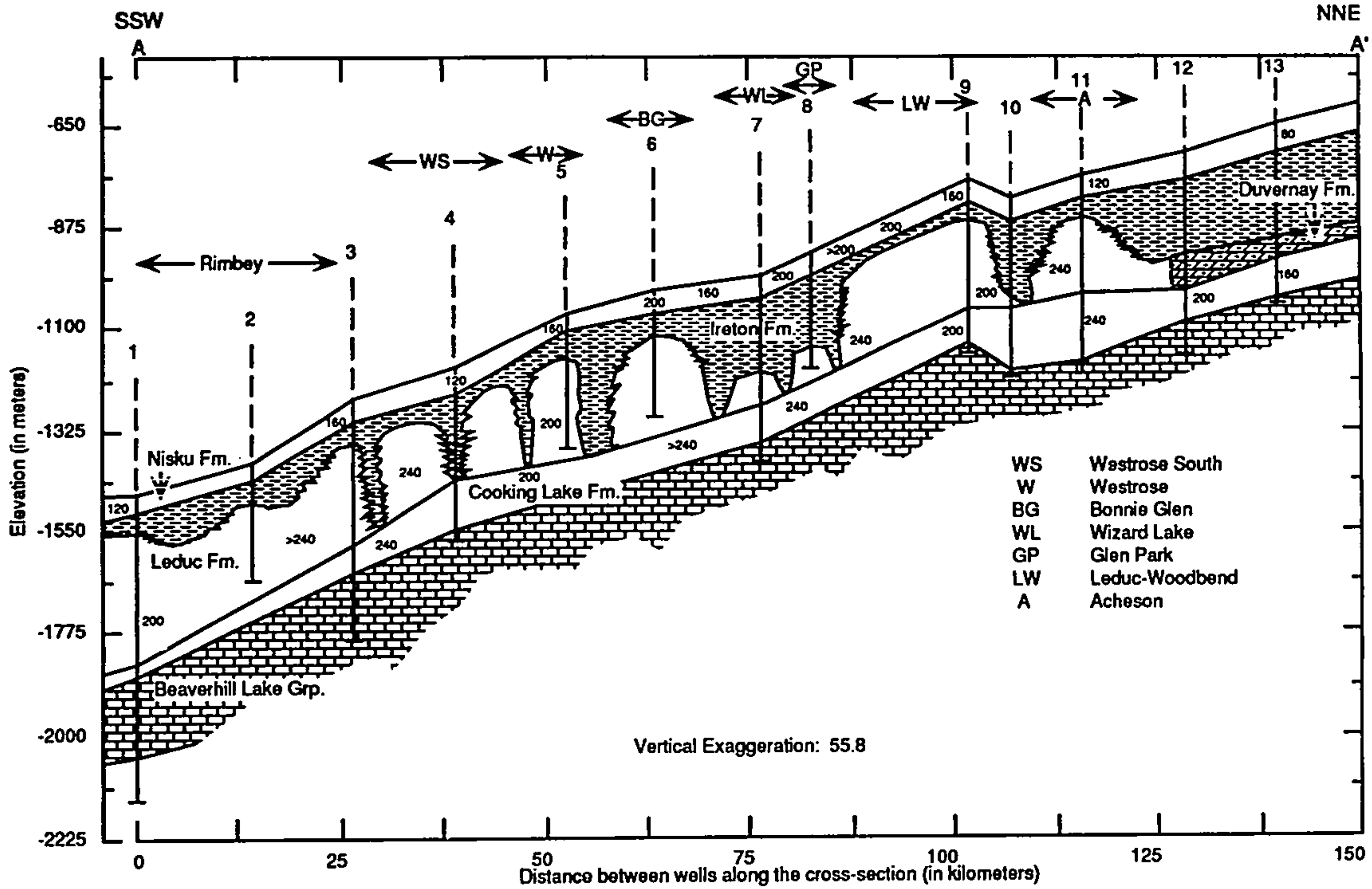

Figure 5.6 Cross-section (A-A') showing salinity (TDS in g/l) distribution

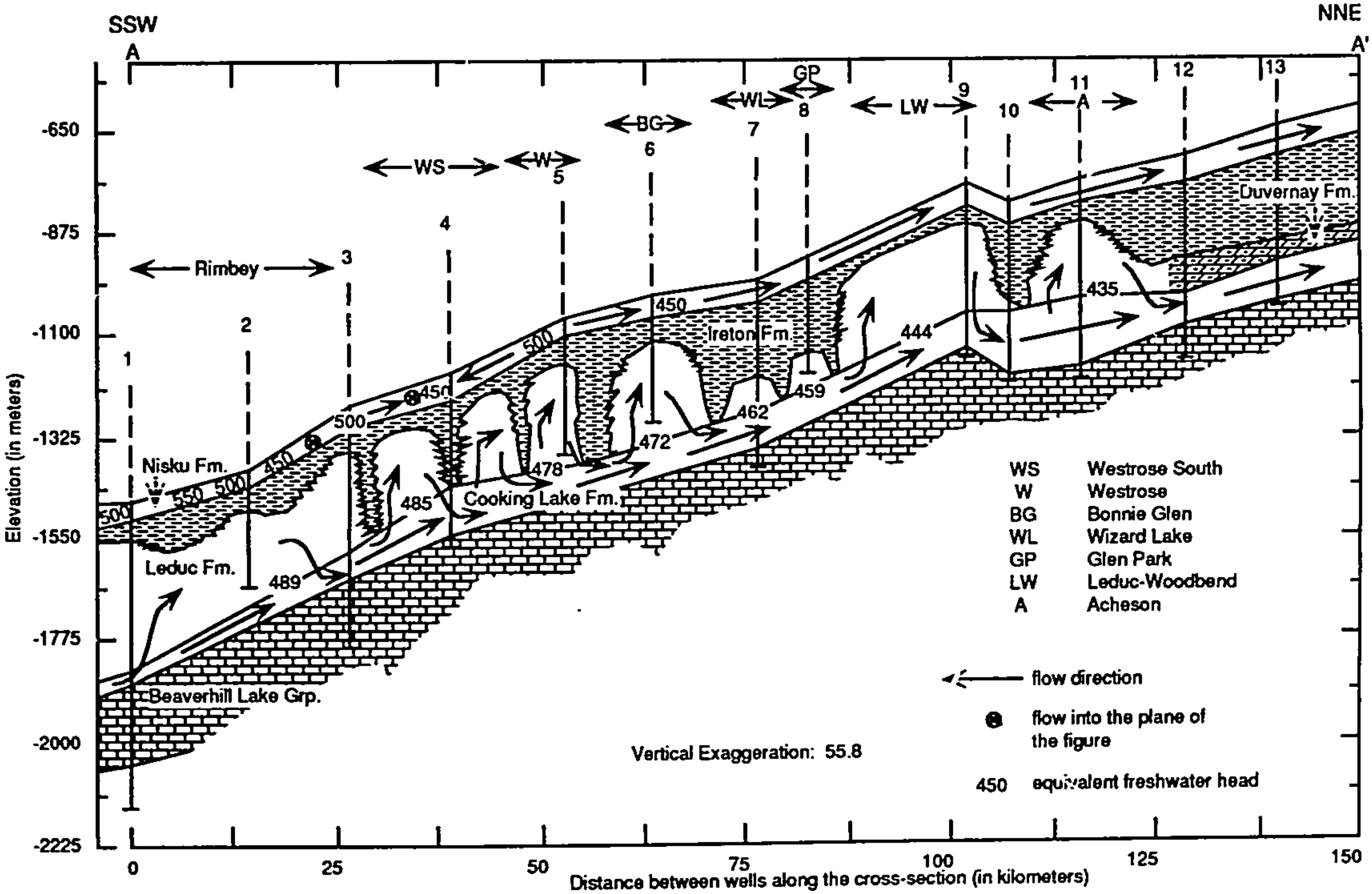

Figure 5.7 Cross-section (A-A') showing equivalent freshwater head distribution in meters and flow directions

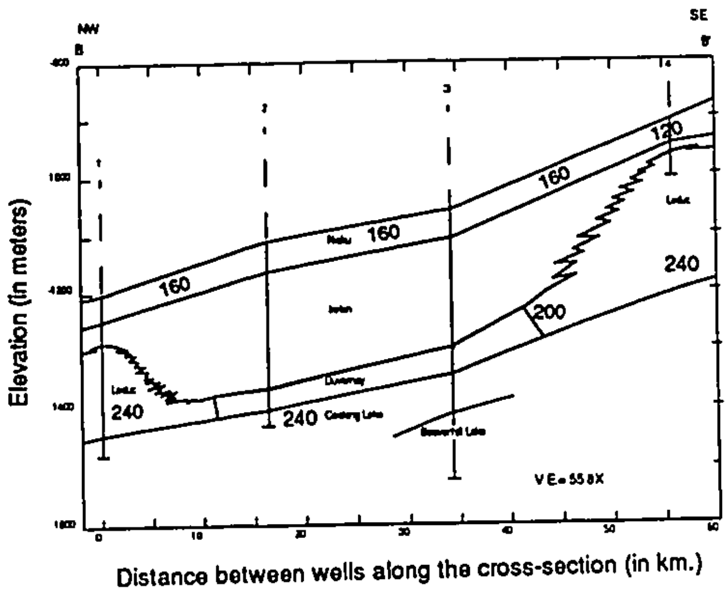

Figure 5.8 Cross-section (B-B') showing salinity (TDS in g/l) distribution

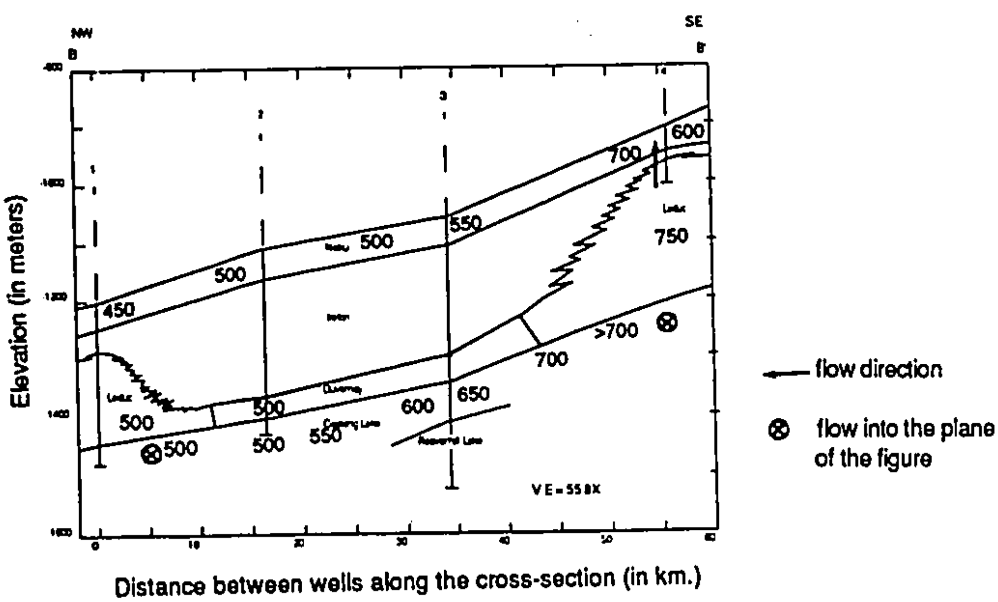

Figure 5.9 Cross-section (B-B') showing equivalent freshwater head distribution in meters

Chapter 6 Conclusions

The major conclusions drawn from this study are enumerated below.

i) Uninterrupted regional northeastward fluid flow within the Leduc and Cooking Lake Formations is active. The fluid flow direction follows the slope of the land surface. In general, regional fluid flow in the Nisku Formation is directed northwards except in the vicinity of the Westrose South reef where fluids tend to move west.

ii) Due probably to the higher rate of energy dissipation along the pre-Cretaceous unconformity, equivalent freshwater heads in the Nisku Formation are lower than those in the Leduc and Cooking Lake Formations along the reef trend. Horizontal fluid flux in the Nisku Formation is 1.36×10^{-8}m/s whereas it is 5.4×10^{-9}m/s within the Cooking Lake Formation. The estimated horizontal fluid flux in the Cooking Lake Formation is 500 times the flux between the Rimbey and Westrose South reefs through the Ireton shales. Therefore, the Cooking Lake Formation can be considered to act as a conduit which is channelling fluids along the reef trend.

iii) Due to weak aquitard characteristics of the relatively thin Ireton shales capping the Bashaw Reef Complex, similar configurations and elevations of the potentiometric surfaces in the Nisku, Leduc and Cooking Lake Formations are observed in this reef complex.

iv) At the Bashaw reef location, the Leduc Formation waters move up and into the Nisku Formation with a fluid flux of 1.49×10^{-8}m/s. Gravity-driven cross-formational flow must be considered as a possible mechanism for the extensive dolomitization of the Nisku Formation observed in its structurally downdip regions.

v) The pre-Cretaceous unconformity plays a vital role in controlling the salinity distribution within the Nisku, Leduc and Cooking Lake Formations. Fluid flow directions show no conspicuous control in the salinity distribution. Mixing of low salinity Cretaceous waters with the Nisku, Leduc and Cooking Lake Formations is seen in the northeastern corner of the study area.

vi) The scattered data in the salinity versus Mg/Ca ratio plots for the Nisku, Leduc and Cooking Lake Formations indicate that waters in these formations have not yet reached equilibrium with respect to calcite and dolomite saturation.

REFERENCES

Akhter, M.S. and C.W. Kreitler, 1990, Reliability and applicability of DST's and bottom-hole pressure measurements in Texas Gulf Coast Tertiary formations: Journal of Petroleum Science and Engineering, 3, p. 287-303.

Alberta Society of Petroleum Geologists, 1960, Oil Fields of Alberta - A reference volume.

Andrichuk, J.M., 1958a, Cooking Lake and Duvernay (Late Devonian) sedimentation in Edmonton area of Central Alberta, Canada: Amer. Assoc. of Petrol. Geol. Bull., 42 (9), p. 2189-2222.

Andrichuk, J.M., 1958b, Stratigraphy and Facies analysis of Upper Devonian reefs in Leduc, Stettler, and Redwater areas, Alberta: Amer. Assoc. of Petrol. Geol. Bull., 42 (1), p. 1-93.

Bachu, S. and J.R. Underschultz, 1992, Regional-Scale Porosity and Permeability Variations, Peace River Arch Area, Alberta, Canada: Amer. Asssoc. of Petrol. Geol. Bull., 76 (April 1992), p. 547-562.

Back, W., 1961, Techniques for mapping of hydrochemical facies: U.S. Geol. Surv. Prof. Paper, (424-D), p. 380-382.

Back, W. and B.B. Hanshaw, 1965, Chemical geohydrology: In Adv. Hydrosci., 2, p. 49-109.

Barfoot, G.L. and S.C.M. Ko, 1987, Assessing, and compensating for, the impact of the Leduc D-3A gas cap blowdown on the other Golden Trend pools: Can. Petrol. Tech., 26 (4), p. 28-36.

Bear, J., 1972, Dynamics of Fluids in Porous Media, Republished by Dover Publications, Inc., 764p.

Belyea, H.R., 1952, Notes on the Devonian System of the North-Central Plains of Alberta: Geol. Survey Canada Paper, 52-27.

Belyea, H.R., 1955, Cross-sections through the Devonian System of the Alberta Plains: Geol. Survey Canada Paper, 55-3, p.1-29.

Burrowes, O.G., and F.F. Krause, 1987, Overview of the Devonian System: Subsurface of Western Canada Basin, *In* Devonian Lithofacies and Reservoir Styles in Alberta, 13th CSPG Core Conference and Display, 2nd International Symposium on the Devonian System, 286p.

Chebotarev, I.I., 1955, Metamorphism of natural waters in the crust of weathering, Part 1-3: Geochimica et Cosmochimica Acta, 8, p. 22-48, 137-170, 198-212.

Cushman, J.H., 1984, On unifying the concepts of scale, instrumentation, and stochastics in the development of multiphase transport theory: Water Resources Research, 20, p. 1668-1676.

Dagan, G., 1989, Flow and transport in porous formations: Springer-Verlag Berlin Heidelberg, 465p.

Dahlberg, E.C., 1982, Applied hydrodynamics in petroleum exploration: New York, Springer-Verlag, 161p.

Davies, P.B., 1987, Dublin, Ohio , Modeling areal, variable-density groundwater flow using equivalent freshwater head - analysis of potentially significant errors: In N.W.W. Association (ed.), Conference on Solving Groundwater Problems with Models, p. 888-903.

de Marsily, G., 1986, Quantitative Hydrogeology: Groundwater Hydrology for Engineers, Academic Press, Inc., 440p.

Deroo, G., T.G. Powell, B. Tissot, and R.G. McCrossan, 1977, The origin and migration of petroleum in the Western Canadian Sedimentary Basin, Alberta - a geochemical and thermal maturation study: Geological Survey of Canada Bull., 262, 136p.

Downing, J.A. and D.Y. Cooke, 1955, Distribution of reefs of Woodbend Group in Alberta, Canada: Amer. Assoc. Petrol. Geol. Bull., 39 (2), p. 189-206.

Freeze, R.A., 1975, A stochastic-conceptual analysis of one-dimensional groundwater flow in nonuniform homogeneous media: Water Resources Research, 11, p. 725-741.

Freeze, R.A. and J.A. Cherry, 1979, Groundwater: Englewood Cliffs, Prentice-Hall, 604p.

Gussow, W.C., 1954, Differential entrapment of oil and gas: a fundamental principle: Amer. Assoc. of Petrol. Geol. Bull., 38 (5), p. 816-853.

Hitchon, B., 1969a, Fluid flow in the Western Canada Sedimentary Basin: 1. Effect of topography.: Water Resour. Res., 5, p. 186-195.

Hitchon, B., 1969b, Fluid flow in the Western Canada Sedimentary Basin: 2. Effect of Geology: Water Resour. Res., 5, p. 460-461.

Hitchon, B. and I. Friedman, 1969, Geochemistry and origin of formation waters in the Wesetern Canada Sedimentary Basin - I. Stable isotopes of hydrogen and oxygen: Geochimica et Cosmochimica Acta, 33 , p. 1321-1349.

Hitchon, B., 1984, Geothermal gradients, hydrodynamics, and hydrocarbon occurrences, Alberta, Canada : Amer. Assoc. of Petrol. Geol. Bull., 68 (6), p. 713-743.

Hnatiuk, J. and J.W. Martinelli, 1967, The relationship of the Westrose D-3 Pool to other pools on the Common Aquifer: Can. Petrol. Tech., 6 (2), p. 43-49.

Horner, D.R., 1951, Pressure build-up in wells: Third World Petrol. Congress, Proc., Sect. II: Leiden, Holland, p. 503-521.

Hubbert, M.K., 1940, The theory of groundwater motion: Journal of Geology, 48 (8), p. 785-944.

Hugo, K.J., 1990, Mechanisms of groundwater flow and oil migration associated with Leduc reefs: Can. Soc. Petrol. Geol. Bull., 38 (3), p. 307-319.

Imperial Oil Limited, Geological Staff, 1950, Devonian Nomenclature in the Edmonton Area, Alberta, Canada: Amer. Assoc. of Petrol. Geol. Bull., 34 (9), p. 1807-25.

Jankowski, J. and G. Jacobson, 1989, Hydrochemical evolution of regional groundwaters to playa brines in Central Australia: Hydrology, 108 , p. 123-173.

Jensen, J.L., D.V. Hinkley and L.W. Lake, 1987, A statistical study of reservoir permeability: distributions, correlations, and averages: SPE Formation Evaluation, p. 461-468.

Johnston, R.H., 1988, Opus Handbook: Formation Waters of Alberta, Opus Petroleum Engineering Ltd., Calgary.

Land, L.S., 1985, The origin of massive dolomite: J. Geol. Educ., 33 , p. 112-125.

Lucia, F.J., 1986, Permeability estimated from subsurface data, Grayburg Formation-Dune field Crane Country, West Texas: SEPM, 86-26, p. 113-117.

Maccagno, M., 1991, The common use of pressure-depth and pressure-elevation plots to analyze groundwater flow: MSc. Thesis (unpublished), University of Alberta.

Machel, H.G. and E.W. Mountjoy, 1986, Chemistry and environments of dolomitization - a reappraisal: Earth Science Reviews, 23 , p. 175-222.

Machel, H.G. and E.W. Mountjoy, 1987, General constraints on extensive dolomitization - and their application to the Devonian carbonates of Western Canada: Can. Soc. Petrol. Geol. Bull., 35 (2), p. 143-158.

McCourt, G.B., 1953, Recent developments in the Leduc-Woodbend Field: Alberta Soc. Petrol. Geol. Bull., 1 (11), p. 39-42.

McCrossan, R.G., 1961, Resistivity mapping and petrophysical study of upper Devonian inter-reef calcareous shales of central Alberta, Canada: Amer. Assoc. Petrol. Geol. Bull., 45 , p. 441-470.

McNamara, L.B. and N.C. Wardlaw, 1991, Geological and statistical description of the Westrose Reservoir, Alberta: Can. Soc. Petrol. Geol. Bull., 39 (4), p. 332-351.

Orr, E. and C. Kreitler, 1985, Interpretation of pressure-depth data from confined underpressured aquifers exemplified by the Deep Basin Brine Aquifer, Palo Duro Basin, Texas: Water Resour. Res., 21 (4), p. 533-544.

Pakhomov, S.I. and I.G. Kissin, 1973, Hydrogeochemistry of magnesium in deep aquifer zones: Akad. Nauk SSSR Doklady, v.209, p. 205-208. [English translation, 1974, Am. Geol. Inst., Doklady Akad, Nauk SSSR, v. 209, p. 200-203].

PUBCO, 1990, CD-ROM, Geobase well database

Reitzel, G.A. and G.O. Callow, 1977, Pool description and performance analysis leads to understanding Golden Spike's miscible flood: Petrol. Tech., 29, p. 867-872.

Roberts, W., 1980, Design and function of oil and gas traps: In W.H. Roberts III and R.J. Cordell (ed.), Problems of Petroleum Migration, AAPG Studies in Geology No. 10, p. 121-169.

Schlumberger, 1989, Log Interpretation Principles/Applications.

Smith, J.E., 1971, The dynamics of shale compaction and evolution of the pore-fluid pressure: Math. Geol., 3 (3), p. 239-263.

Stoakes, F.A., 1980, Nature and control of shale basin fill and its effects on reef growth and termination: upper Devonian Duvernay and Ireton formmations of Alberta: Can. Soc. Petrol. Geol. Bull., 28, p. 345-410.

Stoakes, F.A. and S. Creaney, 1984, Sedimentology of a carbonate source rock: The Duvernay Formation of Central Alberta: In L. Eliuk (ed.), Carbonates in subsurface and outcrops, Can. Soc. Petrol. Geol. Core Conference 1984, p. 132-147.

Tissot, B.P. and D.H. Welte, 1978, Petroleum formation and occurrence. Springer-Verlag, New York, 538p.

Tóth, J., 1962, A theory of groundwater motion in small basins in central Alberta, Canada: Journal of Geophysical Research, 67, p. 4375-4387.

Tóth, J., 1978, Gravity-induced cross-formational fluid flow in Red Earth region, Alberta.: Water Res. Research, 14 (5), p. 805-843.

Tóth, J., 1979, Patterns of dynamic pressure increment of formation fluid flow in large drainage basins exemplified by the Red Earth Region.: Can. Soc. Petrol. Geol., 27 (1), p. 63-86.

Tóth, J., 1980, Cross-Formational Gravity-Flow of Groundwater: A Mechanism of the Transport and Accumulation of Petroleum (The Generalized Hydraulic Theory of Petroleum Migration). In: Problems of Petroleum Migration. W.H. Roberts III and R.J. Cordell (eds.). American Association of Petroleum Geologists, AAPG Studies in Geology No. 10, p. 121-169.

Tóth, J. and T. Corbet, 1986, Post-Paleocene evolution of regional groundwater flow-systems and their relation to petroleum accumulations, Taber area, southern Alberta, Canada.: Can. Soc. Petrol. Geol., 34 (3), p. 339-363.

Tóth, J. and K. Rakhit, 1988, Exploration for reservoir quality rock bodies by mapping and simulation of potentiometric surface anomalies: Can. Soc. Petrol. Geol., 36 (4), p. 362-378.

Tóth, J., 1990, Hydraulic continuity in large sedimentary basins: International Conference on Groundwater in Large Sedimentary Basins, Perth, Australia.

White, D.E., 1965, Saline waters of sedimentary rocks: AAPG, Mem. 4, p. 342-366.

Appendix I

Calculation of equivalent fresh water hydraulic head using pressure measurements in a hydrocarbon pool

The rate of pressure change or vertical pressure gradient ($\gamma=\rho g$) is dependent on the density (ρ) of a fluid. Lighter fluids will show a steeper gradient than heavier fluids. At a given depth, pressures recorded by a DST in a hydrocarbon pool (oil or gas) would be higher than those recorded in the absence of hydrocarbons. Thus, hydraulic heads computed using pressures recorded in hydrocarbon pools are often anomalously high compared to those calculated using pressure measurements within a water column.

In the study area, the Westrose South reef is entirely a gas pool. This reef has been chosen as an example to show how pressure measurements in a gas pool can be used to obtain equivalent freshwater hydraulic heads. Leduc Formation DST's in 7-15-044-1W5, 7-16-044-1W5 and 7-10-045-1W5 were conducted in the gas pool. A pressure-elevation plot generated using these DST's provided a gas gradient represented by the equation $z=5207.6-0.35p$ (Figure A1). Solving this equation using $z=-1453.3$ (the gas-water contact at subsea elevation) gives the coordinates of the intersection of the gas pressure gradient and the gas-water contact. The coordinates of this intersection are (p,z)::(18998.5, -1453.3). At zero pressure the intercept of a pressure gradient on the elevation axis is the hydraulic head. Using the fresh water hydrostatic gradient (9.80665kPa/m) the intercept (fresh water hydraulic head) was calculated as below.

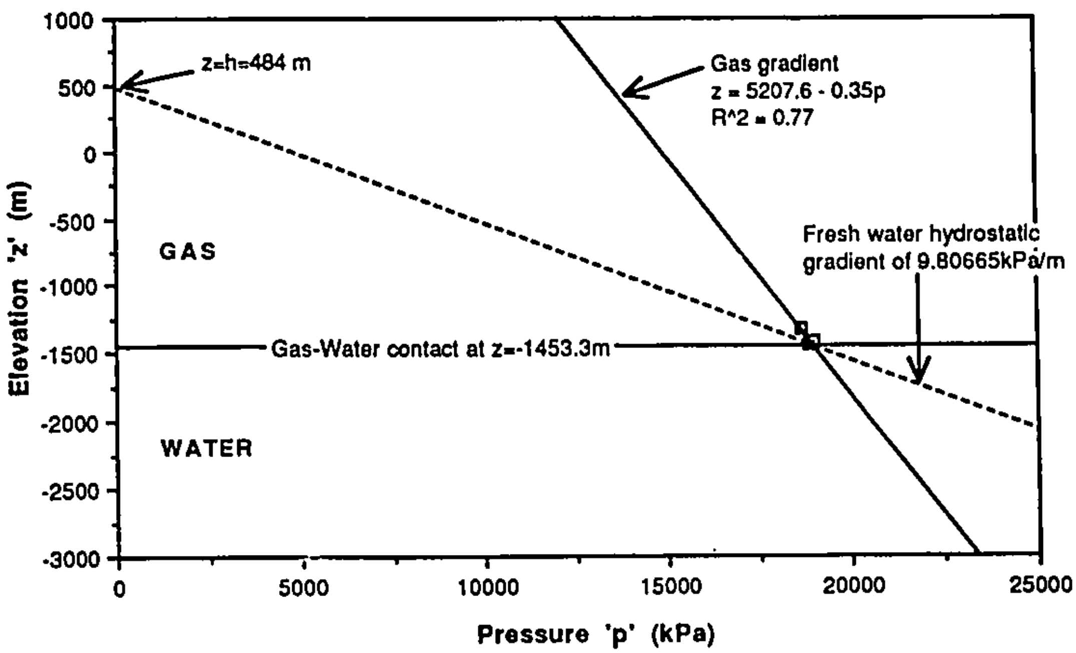

Figure AI Pressure-elevation plot for DST conducted in the gas leg in the Westrose South reef

Since, the slope m of a line in cartesian coordinates is given by : $m = \frac{y_2 - y_1}{x_2 - x_1}$

$$\therefore \quad -9.80665 = \frac{18998.5 - 0}{-1453.3 - h^*}$$

or, $h^* = 484$m (This is the corrected hydraulic head for the DST's conducted in the gas pool)

It is noted that the corrected hydraulic head compares closely with the hydraulic head obtained by using the initial pool pressure (h^*=485m) as well as with those computed using the Leduc Fm. DST's in the water column (h^*= 486 and 488m) of the Westrose South reef.

Appendix II

Fluid flux (or flow intensity) calculations

The specific discharge or fluid flux q_i is defined as the volume of fluid moving through a unit cross-sectional area per unit time. It has the dimensions of $L^3L^{-2}T^{-1}$ (LT^{-1}). In fact, its physical meaning implies the intensity of fluid flow. Using Eq. 4.3 the horizontal and vertical fluxes are given by the following equations -

$$q_x = -K_{xx}\left(\frac{\partial h^*}{\partial x}\right) \quad \text{........................ Eq. (4.6)}$$

and $$q_z = -K_{zz}\left(\frac{\partial h^*}{\partial z} + \rho_r\right) \quad \text{........................ Eq. (4.7)}$$

where,

q_x, q_z are the horizontal and vertical fluxes, respectively.

K_{xx}, K_{zz} are the hydraulic conductivity tensors in the horizontal and vertical directions, respectively. Assuming the principal directions of anisotropy coincide with the coordinate axes. In which case $K_{xx} = K_x$ and $K_{zz} = K_z$.

$\frac{\partial h^*}{\partial x}, \frac{\partial h^*}{\partial z}$ are fresh water hydraulic gradients in the horizontal and vertical directions, respectively.

From Equation 3.6,

$$\frac{\partial h^*}{\partial z} = 1 + \frac{1}{\rho_o g}\frac{\partial p}{\partial z}$$

where

$\frac{\partial p}{\partial z}$ can be known using the relation $-\frac{\partial p}{\partial z} = \frac{\partial p}{\partial d}$

($\frac{\partial p}{\partial d}$ is same as the measured gradient in pressure-depth plots).

The average permeabilities in Table 3 were used to obtain hydraulic conductivities for the reefs in the Rimbey-Meadowbrook Trend. The geometric mean of the permeabilities for all the reefs in the study was the assumed permeability of the Bashaw reef. The hydraulic conductivities were calculated using a viscosity of 0.44×10^{-3} Pa s @ 66^{0}C which is the average bottom hole temperature obtained from the DST's. Hydraulic conductivities for the Nisku, Ireton and Cooking Lake Formations were accepted from Hugo (1990). The values used were 2×10^{-5} m/s, 1.7×10^{-9} m/s, 2×10^{-6}m/s for the respective formations.

A sample calculation of the horizontal flux between Rimbey and Westrose South reefs through the Ireton shale

Hydraulic head at Rimbey reef = 489m
Hydraulic head at Westrose South reef = 485m
Approximate distance between the reefs = 30×10^{3}m
Geometric mean of hydraulic conductivities of Rimbey and Westrose South reefs and Ireton Fm. = 9.78×10^{-8}m/s
Therefore, horizontal flux q_x = 1.3×10^{-11}m/s
$\approx$ 0.0011mm/day

It may be argued that the average temperature at which the viscosity is calculated cannot represent the entire reef trend. Hitchon (1984) showed that the geothermal gradient along the reef trend varies from 30^{0}C/km in the south to 33^{0}C/km in the north of the trend. To be more accurate the bottom-hole temperature for the two reefs should be around 80^{0}C at 2500m depth. At this temperature the recalculated hydraulic conductivity, based on a viscosity of 0.34×10^{-3} Pa s, resulted in a fluid flux of 1.55×10^{-11}m/s ($\approx$0.0013mm/day). It indicates that the error incorporated in using the average temperature for viscosity estimation and consequently fluid flux calculation is insignificant.

A sample calculation of vertical flux in the Bashaw reef

A vertical hydraulic conductivity of 6.76×10^{-8}m/s for the Leduc Fm. in the Bashaw reef was calculated from the geometric mean of the vertical permeabilities of the reefs in the trend.

From the p(d) plot (Figure 4.13) $\frac{\partial p}{\partial d} = 13.409$kPa/m

therefore, $\frac{\partial p}{\partial z} = -13.409$kPa/m

Hence, $\frac{\partial h^*}{\partial z} = 1 + \frac{1}{\rho_o g}\frac{\partial p}{\partial z} = -0.367$

(negative sign means hydraulic head increases downwards; implying upward flow)

The fluid density $\rho = 1.147$g/cm^3 (averaged over 1779.1-2149.4m; refer Leduc waters in Table 7)

$\therefore \quad \rho_r = 0.147$

Using Eq. 4.7 the vertical flux $q_z = 1.487 \times 10^{-8}$m/s
≈ 1.28mm/day

Fluids from the Bashaw reef move up and into the Nisku Fm. with an intensity of 1.487×10^{-8}m/s. If the total area through which fluids move is known the volumetric flow may be estimated by multiplying the fluid flux and total area.

Appendix III

Data and tables used in the thesis

Table 1 Wells used for cross-sections A-A' & B-B'

Well nos.	Wells used for cross-section A-A'
1	14-05-041-2W5
2	07-22-042-2W5
3	03-29-043-1W5
4	12-25-044-1W5
5	02-10-046-28W4
6	07-07-047-27W4
7	03-22-048-27W4
8	07-02-049-27W4
9	08-34-050-26W4
10	06-11-051-26W4
11	14-03-052-26W4
12	10-04-053-25W4
13	07-10-054-25W4

Well nos.	Wells used for cross-section B-B'
1	08-09-044-1W5
2	11-34-043-27W4
3	03-26-042-26W4
4	06-26-041-24W4

Table 2 Well scale permeability and porosity for 60 wells in the Leduc Formation

LSD. Sec. T. R. M.	Cored Interval (m)		Average Permeability (md)		Av. Porosity
	Top	Bottom	Horizontal 'kx'	Vertical 'kz'	%
14 34 045 28 4	2219.2	2226.0	8.96	3.19	4.52
02 03 046 28 4	2204.0	2211.2	7.60	2.25	8.13
01 10 046 28 4	2185.0	2196.6	26.80	1.08	4.76
09 14 046 28 4	2030.6	2087.8	41.54	2.01	6 75
15 24 046 28 4	2012.6	2180.8	514.80	6.02	10.53
14 36 046 28 4	2035.1	2207.2	313.10	4.55	10.22
15 17 047 27 4	2137.9	2139.8	140.10	1.12	12.50
07 29 047 27 4	2110.3	2151.6	690.50	2.44	8.83
01 05 048 27 4	2106.5	2114.1	3.35	0.38	3.83
07 09 048 27 4	2014.1	2028.7	508.03	8.26	8.03
16 16 048 27 4	1840.4	1876.8	350.03	36.05	11.74
03 22 048 27 4	1986.0	2136.3	202.20	5.24	10.75
01 28 048 27 4	1997.6	2008.1	144.40	2.23	9.16
14 25 049 26 4	1633.1	1639.2	1033.40	76.38	10.71
14 34 049 26 4	1647.7	1651.4	113.86	5.32	5.10
11 02 049 27 4	1903.0	1914.1	128.30	3.21	7.68
04 24 049 27 4	1705.1	1709.0	11.55	0.75	8.29
03 06 050 26 4	1570.3	1590.4	6.74	-	9.71
01 11 050 26 4	1629.2	1639.9	86.14	7.15	9.14
08 34 050 26 4	1735.0	1737.5	0.34	-	6.90
10 12 050 27 4	1652.0	1670.0	94.27	2.44	7.93
14 15 051 26 4	1611.5	1623.7	731.00	37.39	11.73
06 21 051 26 4	1595.1	1620.0	123.30	5.96	8.16
05 24 051 27 4	1807.0	1813.0	3.29	0.50	8.51
13 24 051 27 4	1807.2	1813.9	4.55	1.51	9.98
04 26 051 27 4	1634.3	1647.6	93.97	6.51	9.83
	1656.3	1665.1			
08 26 051 27 4	1813.8	1824.6	3.99	0.67	6.71
01 27 051 27 4	1668.8	1806.2	86.96	8.59	9.40
07 34 051 27 4	1819.8	1824.5	0.60	1.13	5.38
13 03 052 26 4	1534.1	1556.5	165.20	9.09	11.63
12 07 052 26 4	1389.2	1395.7	6.00	2.34	9.80
06 22 052 26 4	1563.1	1666.8	218.36	4.34	7.49

LSD. Sec. T. R. M.	Cored Interval (m)		Average Permeability (md)		Av. Porosity
	Top	Bottom	Horizontal 'kx'	Vertical 'kz'	%
15 34 052 26 4	1551.1	1553.8	708.19	8.14	9.45
07 02 053 26 4	1624.0	1637.7	7.65	0.28	9.47
05 25 053 26 4	1431.3	1490.5	942.06	4.19	13.38
10 36 053 26 4	1401.5	1404.1	53.81	-	6.07
13 18 054 25 4	1621.8	1628.4	11.29	0.53	4.76
05 13 054 26 4	1614.2	1628.7	172.89	4.26	6.31
08 14 054 26 4	1554.3	1598.9	58.60	1.59	6.11
	1612.4	1618.3			
14 05 041 02 5	2512.5	2535.9	6.53	1.20	6.48
11 03 042 02 5	2374.1	2403.6	103.40	2.92	6.14
09 14 042 02 5	2382.9	2389.0	28.06	5.06	5.33
01 23 042 02 5	2375.6	2400.9	39.21	2.15	7.48
03 01 043 02 5	2424.7	2430.9	62.03	5.72	8.99
11 01 043 02 5	2420.1	2426.6	103.02	2.71	7.47
01 13 043 02 5	2392.1	2396.1	68.27	1.69	8.98
11 18 043 01 5	2390.9	2394.7	65.94	2.43	8.68
11 20 043 01 5	2370.1	2417.0	75.90	5.22	6.17
01 25 043 02 5	2448.5	2455.3	6.75	1.15	4.78
11 28 043 01 5	2426.5	2457.0	7.30	0.56	6.26
10 33 043 01 5	2395.7	2430.2	4.07	0.15	4.78
10 14 044 01 5	2322.5	2325.2	158.38	0.76	8.11
	2329.9	2334.1			
07 15 044 01 5	2225.0	2330.5	32.57	1.36	7.66
07 16 044 01 5	2348.2	2357.9	94.86	6.82	8.32
11 26 044 01 5	2370.1	2378.9	55.30	2.38	12.30
05 01 045 01 5	2325.9	2331.7	21.80	0.57	6.17
01 04 045 01 5	2371.3	2386.6	19.28	1.15	6.56
07 10 045 01 5	2300.9	2322.9	5.97	0.89	7.10
09 25 045 01 5	2179.4	2247.9	237.70	40.70	10.41
09 36 045 01 5	2216.5	2243.8	18.30	4.98	7.27

Table 3 Average core permeabilities and porosities for individual reef

Reefs	Permeability (md)		Porosity	No. of wells	K (m/s)	
	Horizontal	Vertical	%		Horizontal	Vertical
St. Albert	48.54	1.53	5.73	3	1.07E-06	3.37E-08
Big Lake	225.13	4.19	9.73	2	4.95E-06	9.22E-08
Acheson	118.24	3.08	9.51	4	2.60E-06	6.78E-08
Leduc-Woodbend	50.87	7.37	8.63	9	1.12E-06	1.62E-07
Glen Park	128.30	3.21	7.68	1	2.82E-06	7.06E-08
Wizard Lake	268.43	7.68	9.92	4	5.90E-06	1.69E-07
Bonnie Glen	353.37	2.94	10.52	4	7.77E-06	6.47E-08
Westrose	23.99	4.36	7.02	5	5.28E-07	9.59E-08
Westrose South	23.22	0.98	7.47	9	5.11E-07	2.16E-08
Rimbey	48.98	2.86	7.30	9	1.08E-06	6.29E-08
Golden Spike	13.73	1.78	8.32	6	3.02E-07	3.92E-08
Bashaw		3.07				6.76E-08

Notes:

1. Reef permeabilities are geometric averages whereas porosities are arithmetic averages
2. Permeability in Bashaw reef is the geometric mean of all the other reef permeabilities
3. Hydraulic conductivity (K) is calculated using K=k*rho*g/mu

where k=permeability of the reef, rho=density of pure water, g=acceleration due to gravity, and mu=viscosity of 0.44e-03 Pa s @ 66 deg C.

Table 4 Drill Stem Tests used for the Nisku Formation

LSD. Sec. T. R. M.	DST	INTERVAL (m)		K.B.	Elevation	Recorder	Stabilized	Recovery	Fresh water
	DATE	From	To	(m)	(m)	Depth (m)	Pressure (kPa)		Head (m)
10-02-040-24-W-4	650610	1877	1888	901	-971	1872	16458	Gas	707.25
04-11-040-24-W-4	650211	1867	1873	906	-964	1870	16618	Water	730.56
07-13-040-24-W-4	640910	1845	1851	913	-935	1848	16023	Mud	698.89
12-24-040-24-W-4	621107	1792	1808	862	-941	1803	16224	Mud	713.39
04-32-040-24-W-4	620610	1841	1849	847	-997	1844	17054	Water	742.02
13-36-040-24-W-4	561216	1783	1795	836	-958	1794	16651	Water	739.93
10-05-040-25-W-4	620519	2016	2035	941	-1069	2010	18029	Oil	769.45
08-08-040-25-W-4	820409	1978	1993	920	-1059	1979	17155	Gas	690.32
05-16-040-25-W-4	770317	1975	1996	914	-1070	1984	17225	Gas/Oil	686.46
08-17-040-25-W-4	830912	1989	1995	922	-1071	1993	16604	Water	622.14
04-27-040-25-W-4	570726	1981	1988	937	-1051	1988	16765	Water	658.55
06-27-040-25-W-4	840515	1945	1963	918	-1029	1947	17374	Mud	742.65
02-34-040-25-W-4	640310	1926	1942	894	-1046	1940	17723	Mud	761.24
13-36-040-25-W-4	590219	1889	1899	855	-1040	1895	17882	Oil	783.46
12-14-040-26-W-4	890115	2042	2070	907	-1126	2033	17732	-	682.16
01-07-040-27-W-4	680227	2228	2248	935	-1301	2236	19506	Gas	688.06
09-01-041-24-W-4	640613	1756	1760	810	-948	1758	16217	Water	705.67
02-14-041-24-W-4	671020	1786	1793	858	-930	1788	15641	Water	664.94
10-16-041-24-W-4	750807	1877	1890	878	-1010	1888	16539	Water	676.51
06-19-041-24-W-4	761013	1859	1890	867	-993	1860	16681	Water	707.99
12-01-041-25-W-4	590418	1856	1900	857	-1040	1897	17751	Mud/Oil	770.10
11-11-041-02-W-5	800912	2454	2473	1000	-1455	2455	18875	Mud	469.71
11-15-041-02-W-5	791226	2438	2467	984	-1456	2440	19228	Water	504.71
14-15-041-02-W-5	611024	2427	2433	971	-1461	2432	19098	Gas/Water	486.45
04-20-041-02-W-5	591122	2429	2451	975	-1450	2425	18974	Water	484.81
03-22-041-02-W-5	810115	2391	2420	954	-1431	2385	18908	Mud/Water	497.08

LSD. Sec. T. R. M.	DST	INTERVAL (m)		K.B.	Elevation	Recorder	Stabilized	Recovery	Fresh water
	DATE	From	To	(m)	(m)	Depth (m)	Pressure (kPa)		Head (m)
07-28-041-02-W-5	660921	2384	2415	938	-1455	2393	19176	Water	500.41
06-29-041-02-W-5	900131	2392	2412	937	-1458	2395	18753	Water	454.27
16-32-041-02-W-5	841027	2382	2405	968	-1415	2383	18972	Water	519.61
10-05-042-24-W-4	621018	1890	1898	883	-1011	1894	16289	Mud	650.02
16-04-042-01-W-5	870809	2306	2329	938	-1357	2295	18264	Water	505.41
14-15-042-02-W-5	831026	2294	2307	907	-1389	2296	18237	Oil	470.66
06-22-042-02-W-5	830817	2279	2289	905	-1375	2280	18379	Mud	499.14
07-22-042-02-W-5	840607	2306	2328	903	-1405	2308	18493	Water	480.76
11-35-042-02-W-5	570531	2307	2335	940	-1393	2333	18173	Water	460.13
09-02-043-24-W-4	780728	1700	1715	869	-832	1701	12954	-	488.94
11-08-043-01-W-5	610113	2210	2221	919	-1285	2204	17232	-	472.17
10-36-043-01-W-5	551228	2151	2162	937	-1209	2146	16286	Water	451.71
09-02-043-02-W-5	570404	2294	2306	949	-1346	2295	17409	Oil/Mud	429.22
09-23-043-02-W-5	610201	2257	2275	917	-1358	2275	17815	Mud	458.62
02-08-044-27-W-4	550526	1980	1986	850	-1134	1984	15895	Water	486.84
14-26-044-27-W-4	610629	1926	1934	862	-1068	1930	14376	Water	397.94
10-23-044-28-W-4	620329	2100	2126	938	-1156	2094	15679	Water	442.81
10-08-044-01-W-5	600128	2215	2247	964	-1255	2219	16651	Mud	442.93
11-26-044-01-W-5	600617	2147	2157	942	-1211	2153	16079	Mud/Water	428.60
07-34-044-01-W-5	571121	2173	2196	966	-1204	2170	16550	Water	483.63
06-02-045-26-W-4	811221	1852	1877	844	-1009	1853	13925	Water	410.95
14-11-045-27-W-4	531227	1912	1918	860	-1052	1912	14479	Water	424.45
14-10-045-28-W-4	620830	2007	2035	853	-1181	2034	15837	Water	433.92
12-02-045-01-W-5	600608	2060	2075	891	-1183	2074	16662	Oil	516.05
14-13-045-01-W-5	620509	2022	2037	855	-1170	2025	15688	Water	429.73
05-23-045-01-W-5	730722	2036	2054	872	-1170	2042	15904	Water	451.76

LSD. Sec. T. R. M.	DST	INTERVAL (m)		K.B.	Elevation	Recorder	Stabilized	Recovery	Fresh water
	DATE	From	To	(m)	(m)	Depth (m)	Pressure (kPa)		Head (m)
11-24-045-01-W-5	590901	1986	1995	834	-1158	1992	15791	Water/Oil	452.23
14-21-045-02-W-5	600828	2216	2234	920	-1302	2222	17209	Water	452.83
07-11-046-28-W-4	680526	1984	2002	853	-1137	1990	15555	Water	449.17
09-13-046-28-W-4	540807	1936	1948	858	-1077	1935	14980	Water	450.53
10-09-046-02-W-5	660117	2221	2231	963	-1259	2222	16816	Water	455.75
10-25-046-02-W-5	660717	2121	2129	919	-1205	2124	16099	Water	436.64
11-36-047-24-W-4	610820	1543	1561	771	-781	1552	12087	Water	451.53
10-35-047-25-W-4	720104	1612	1627	773	-853	1626	12393	Mud/Water	410.73
13-09-047-27-W-4	651016	1920	1928	857	-1063	1920	14425	Water	407.94
13-13-047-28-W-4	660807	1975	2007	893	-1113	2006	15169	Water	433.81
06-02-047-02-W-5	610624	2090	2096	892	-1198	2090	16079	Water	441.60
10-31-048-26-W-4	550410	1674	1683	756	-918	1674	13046	Water	412.32
01-33-048-26-W-4	620128	1666	1671	762	-908	1670	12852	Oil/Water	402.54
10-34-048-26-W-4	630213	1657	1663	761	-901	1662	12886	Water	413.01
02-21-048-01-W-5	620205	1879	1884	798	-1084	1882	14810	Water	426.20
10-20-049-23-W-4	620611	1452	1459	761	-686	1447	10790	Oil/Water	414.27
10-34-049-25-W-4	620522	1510	1532	728	-803	1531	11835	Water	403.83
02-23-049-28-W-4	580301	1734	1758	748	-987	1735	13824	Water	422.66
16-33-049-01-W-5	540209	1765	1768	721	-1044	1765	14797	Water	464.87
13-16-050-24-W-4	611227	1417	1423	712	-711	1423	10942	Mud/Water	404.77
10-25-050-24-W-4	790316	1399	1404	740	-662	1402	10730	Gas	432.16
06-04-050-25-W-4	810301	1508	1513	715	-794	1509	11900	Water	419.46
07-20-050-27-W-4	711121	1612	1631	708	-911	1619	13042	Water	418.91
12-28-050-27-W-4	650131	1600	1609	704	-900	1604	12893	Water	414.72
04-20-050-02-W-5	581218	1855	1870	772	-1097	1869	14927	Mud	425.13
05-20-050-02-W-5	650912	1847	1854	771	-1072	1843	14789	Water	436.06

LSD. Sec. T. R. M.	DST	INTERVAL (m)		K.B.	Elevation	Recorder	Stabilized	Recovery	Fresh water
	DATE	From	To	(m)	(m)	Depth (m)	Pressure (kPa)		Head (m)
06-20-051-23-W-4	810915	1366	1376	743	-624	1367	10257	Water	421.92
10-04-051-24-W-4	620627	1402	1412	708	-699	1407	10852	Water	407.60
10-10-051-24-W-4	711227	1385	1396	709	-678	1387	10770	Water	420.23
02-04-051-25-W-4	690920	1479	1491	702	-786	1488	11776	Mud	414.82
06-25-051-25-W-4	570928	1419	1436	690	-729	1419	11376	Water	431.03
06-11-051-26-W-4	540718	1511	1516	703	-808	1511	12238	Water	439.93
14-31-051-26-W-4	540714	1533	1548	705	-828	1533	12117	Mud	407.59
03-04-052-25-W-4	800701	1443	1452	687	-757	1444	11493	Water	414.96
13-03-052-26-W-4	550717	1449	1453	707	-743	1450	11209	Water	400.00
09-09-052-26-W-4	610309	1455	1460	711	-747	1458	11142	Water/Oil	389.17
02-10-052-26-W-4	661013	1442	1480	707	-768	1475	11480	Water	402.63
09-16-052-26-W-4	631216	1474	1477	717	-748	1465	11363	Oil	410.70
10-05-052-02-W-5	671219	1740	1759	746	-999	1745	13976	Mud	426.16

Table 5 Drill Stem Tests used for the Leduc Formation

LSD. Sec. T. R. M.	DST DATE	INTERVAL(m) From	To	K.B. (m)	Elevation (m)	Recorder Depth (m)	Stabilized Pressure (kPa)	Recovery	Fresh water Head (m)
11 08 041 24 4	551016	1892.8	1898.9	855.6	-1041	1896.6	17761	Water	770.5
07 12 041 24 4	691024	1777.0	1786.1	807.1	-976	1783.1	15713	Water	626.0
06 26 041 24 4	610708	1828.5	1829.7	864.7	-964	1828.7	16695	Water	738.6
10 34 041 24 4	691219	1854.7	1863.9	870.2	-992	1862.2	15916	Water	630.9
12 36 041 24 4	650701	1804.4	1828.8	848.6	-961	1809.6	16136	Water	684.5
12 01 041 25 4	590420	1907.4	1913.5	857.4	-1053	1910.4	17917	Water	774.0
07 10 041 25 4	620411	1957.4	1962.3	671.1	-1090	1961.1	18190	Water	764.8
06 25 041 25 4	580618	1946.1	1952.2	882.1	-1068	1950.1	17976	Water	765.3
10 36 041 25 4	630726	2086.4	2106.2	894.0	-1200	2094.0	19223	Water	759.9
01 15 042 24 4	801128	1854.0	1859.0	882.6	-972	1854.6	13764	Water	431.1
08 16 054 25 4	740313	1621.8	1627.9	689.8	-937	1626.8	12850	Water	373.3
03 26 054 26 4	831111	1640.0	1650.0	700.0	-947	1647.0	13009	Water	379.9
14 15 041 02 5	611104	2574.0	2596.9	970.8	-1608	2578.8	20553	Water	488.0
04 20 041 02 5	591120	2508.5	2512.5	975.1	-1537	2512.1	19988	Water	501.1
11 35 043 01 5	590128	2443.0	2465.8	925.1	-1538	2463.1	19850	Water	486.4
10 08 044 01 5	600203	2453.6	2456.7	963.8	-1493	2456.8	19423	Water	487.7
07 10 045 01 5	*590918*	*2296.4*	*2300.9*	*864.7*	*-1435*	*2299.7*	*18844*	*Gas*	*486.9*
07 15 044 01 5	*590620*	*2221.7*	*2224.7*	*908.0*	*-1317*	*2225.0*	*18644*	*Water*	*584.5*
07 16 044 01 5	*600702*	*2326.8*	*2348.2*	*928.1*	*-1419*	*2347.1*	*18961*	*Gas*	*514.4*

Note: DST's in italics are in a gas leg.

Corrected fresh water hydraulic head for these DST's is 484m (see Appendix I).

Table 6 Drill Stem Tests used for the Cooking Lake Formation

LSD. Sec. T. R. M.	DST	INTERVAL(m)		K.B.	Elevation	Recorder	Stabilized	Recovery	Fresh water
	DATE	From	To	(m)	(m)	Depth(m)	Pressure (kPa)		Head (m)
10 02 042 25 4	690108	2135.7	2202.2	920.5	-1281.7	2202.2	19498.7	Water	706.6
05 02 044 28 4	580813	2436.0	2441.4	912.6	-1526.7	2439.3	19819.0	Water	494.3
10 17 053 23 4	650726	1515.2	1531.9	654.7	-876.3	1531.0	12691.4	Water	417.9
14 18 054 25 4	610108	1622.5	1630.1	686.4	-940.6	1627.0	12889.1	Mud	373.7
16 20 054 25 4	601224	1634.9	1641.3	691.3	-950.1	1641.4	12939.4	Water	369.4

Table 7 Average interval densities and vertical pressure gradients for the formations (used for nominal gradient calculations)

	NISKU FORMATION					LEDUC FORMATION					COOKING LAKE FORMATION			
From	To	ρ	ρ	γ	From	To	ρ	ρ	γ	From	To	ρ	ρ	γ
(m)	(m)	(g/cm3)	(g/cm3)	(kPa/m)	(m)	(m)	(g/cm3)	(g/cm3)	(kPa/m)	(m)	(m)	(g/cm3)	(g/cm3)	(kPa/m)
1243.6	1325.9	1.079												
1254.9	1262.2	1.078	1.078	10.568										
1259.7	1283.2	1.076												
1299.4	1303.0	1.046												
1311.9	1315.2	1.049												
1327.7	1330.8	1.080												
1339.6	1343.3	1.061												
1344.2	1362.2	1.065	1.062	10.412										
1385.3	1399.0	1.079												
1391.4	1396.0	1.082												
1396.3	1399.3	1.032												
1405.7	1411.8	1.080			1478.3	1482.9	1.094	1.094	10.728	1496.6	1503.3	1.122	1.122	11.003
1414.3	1416.7	1.080												
1417.3	1423.4	1.076												
1432.0	1444.4	1.070	1.077	10.557										
1444.8	1450.8	1.082												
1449.6	1457.6	1.073												
1451.5	1459.1	1.073												
1479.8	1490.5	1.078												
1542.6	1560.9	1.076			1559.4	1563.3	1.145			1515.2	1531.9	1.107	1.107	10.856
1544.1	1551.4	1.100			1562.1	1568.2	1.144	1.151	11.291					
1563.6	1592.9	1.138			1586.8	1588.3	1.165							
1578.3	1606.9	1.122	1.107	10.856										
1585.9	1590.4	1.122												
1590.8	1595.6	1.084												
1604.2	1611.5	1.102			1625.2	1626.4	1.109			1612.7	1621.5	1.086		
1610.3	1614.8	1.116	1.099	10.778	1638.3	1639.8	1.155			1613.3	1618.5	1.103		
1612.4	1626.7	1.079			1642.9	1647.4	1.108	1.131	11.086	1621.8	1640.1	1.116		
					1668.5	1672.1	1.150			1645.9	1655.1	1.089	1.111	10.895
										1677.9	1702.0	1.132		
										1692.6	1699.3	1.140		
1727.6	1734.3	1.107			1729.4	1736.8	1.162			1706.9	1723.0	1.128		
1734.3	1758.1	1.105	1.102	10.807	1731.3	1737.4	1.164			1713.0	1722.1	1.170		
1773.0	1780.9	1.094			1738.6		1.144			1728.2	1734.9	1.142		
					1760.2	1761.4	1.147	1.152	11.297	1734.3	1767.8	1.123	1.138	11.159
					1779.1	1784.6	1.156			1745.0	1761.1	1.085		
					1780.0	1788.9	1.139			1752.6	1759.3	1.160		
										1773.0	1783.1	1.157		
1847.4	1853.5	1.102			1800.1	1823.0	1.130			1800.5	1802.9	1.166	1.166	11.435
1852.0	1877.0	1.112	1.098	10.764	1804.1	1813.6	1.166	1.150	11.281					
1862.9	1885.2	1.079			1894.3	1905.9	1.155							
1950.7	1957.1	1.132			1926.9	1930.6	1.143			1934.0	1941.6	1.153	1.153	11.307
1954.4	1969.6	1.121			1937.9	1939.4	1.165	1.154	11.317					
1956.8	1964.1	1.066	1.100	10.787										
1975.1	2007.1	1.081												
2006.8	2034.5	1.107	1.107	10.856	2011.7	2019.3	1.162	1.162	11.395					

	NISKU FORMATION					LEDUC FORMATION					COOKING LAKE FORMATION			
From	To	p	ρ	γ	From	To	p	ρ	γ	From	To	p	ρ	γ
(m)	(m)	(g/cm3)	(g/cm3)	(kPa/m)	(m)	(m)	(g/cm3)	(g/cm3)	(kPa/m)	(m)	(m)	(g/cm3)	(g/cm3)	(kPa/m)
2100.1	2126.0	1.121			2133.0	2149.4	1.104	1.104	10.827	2106.2	2133.6	1.144		
2121.4	2129.0	1.119	1.116	10.944						2156.8	2161.6	1.168	1.156	11.336
2151.0	2161.6	1.108												
2215.0	2240.3	1.086			2218.9	2227.8	1.117			2240.3	2259.2	1.150	1.150	11.278
2246.4	2256.1	1.079	1.083	10.616	2226.0	2241.2	1.160	1.147	11.245					
					2251.9	2260.1	1.163							
					2320.4	2328.4	1.133			2337.8	2356.1	1.123	1.123	11.013
					2393.3	2393.9	1.170	1.152	11.292					
2453.9	2473.1	1.084	1.084	10.630	2417.7	2420.4	1.162	1.162	11.395	2443.0	2465.8	1.161	1.161	11.386
					2574.0	2596.9	1.140	1.140	11.180					
NOTES	p=	Density												
	ρ=	Average Density												
	γ=	Average Density x 9.80665												

Table 8a Water chemistry data for the Nisku Formation

No.	LSD.Sec.T.R.M.	INTERVAL(m)		Depth(m)	K.B.(m)	Elev.(m)	pH	Density	TDSmg/l	Na	Ca	Mg	HCO3	SO4	Cl
1	02 11 052 25 4	1396.29	1399.34	1397.8			7.10	1.032	68598	22500	2930	765	333	570	41500
2	05 04 054 24 4	1299.36	1303.02	1301.2	683.06	-618.1	6.70	1.046	69874	21243	4088	1022	833	789	41899
3	07 10 054 25 4	1311.86	1315.21	1313.5	661.72	-651.8	6.60	1.049	71251	21400	4280	1145	521	1205	42700
4	02 01 052 24 4	1339.60	1343.25	1341.4			6.50	1.061	87671	25450	6230	1315	612	1064	53000
5	04 22 054 23 4	1179.88	1184.76	1182.3			7.15		88853	27540	4802	1330	305	754	54122
6	09 16 051 23 4	1344.17	1362.15	1353.2			6.90	1.065	93555	26800	6600	1730	392	833	57200
7	02 28 048 02 5	1956.82	1964.13	1960.5			6.60	1.066	94000		*8332*		550	500	56272
8	14 21 045 02 5	2246.38	2256.13	2251.3	919.73	-1331.5	7.30	1.079	100168	26535	8516	2112	380	2625	60000
9	10 20 049 23 4	1451.46	1459.08	1455.3	760.48	-694.8	6.50	1.073	102210		*10510*		812	1038	62302
10	10 35 047 25 4	1612.39	1626.72	1619.6	773.28	-846.3	7.70	1.079	102989	26257	6807	4131	500	3794	61500
11	08 06 053 23 4	1254.86	1262.18	1258.5			6.50	1.078	105328	31100	6340	2110	158	920	64700
12	14 31 052 23 4	1243.58	1325.88	1284.7	667.82	-616.9	5.70	1.079	106590	32079	6422	1662	960	1267	64200
13	14 22 049 23 4	1431.95	1444.45	1438.2			6.53	1.070	107655	34100	5200	1510	885	1060	64900
14	10 10 051 24 4	1385.32	1399.03	1392.2	709.27	-682.9	7.10	1.079	107764	33239	6350	1298	590	1287	65000
15	09 01 053 24 4	1259.74	1283.21	1271.5	661.66	-609.8	6.30	1.076	108713	32853	6523	1648	891	1197	65601
16	15 14 048 23 4	1449.63	1457.55	1453.6			7.00	1.073	110086	32990	6968	1592	825	1346	66365
17	13 13 047 28 4	1975.10	2007.11	1991.1	893.00	-1098.1	6.20	1.081	110961	32235	8040	1565	361	1840	66920
18	10 05 051 25 4	1497.18	1504.49	1500.8	697.69	-803.1			112978	34700	7320	1060	486	512	68900
19	11 36 047 24 4	1542.59	1560.88	1551.7			6.60	1.076	115195	34546	7520	1580	856	48	70645
20	13 03 052 26 4	1444.75	1450.85	1447.8	706.53	-741.3	6.60	1.082	115683	35912	6588	1454	293	1296	70140
21	15 21 047 23 4	1479.80	1490.47	1485.1				1.078	115828	35700	7580	1820	420	1308	69000
22	10 04 053 25 4	1391.41	1395.98	1393.7	680.62	-713.1	6.40	1.082	116568	36500	7050	938	790	1190	70100
23	08 02 041 25 4	1862.94	1885.19	1874.1	858.01	-1016.1	5.10	1.079	118251	12780	14090	5492	580	469	73500
24	04 11 053 27 4	1499.01	1503.58	1501.3					120079	39600	6260	406	592	821	72400
25	10 23 044 28 4	2100.07	2125.98	2113.0	937.56	-1175.5	6.80	1.121	171590		*10611*		289	1100	108159
26	01 04 052 27 4	1590.75	1595.63	1593.2			6.00	1.084	121059	36067	8033	1673	865	844	73577
27	07 26 052 26 4	1414.27	1416.71	1415.5	715.37	-700.1	6.65	1.080	122779	42058	7202	1674	768	1205	69502
28	11 11 041 02 5	2453.94	2473.15	2463.5	998.83	-1464.7	7.70	1.084	124580	36770	5245	4143	610	9662	66650

No.	LSD.Sec.T.R.M.	INTERVAL(m)		Depth(m)	K.B.(m)	Elev.(m)	pH	Density	TDSmg/l	Na	Ca	Mg	HCO3	SO4	Cl
29	10 08 044 01 5	2214.98	2240.28	2227.6			7.60	1.086	124696	38538	7581	1314	130	1969	75164
30	05 05 042 23 4	1773.02	1780.95	1777.0	872.95	-904.0	7.61	1.094	129000	30800	8200	2140	1700	3500	76000
31	02 11 053 26 4	1405.74	1411.83	1408.8	708.05	-700.7	7.40	1.080	132694	41802	7916	990	564	1420	80002
32	14 23 051 27 4	1544.12	1551.43	1547.8	713.54	-834.2	6.70	1.100	139887	40946	9469	2321	560	891	85700
33	10 36 043 01 5	2150.97	2161.64	2156.3				1.108	140461	20833	21300	6850	1128	4680	85670
34	05 20 050 02 5	1847.39	1853.49	1850.4	767.18	-1083.3	6.51	1.102	146891	44047	9688	1934	813	720	89689
35	02 02 049 27 4	1727.61	1734.31	1731.0	806.20	-924.8	6.40	1.107	160680	48229	10175	2170	206	1900	97700
36	11 31 048 25 4	1604.16	1611.48	1607.8			6.80	1.102	161300	45200	12203	2995	244	818	99840
37	05 23 049 26 4	1610.26	1614.83	1612.5	738.23	-874.3	7.15	1.116	165414	49138	12043	1677	178	728	101061
38	14 10 045 28 4	2006.80	2034.54	2020.7	852.92	-1167.7	6.30	1.107	167767	50224	11559	1832	710	2242	101200
39	10 25 046 02 5	2121.41	2129.03	2125.2	919.28	-1205.9	7.31	1.119	170476	49136	14104	1461	532	1188	103574
40	06 02 045 26 4	1851.96	1876.96	1864.5	846.43	-1018.0	6.40	1.112	170944	49269	11230	2126	198	2189	103000
41	07 11 046 28 4	1984.25	2001.93	1993.1	851.00	-1142.1	5.90		178367	56013	11355	982	490	1727	107800
42	03 05 047 27 4	1954.38	1969.62	1962.0			7.75	1.121	178862	50736	14722	2223	260	1185	109736
43	04 35 044 23 4	1585.87	1590.45	1588.2			6.90	1.122	194556	65500	8630	939	430	557	118500
44	12 21 044 27 4	1950.72	1957.12	1953.9			6.50	1.132	199694	59432	14236	2254	465	678	122629
45	14 04 050 26 4	1563.62	1592.88	1578.3	732.13	-846.1	6.30	1.138	202683	55295	17257	3596	130	555	125800
46	02 08 049 25 4	1578.25	1606.91	1592.6	737.62	-855.0	6.30	1.122	205588	69023	12154	2374	154	901	120982
47	13 16 050 24 4	1417.32	1423.42	1420.4	711.71	-708.7	7.30	1.076	*107510*		*8867*		542	1284	65098
48	06 01 054 26 4	1327.71	1330.76	1329.2			5.60	1.080	*109030*		*12480*		700	200	67400
49	02 23 049 28 4	1734.31	1758.09	1746.2	747.52	-998.7	7.00	1.105	*140670*		*13280*		447	1081	96309
						AVERAGE	6.71	1.088	128939	38026	9079	1985	551.8	1448	78237
						STD	0.58	0.023	35390.8	12354	3616	1232	299.9	1484	21996
						COUNT	45	45	49	43	49	43	49	49	49
						NOTE:	Calculated TDS values are enlisted; values italicized are at ignition								
							Italicized values in Calcium column represent (Ca+Mg)								
							Cations and Anions are in mg/l; Density in g/cc								

Table 8b Water chemistry data for the Nisku Formation

No.	LSD. Sec.T.R.M.	Na	Ca	Mg	HCO3	SO4	Cl	Mg/Ca	Na/Cl	(HCO3/Cl)*100	SO4/Cl	SO4/HCO3
1	02 11 052 25 4	978.69	146.21	62.94	5.46	11.87	1170.66	0.430	0.836	0.466	0.010	2.175
2	05 04 054 24 4	924.01	203.99	84.08	13.65	16.43	1181.92	0.412	0.782	1.155	0.014	1.203
3	07 10 054 25 4	930.84	213.57	94.20	8.54	25.09	1204.51	0.441	0.773	0.709	0.021	2.938
4	02 01 052 24 4	1107.00	310.88	108.19	10.03	22.15	1495.06	0.348	0.740	0.671	0.015	2.209
5	04 22 054 23 4	1197.91	239.62	109.42	5.00	15.70	1526.71	0.457	0.785	0.327	0.010	3.141
6	09 16 051 23 4	1165.72	329.34	142.33	6.42	17.34	1613.54	0.432	0.722	0.398	0.011	2.700
7	02 28 048 02 5		415.77		9.01	10.41	1587.36			0.568	0.007	1.155
8	14 21 045 02 5	1154.20	424.95	173.76	6.23	54.65	1692.52	0.409	0.682	0.368	0.032	8.776
9	10 20 049 23 4		524.45		13.31	21.61	1757.46			0.757	0.012	1.624
10	10 35 047 25 4	1142.11	339.67	339.86	8.19	78.99	1734.84	1.001	0.658	0.472	0.046	9.640
11	08 06 053 23 4	1352.76	316.37	173.59	2.59	19.15	1825.11	0.549	0.741	0.142	0.010	7.398
12	14 31 052 23 4	1395.35	320.46	136.73	15.73	26.38	1811.00	0.427	0.770	0.869	0.015	1.677
13	14 22 049 23 4	1483.25	259.48	124.23	14.50	22.07	1830.75	0.479	0.810	0.792	0.012	1.522
14	10 10 051 24 4	1445.80	316.87	106.79	9.67	26.80	1833.57	0.337	0.789	0.527	0.015	2.771
15	09 01 053 24 4	1429.01	325.50	135.58	14.60	24.92	1850.52	0.417	0.772	0.789	0.013	1.707
16	15 14 048 23 4	1434.97	347.70	130.97	13.52	28.02	1872.07	0.377	0.767	0.722	0.015	2.073
17	13 13 047 28 4	1402.13	401.20	128.75	5.92	38.31	1887.73	0.321	0.743	0.313	0.020	6.475
18	10 05 051 25 4	1509.35	365.27	87.21	7.96	10.66	1943.58	0.239	0.777	0.410	0.005	1.338
19	11 36 047 24 4	1502.65	375.25	129.99	14.03	1.00	1992.81	0.346	0.754	0.704	0.001	0.071
20	13 03 052 26 4	1562.07	328.74	119.62	4.80	26.98	1978.56	0.364	0.789	0.243	0.014	5.619
21	15 21 047 23 4	1552.85	378.24	149.73	6.88	27.23	1946.40	0.396	0.798	0.354	0.014	3.957
22	10 04 053 25 4	1587.65	351.80	77.17	12.95	24.78	1977.43	0.219	0.803	0.655	0.013	1.914
23	08 02 041 25 4	555.89	703.09	451.83	9.51	9.76	2073.34	0.643	0.268	0.458	0.005	1.027
24	04 11 053 27 4	1722.49	312.38	33.40	9.70	17.09	2042.31	0.107	0.843	0.475	0.008	1.762
25	10 23 044 28 4		529.49		4.74	22.90	3051.03			0.155	0.008	4.836
26	01 04 052 27 4	1568.81	400.85	137.64	14.18	17.57	2075.51	0.343	0.756	0.683	0.008	1.240
27	07 26 052 26 4	1829.40	359.38	137.72	12.59	25.09	1960.56	0.383	0.933	0.642	0.013	1.993
28	11 11 041 02 5	1599.39	261.73	340.85	10.00	201.17	1880.11	1.302	0.851	0.532	0.107	20.123

No.	LSD. Sec.T.R.M.	Na	Ca	Mg	HCO3	SO4	Cl	Mg/Ca	Na/Cl	(HCO3/Cl)*100	SO4/Cl	SO4/HCO3
29	10 08 044 01 5	1676.29	378.29	108.10	2.13	41.00	2120.28	**0.286**	0.791	0.100	0.019	19.243
30	05 05 042 23 4	1339.71	409.18	176.06	27.86	72.87	2143.86	**0.430**	0.625	1.300	0.034	2.616
31	02 11 053 26 4	1818.27	395.01	81.45	9.24	29.56	2256.76	**0.206**	0.806	0.410	0.013	3.199
32	14 23 051 27 4	1781.04	472.50	190.95	9.18	18.55	2417.49	**0.404**	0.737	0.380	0.008	2.021
33	10 36 043 01 5	906.18	1062.87	563.55	18.49	97.44	2416.64	**0.530**	0.375	0.765	0.040	5.271
34	05 20 050 02 5	1915.92	483.43	159.11	13.32	14.99	2530.01	**0.329**	0.757	0.527	0.006	1.125
35	02 02 049 27 4	2097.83	507.73	178.53	3.38	39.56	2755.99	**0.352**	0.761	0.122	0.014	11.718
36	11 31 048 25 4	1966.07	608.93	246.40	4.00	17.03	2816.36	**0.405**	0.698	0.142	0.006	4.259
37	05 23 049 26 4	2137.36	600.95	137.97	2.92	15.16	2850.80	**0.230**	0.750	0.102	0.005	5.196
38	14 10 045 28 4	2184.60	576.80	150.72	11.64	46.68	2854.72	**0.261**	0.765	0.408	0.016	4.012
39	10 25 046 02 5	2137.28	703.79	120.20	8.72	24.73	2921.69	**0.171**	0.732	0.298	0.008	2.837
40	06 02 045 26 4	2143.06	560.38	174.91	3.24	45.58	2905.50	**0.312**	0.738	0.112	0.016	14.046
41	07 11 046 28 4	2436.41	566.62	80.79	8.03	35.96	3040.90	**0.143**	0.801	0.264	0.012	4.478
42	03 05 047 27 4	2206.87	734.63	182.89	4.26	24.67	3095.51	**0.249**	0.713	0.138	0.008	5.790
43	04 35 044 23 4	2849.06	430.64	77.25	7.05	11.60	3342.74	**0.179**	0.852	0.211	0.003	1.646
44	12 21 044 27 4	2585.12	710.38	185.44	7.62	14.12	3459.21	**0.261**	0.747	0.220	0.004	1.852
45	14 04 050 26 4	2405.18	861.13	295.85	2.13	11.56	3548.66	**0.344**	0.678	0.060	0.003	5.424
46	02 08 049 25 4	3002.31	606.49	195.31	2.52	18.76	3412.75	**0.322**	0.880	0.074	0.005	7.433
47	13 16 050 24 4		442.47		8.88	26.73	1836.33			0.484	0.015	3.010
48	06 01 054 26 4		622.75		11.47	4.16	1901.27			0.603	0.002	0.363
49	02 23 049 28 4		662.67		7.33	22.51	2716.76			0.270	0.008	3.072
	AVERAGE	1654.02	453.06	163.30	9.04	30.15	2206.96	0.386	0.748	0.456	0.015	4.320
	STD	537.36	180.46	101.32	4.92	30.90	620.48	0.206	0.112	0.278	0.016	4.309
	COUNT	43	49	43	49	49	49	43	43	49	49	49
	NOTE: Cations and Anions are in meq/l											

Table 9a Water chemistry data for the Leduc Formation

No.	LSD.Sec.T.R.M.	INTERVAL(m)		Depth(m)	K.B.(m)	Elev.(m)	pH	Density	TDSmg/l	Na	Ca	Mg	HCO3	SO4	Cl
1	01 02 042 25 4	2133	2149	2141.2			7.00	1.104	139195	30042	17640	3436	505	1181	86391
2	14 15 041 02 5	2574	2597	2585.5	970.79	-1614.7	5.70	1.140	148227	32230	16950	4870	363	550	93264
3	15 02 053 26 4						6.40	1.109	152007	36190	14990	3280	207	963	94600
4	13 18 054 25 4	1625	1626	1625.8	689.15	-936.7	6.13	1.109	161693	44662	13901	2294	411	756	99097
5	04 22 054 23 4	1487	1490	1488.3			6.25		164325	48492	11549	2259	55	690	101280
6	04 06 051 25 4	1643	1647	1645.2			6.80	1.108	165367	40200	18800	2770	115	372	103000
7	07 11 046 28 4	2219	2228	2223.4	852.53	-1370.8	6.30	1.117	171363	42920	20500	2892	230	1621	103200
8	08 24 049 26 4	1800	1823	1811.6	724.51	-1087.1	6.70	1.130	191921	39000	24500	4155	176	772	120800
9	07 34 041 23 4	1780	1789	1784.5	859.23	-925.2	6.75	1.139	199745	52137	20000	2840	1430	448	122890
10	10 11 041 25 4	1927	1931	1928.8			6.75	1.143	203000	51301	21449	3123	867	662	124815
11	08 09 052 26 4	1562	1568	1565.1	709.88	-855.3	6.50	1.144	211045	54330	21065	3659	300	451	131240
12	10 14 044 01 5	2320	2328	2324.4	872.64	-1451.8	5.80	1.133	211897	49844	24264	4496	500	593	132200
13	07 34 052 26 4	1559	1563	1561.3	720.85	-840.5	6.36	1.145	212540	53490	22857	3203	251	454	131366
14	02 01 046 01 5	2252	2260	2256.0	915.92	-1340.1	6.30	1.163	218232	43600	26790	4641	366	1325	138300
15	11 07 041 24 4	1894	1906	1900.1	862.28	-1037.8	6.00	1.155	218290	57165	20020	4350	730	625	135400
16	05 36 051 26 4	1779	1785	1781.9			6.13	1.156	220063	47400	29800	4280	232	351	138000
17	16 23 049 27 4	1729	1737	1733.1	733.04	-1000.0	6.10	1.162	221698	47302	30334	4414	224	319	139105
18	06 29 049 25 4	1638	1640	1639.1	713.84	-925.2	5.90	1.155	221724	67339	16615	1120	171	339	136140
19	13 34 048 27 4	2012	2019	2015.5			7.00	1.162	222982	47136	30758	4543	135	500	139910
20	08 05 050 25 4	1760	1761	1760.8	711.1	-1049.7	6.40	1.147	223607	48473	29463	4755	150	328	140438
21	02 12 042 23 4	1739			861.67	861.7	6.50	1.144	224245	47742	30209	4825	632	84	140645
22	02 04 051 25 4	1731	1737	1734.3			5.50	1.164	226362	50463	28829	4617	144	309	142000
23	11 20 046 27 4	2226	2241	2233.6	867.16	-1366.4	6.50	1.160	228220	46617	25270	10074	255	621	145383
24	04 01 050 26 4	1668	1672	1670.3	719.02	-951.3	5.70	1.150	230375	50678	28370	4306	148	360	143400
25	10 13 050 27 4	1587	1588	1587.6	675.13	-912.4	5.90	1.165	236141	52308	30931	4356	214	328	147481
26	02 02 049 27 4	1938	1939	1938.7	759.56	-1179.1	5.60	1.165	239143	52189	32470	4102	156	346	149256
27	11 07 043 01 5	2393	2394	2393.6	910.44	-1483.2	5.20	1.170	242092	57955	30369	2542	54	334	149737

No.	LSD.Sec.T.R.M.	INTERVAL(m)		Depth(m)	K.B.(m)	Elev.(m)	pH	Density	TDSmg/l	Na	Ca	Mg	HCO3	SO4	Cl
28	03 24 042 02 5	2418	2420	2419.0	933.6	-1485.4	6.30	1.162	244790	61005	28347	2758	309	467	151598
29	05 24 051 27 4	1804	1814	1808.8	709.88	-1099.0	6.00	1.166	252935	66449	25064	3530	216	311	156241
30	06 01 054 26 4	1478	1483	1480.6			5.80	1.094	*132850*		*17400*		500	70	81150
						AVERAGE	6.21	1.143	204536	48919	23650	3879	335	551	127278
						STD	0.45	0.022	33909	8672.4	5961.6	1523.7	285	345	21536
						COUNT	30	29	30	29	30	29	30	30	30
						NOTE: Calculated TDS values are enlisted; values italicized are at ignition									
						Italicized values in Calcium column represent (Ca+Mg)									
						Cations and Anions [illegible]re in mg/l; Density in g/cc									

Table 9b Water chemistry data for the Leduc Formation

No.	LSD.Sec.T.R.M.	Na	Ca	Mg	HCO3	SO4	Cl	Mg/Ca	Na/Cl	(HCO3/Cl)*100	SO4/Cl	SO4/HCO3
1	01 02 042 25 4	1306.74	880.24	282.68	8.28	24.59	2436.98	0.3211	0.536	0.340	0.010	2.971
2	14 15 041 02 5	1401.91	845.81	400.66	5.95	11.45	2630.86	0.4737	0.533	0.226	0.004	1.925
3	15 02 053 26 4	1574.16	748.00	269.85	3.39	20.05	2668.55	0.3608	0.59	0.127	0.008	5.910
4	13 18 054 25 4	1942.67	693.66	188.73	6.74	15.74	2795.40	0.2721	0.695	0.241	0.006	2.337
5	04 22 054 23 4	2109.26	576.30	185.85	0.90	14.37	2856.98	0.3225	0.738	0.032	0.005	15.938
6	04 06 051 25 4	1748.59	938.12	227.89	1.88	7.75	2905.50	0.2429	0.602	0.065	0.003	4.110
7	07 11 046 28 4	1866.90	1022.95	237.93	3.77	33.75	2911.14	0.2326	0.641	0.129	0.012	8.954
8	08 24 049 26 4	1696.39	1222.55	341.83	2.88	16.07	3407.62	0.2796	0.498	0.085	0.005	5.573
9	07 34 041 23 4	2267.81	998.00	233.65	23.43	9.33	3466.57	0.2341	0.654	0.676	0.003	0.398
10	10 11 041 25 4	2231.45	1070.31	256.93	14.21	13.78	3520.87	0.2401	0.634	0.404	0.004	0.970
11	08 09 052 26 4	2363.20	1051.15	301.03	4.92	9.39	3702.12	0.2864	0.638	0.133	0.003	1.910
12	10 14 044 01 5	2168.07	1210.78	369.89	8.19	12.35	3729.20	0.3055	0.581	0.220	0.003	1.507
13	07 34 052 26 4	2326.66	1140.57	263.51	4.11	9.45	3705.67	0.231	0.628	0.111	0.003	2.298
14	02 01 046 01 5	1896.48	1336.83	381.82	6.00	27.59	3901.27	0.2856	0.486	0.154	0.007	4.599
15	11 07 041 24 4	2486.52	999.00	357.88	11.96	13.01	3819.46	0.3582	0.651	0.313	0.003	1.088
16	05 36 051 26 4	2061.77	1487.03	352.12	3.80	7.31	3892.81	0.2368	0.53	0.098	0.002	1.922
17	16 23 049 27 4	2057.50	1513.67	363.14	3.67	6.64	3923.98	0.2399	0.524	0.094	0.002	1.809
18	06 29 049 25 4	2929.06	829.09	92.14	2.80	7.06	3840.34	0.1111	0.763	0.073	0.002	2.519
19	13 34 048 27 4	2050.28	1534.83	373.76	2.21	10.41	3946.69	0.2435	0.519	0.056	0.003	4.705
20	08 05 050 25 4	2108.44	1470.21	391.20	2.46	6.83	3961.58	0.2661	0.532	0.062	0.002	2.778
21	02 12 042 23 4	2076.64	1507.44	396.96	10.36	1.75	3967.42	0.2633	0.523	0.261	0.000	0.169
22	02 04 051 25 4	2195.00	1438.57	379.84	2.36	6.43	4005.64	0.264	0.548	0.059	0.002	2.726
23	11 20 046 27 4	2027.71	1260.98	828.79	4.18	12.93	4101.07	0.6573	0.494	0.102	0.003	3.094
24	04 01 050 26 4	2204.35	1415.67	354.26	2.43	7.50	4045.13	0.2502	0.545	0.060	0.002	3.090
25	10 13 050 27 4	2275.25	1543.46	358.37	3.51	6.83	4160.25	0.2322	0.547	0.084	0.002	1.947
26	02 02 049 27 4	2270.07	1620.26	337.47	2.56	7.20	4210.32	0.2083	0.539	0.061	0.002	2.818
27	11 07 043 01 5	2520.88	1515.42	209.13	0.88	6.95	4223.89	0.138	0.597	0.021	0.002	7.858

No.	LSD.Sec.T.R.M.	Na	Ca	Mg	HCO3	SO4	Cl	Mg/Ca	Na/Cl	(HCO3/Cl)*100	SO4/Cl	SO4/HCO3
28	03 24 042 02 5	2653.55	1414.52	226.90	5.06	9.72	4276.39	0.1604	0.621	0.118	0.002	1.920
29	05 24 051 27 4	2890.34	1250.70	290.42	3.54	6.48	4407.36	0.2322	0.656	0.080	0.001	1.829
30	06 01 054 26 4		868.26		8.19	1.46	2289.14			0.358	0.001	0.178
	AVERAGE	2127.85	1180.15	319.13	5.49	11.47	3590.34	0.274	0.588	0.161	0.003	3.328
	STD	377.23	297.48	125.35	4.66	7.18	607.50	0.101	0.073	0.142	0.003	3.150
	COUNT	29	30	29	30	30	30	29	29	30	30	30
	NOTE: Cations and Anions are in meq/l											

Table 10a Water chemistry data for the Cooking Lake Formation

No.	LSD.Sec.T.R.M.	INTERVAL(m)		Depth(m)	K.B.(m)	Elev.(m)	pH	Density	TDSmg/l	Na	Ca	Mg	HCO3	SO4	Cl
1	15 14 048 23 4	1745.0	1761.1	1753.06			7.00	1.085	124199	24234	18652	2719	200	798	77596
2	02 01 052 24 4	1645.9	1655.1	1650.49			7.30	1.089	128135	36500	9860	1930	160	785	78900
3	05 04 054 24 4	1612.7	1621.5	1617.12	77.99	-934.1	6.90	1.086	131908	34915	12992	1715	500	980	80806
4	07 10 054 25 4	1613.3	1618.5	1615.9	75.55	-954.2	5.90	1.103	149743	43300	11000	2225	386	832	92000
5	14 13 045 01 5	2337.8	2356.1	2346.96	97.65	-1491.7	6.95	1.123	159975	33852	21770	3340	193	1840	98980
6	07 27 051 23 4	1621.8	1640.1	1630.98			6.70	1.116	161600		*17420*		<1000	100-2000	100300
7	10 17 053 23 4	1515.2	1531.9	1523.54	74.77	-868.7	6.87	1.107	168475	50404	11691	1928	134	724	103190
8	02 32 054 23 4	1496.6	1503.3	1499.92			7.30	1.122	173744	53000	12279	2487	122	756	110100
9	04 24 050 26 4	1734.3	1767.8	1751.08	81.22	-1039.7	6.10	1.123	179085	39921	22192	4050	351	583	111988
10	01 24 053 26 4	1677.9	1702.0	1689.96	78.27	-1004.5	6.30	1.132	198036	48720	19540	4909	327	582	121800
11	11 18 047 26 4	2106.2	2133.6	2119.88	91.07	-1322.2	6.00	1.144	202436	46663	24264	4170	135	804	126400
12	02 30 052 25 4	1728.2	1734.9	1731.57	79.87	-1032.1	7.40	1.142	209369	50087	23826	4032	295	479	130650
13	10 04 053 25 4	1692.6	1699.3	1695.91	77.71	-1015.3	5.90	1.140	210090	57200	19600	2610	221	459	130000
14	02 06 046 27 4	2240.3	2259.2	2249.73			6.10	1.150	214395	52264	24865	3159	270	637	133200
15	08 16 051 25 4	1752.6	1759.3	1755.95	79.73	-1057.7	7.00	1.160	225879	51267	28123	4446	270	473	141300
16	11 35 043 01 5	2443.0	2465.8	2454.4	105.58	-1529.6	6.60	1.161	229354	56599	24236	4597	560	362	143000
17	09 22 051 27 4	1841.6	1847.7	1844.65	81.71	-1129.0	6.10		232461	64079	20220	3430	146	329	144257
18	06 07 050 25 4	1773.0	1783.1	1778.05	81.29	-1066.0	6.20	1.157	233127	49874	30070	4301	425	463	144900
19	04 10 049 26 4	1934.0	1941.6	1937.77			6.00	1.153	233417	66800	16440	4450	352	375	145000
20	03 19 047 27 4	2156.8	2161.6	2159.2	98.73	-1294.5	5.98	1.168	260950	61394	31995	3994	230	256	162207
21	07 22 054 26 4	1706.9	1723.0	1714.96	77.39	-1037.1	6.00	1.128	*175780*		*22037*		270	112	112815
22	13 16 050 24 4	1713.0	1722.1	1717.55	81.26	-1005.8	6.30	1.170	*231970*		*50570*		185	212	154808
23	02 22 046 23 4	1800.5	1802.9	1801.67			5.60	1.166	*233100*		*32670*		<1000	100-2000	146100
						AVERAGE	6.46	1.133	194445	48478	22014	3394	273	611	121317
						STD	0.53	0.027	39281.9	10983	9002	1028	122	364	25241
						COUNT	23	22	23	19	23	19	21	21	23

NOTE: Calculated TDS values are enlisted; values italicized are at ignition

Italicized values in Calcium column represent (Ca+Mg)

Cations and Anions are in mg/l; Density in g/cc

Table 10b Water chemistry data for the Cooking Lake Formation

No.	LSD.Sec.T.R.M.	Na	Ca	Mg	HCO3	SO4	Cl	Mg/Ca	Na/Cl	(HCO3/Cl)*100	SO4/Cl	SO4/HCO3
1	15 14 048 23 4	1054.11	930.74	223.69	3.28	16.61	2188.89	0.240	0.482	0.150	0.008	5.069
2	02 01 052 24 4	1587.65	492.02	158.78	2.62	16.34	2225.67	0.323	0.713	0.118	0.007	6.233
3	05 04 054 24 4	1518.70	648.30	141.09	8.19	20.40	2279.44	0.218	0.666	0.359	0.009	2.490
4	07 10 054 25 4	1883.43	548.90	183.05	6.33	17.32	2595.20	0.333	0.726	0.244	0.007	2.738
5	14 13 045 01 5	1472.47	1086.33	274.78	3.16	38.31	2792.10	0.253	0.527	0.113	0.014	12.112
6	07 27 051 23 4		869.26				2829.34					
7	10 17 053 23 4	2192.43	583.38	158.62	2.20	15.07	2910.86	0.272	0.753	0.075	0.005	6.864
8	02 32 054 23 4	2305.35	612.72	204.61	2.00	15.74	3105.78	0.334	0.742	0.064	0.005	7.873
9	04 24 050 26 4	1736.45	1107.39	333.20	5.75	12.14	3159.04	0.301	0.550	0.182	0.004	2.110
10	01 24 053 26 4	2119.18	975.05	403.87	5.36	12.12	3435.83	0.414	0.617	0.156	0.004	2.261
11	11 18 047 26 4	2029.71	1210.78	343.07	2.21	16.74	3565.59	0.283	0.569	0.062	0.005	7.566
12	02 30 052 25 4	2178.64	1188.92	331.72	4.83	9.97	3685.47	0.279	0.591	0.131	0.003	2.063
13	10 04 053 25 4	2488.04	978.04	214.73	3.62	9.56	3667.14	0.220	0.678	0.099	0.003	2.639
14	02 06 046 27 4	2273.34	1240.77	259.89	4.42	13.26	3757.40	0.209	0.605	0.118	0.004	2.997
15	08 16 051 25 4	2229.97	1403.34	365.78	4.42	9.85	3985.90	0.261	0.559	0.111	0.002	2.226
16	11 35 043 01 5	2461.90	1209.38	378.20	9.18	7.54	4033.85	0.313	0.610	0.228	0.002	0.821
17	09 22 051 27 4	2787.26	1008.98	282.19	2.39	6.85	4069.31	0.280	0.685	0.059	0.002	2.863
18	06 07 050 25 4	2169.38	1500.50	353.85	6.96	9.64	4087.45	0.236	0.531	0.170	0.002	1.384
19	04 1C 049 26 4	2905.61	820.36	366.10	5.77	7.81	4090.27	0.446	0.710	0.141	0.002	1.353
20	03 19 047 27 4	2670.47	1596.56	328.59	3.77	5.33	4575.66	0.206	0.584	0.082	0.001	1.414
21	07 22 054 26 4		1099.65		4.42	2.33	3182.37			0.139	0.001	0.527
22	13 16 050 24 4		2523.45		3.03	4.41	4366.94			0.069	0.001	1.456
23	02 22 046 23 4		1630.24				4121.30					
	AVERAGE	2108.64	1098.48	279.25	4.47	12.73	3422.21	0.285	0.626	0.137	0.004	3.574
	STD	477.73	449.20	84.56	2.01	7.57	712.01	0.065	0.081	0.072	0.003	2.956
	COUNT	19	23	19	21	21	23	19	19	21	21	21
	NOTE: Cations and Anions are in meq/l											